New developments in wide bandgap CdZnTe (CZT) semiconductor detectors

Aleksey Bolotnikov

Brookhaven National Laboratory
Upton, NY

May 18, 2012

1. Introduction

- BNL's Nonproliferation and National Security Department (NNS)
- Finding solutions and developments related to
  - Nonproliferation of nuclear materials (security of nuclear plants and other facilities)
  - Arms control
  - Movement of spent fuel
  - National security (points of entry, safeguard)
- Detector development efforts: neutron and gamma-ray detectors

- Three research areas:
  - CdZnTe material growth (new)
  - material characterization (samples from vendors)
  - detector development and testing

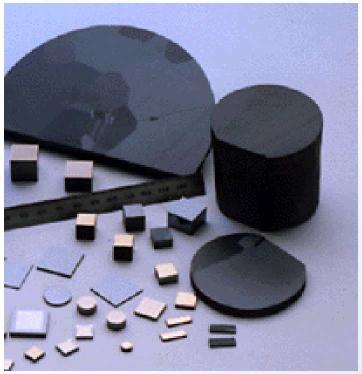

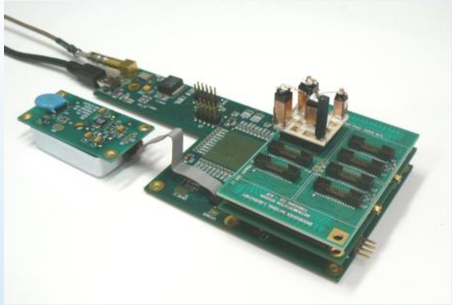

Advantages of Cadmium Zinc Telluride (CZT) Material

CZT is very attractive material for radiation detectors. Its feasibility has been demonstrated in many applications

	CZT	Ge	Si	TlBr	Hg$_2$I
• High average Z	49.1	32	14	80	80
• High density (g/cm^3)	5.78	5.32	2.33	7.56	6.4
• High resistivity (Ω–cm)	10^{10}	47	2.3×10^5	10^{12}	10^{12}

- chemically reactive
- difficult to handle
- toxic

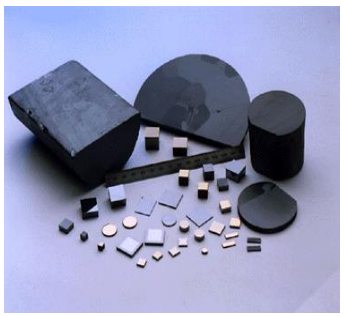

TlBr

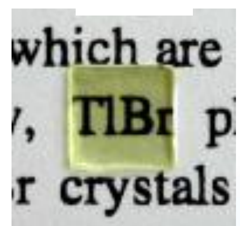

HgI$_2$

• Provide high energy resolution close to Ge (0.5% at 662 keV)
• Do not require cooling (best results usually obtained at ~5-10 C)
• Provide sub-millimeter spatial resolution for imaging devices
• Device fabrication utilizes technologies developed in semiconductor industry which make CZT detectors less expensive and more robust

National and Homeland Security

- Nonproliferation of nuclear materials
- Secondary inspection for portals
- Safeguards measurements
- Forensics and attribution
- Nuclear waste management

Medical Imaging

- SPECT, PET and CT scanners
- Bone densitometers
- Medical probes

Basic science

- Astrophysics
- Gamma-Ray Spectroscopy
- Synchrotron X-ray research

Industrial imaging

- Bore-hole logging
- X-ray and gamma-ray cameras
- XRF material analyses

→

Variety of applications requires detectors with spectroscopic and imaging capabilities

Long-term, widespread and un-met need for advanced detectors

Progress in CZT detector development

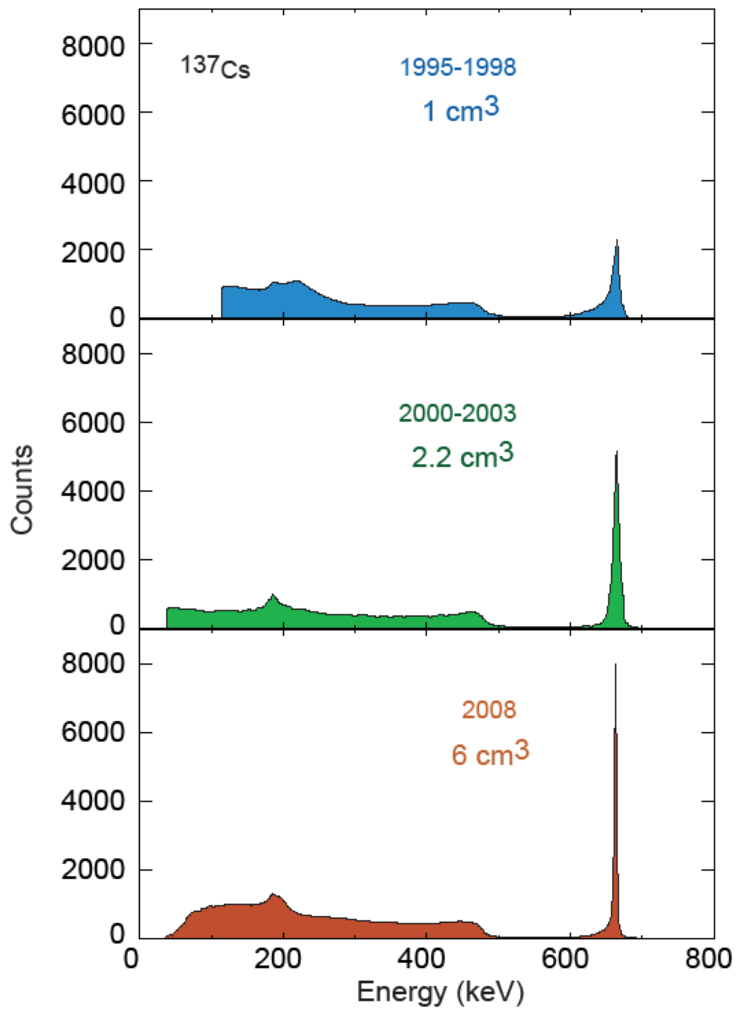

CZT detectors have been proposed more that a decade ago with a goal to replace HPGe in the field applications

Despite of significant progress in detector technologies and electronics we are still far from achieving this goal

We believe, that today's commercial CZT material have excessively high concentrations of the extended defects, which limit the size and performance of CZT detectors

X-ray and gamma spectrometers required for many security and medical applications

Traditional Nuclear
Radiation Spectrometers

- Ge – High energy resolution, cryogenic cooling
- NaI Scintillators – Low energy resolution

Room-Temperature
Wide Band-gap Semiconductor Spectrometers

- No cooling requirements
- High energy resolution
- High spatial resolution

Brookhaven Science Associates

Spectra of ^{152}Eu source measured with different detectors

Detectors with high resolution preserve more information about a source

Comparison of NaI, HPGe and CZT Detectors

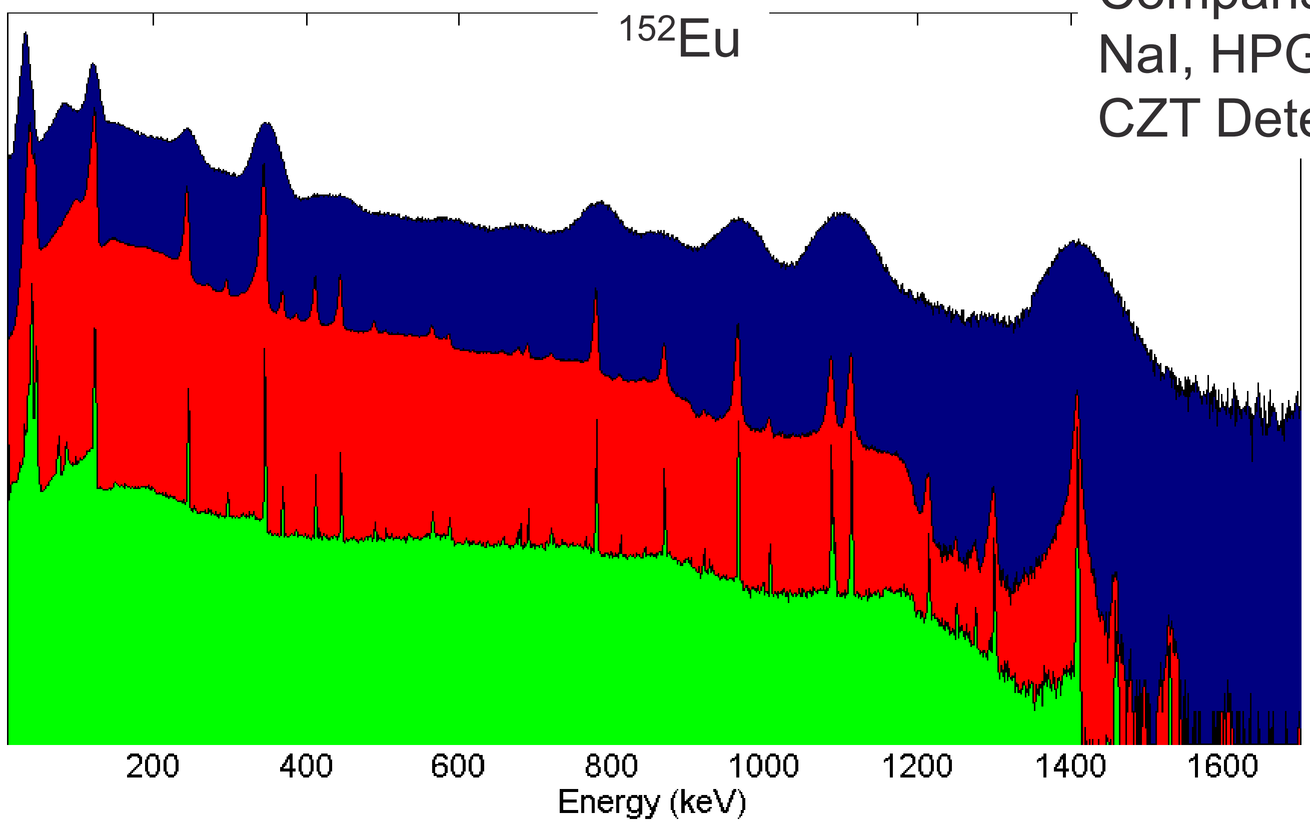

Z. He et al., University of Michigan

Many candidate materials considered for detector and photo-voltaic applications

(1) Improve our ability to precisely image the distribution of radionuclides in bodies;

(2) Enhance our capability to detect the trafficking, storage, and use of radiological materials and devices.

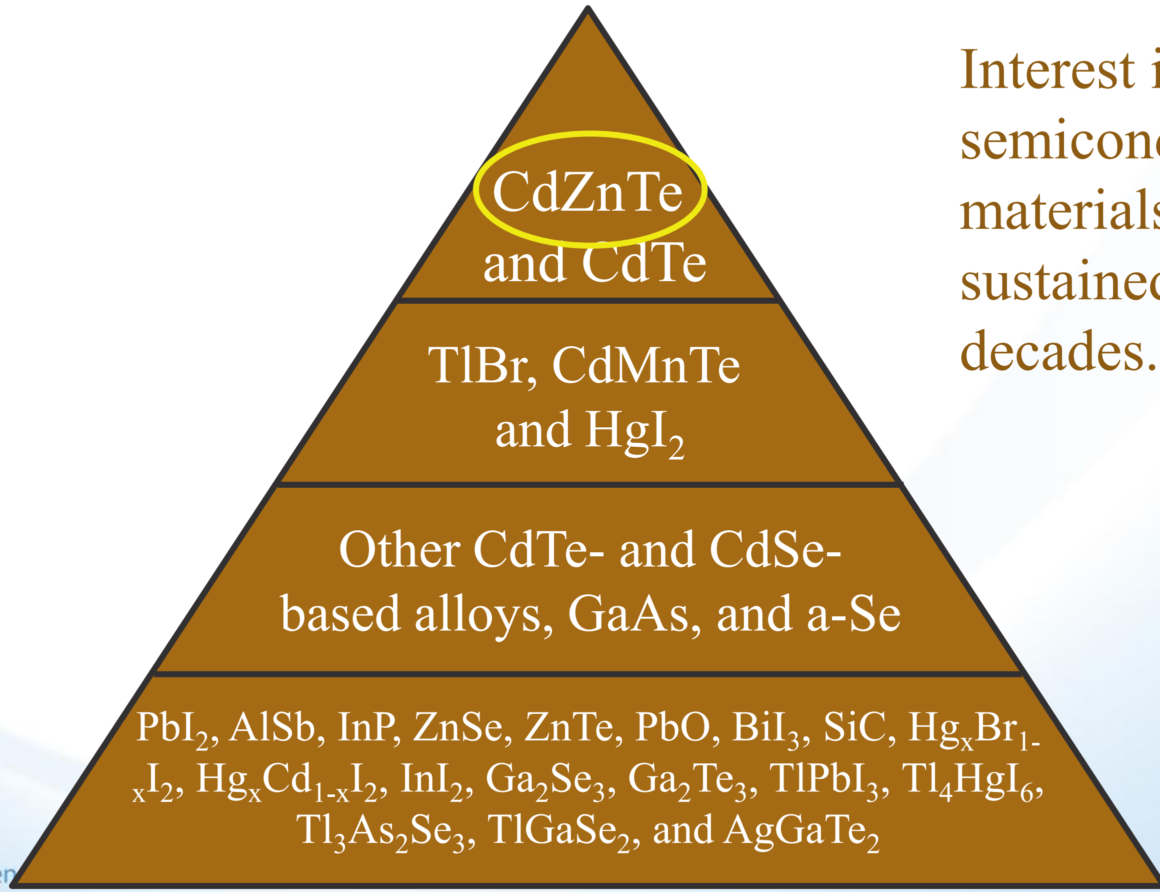

Interest in wide band gap semiconductor detector materials has been sustained for over three decades.

Cadmium Zinc Telluride (CZT) detectors capable of energy resolution close to High-Purity Germanium

Enriched Uranium (95%) Spectrum Taken with Cadmium Zinc Telluride Detector

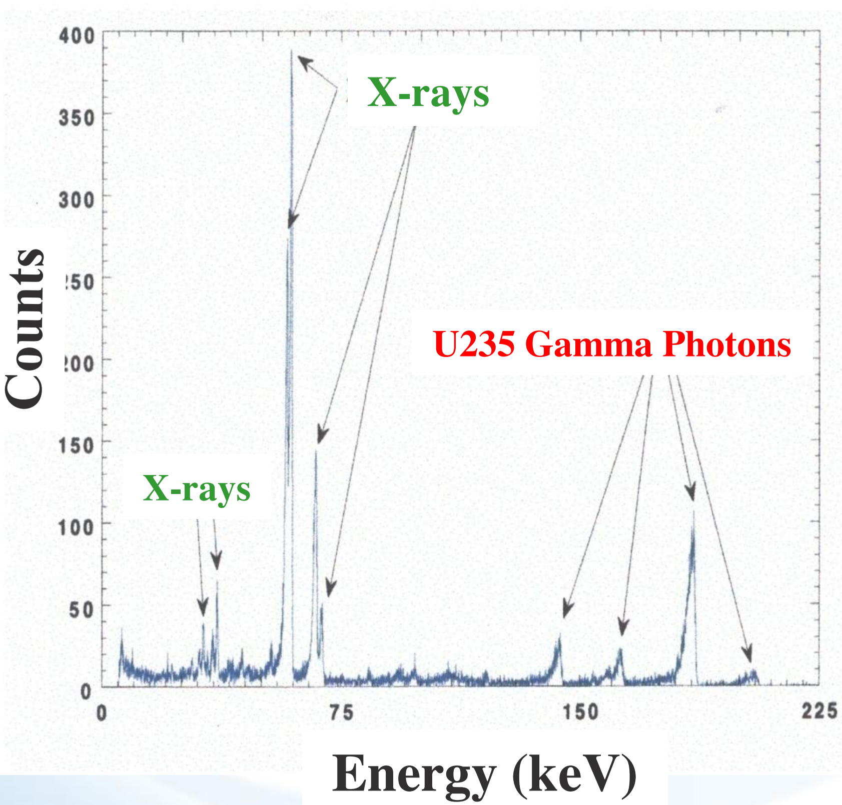

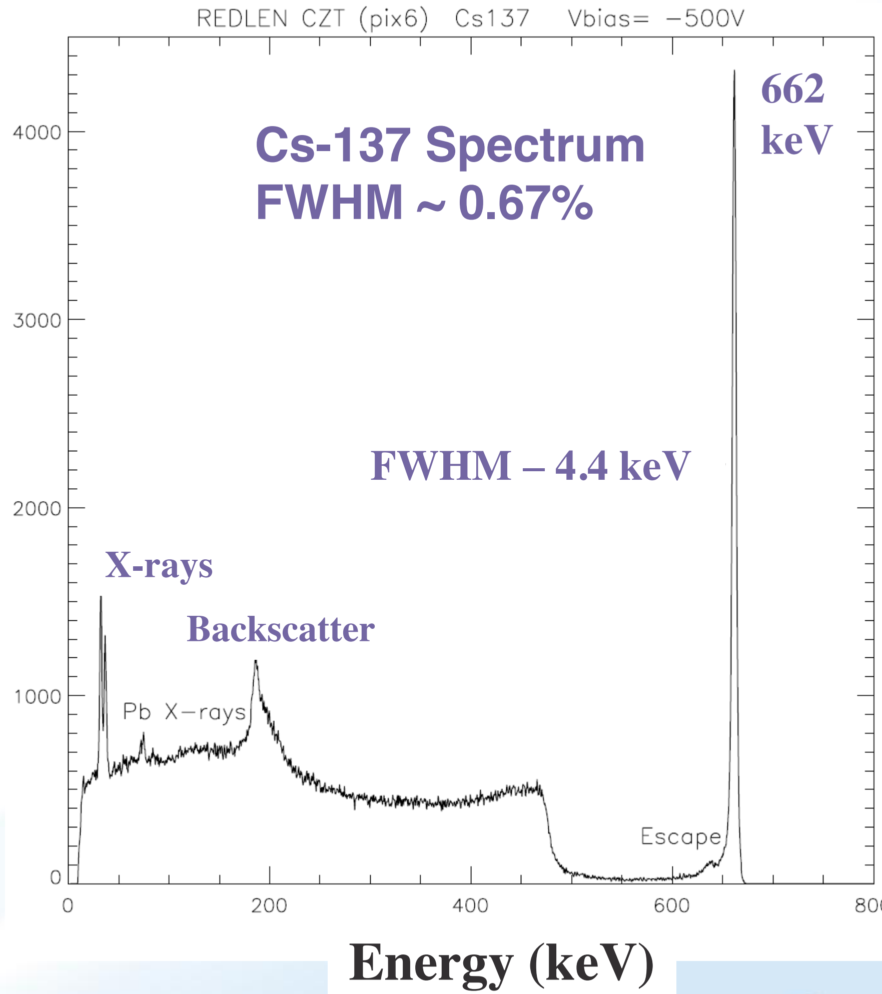

Brookhaven Science Associates

Mobility-Lifetime Products

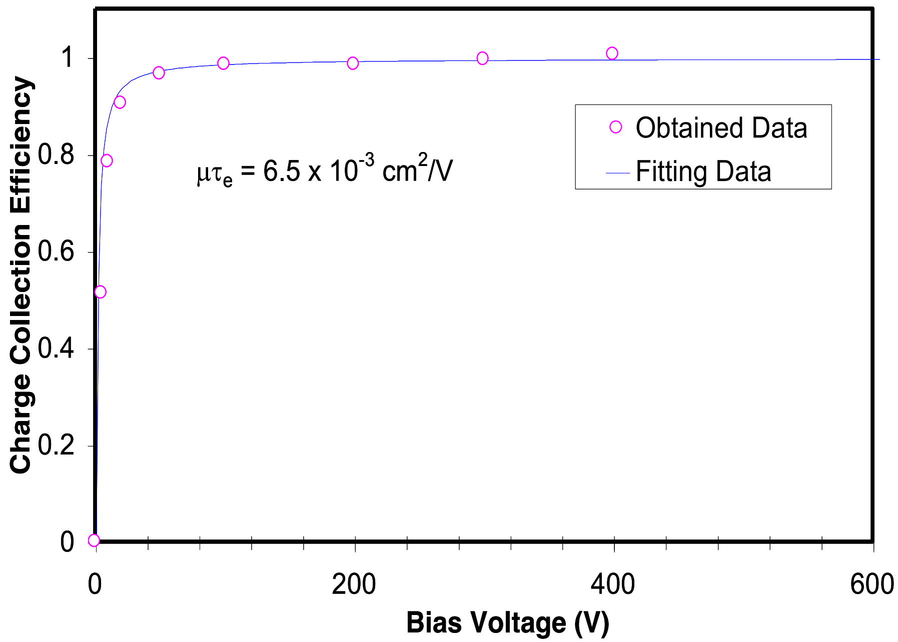

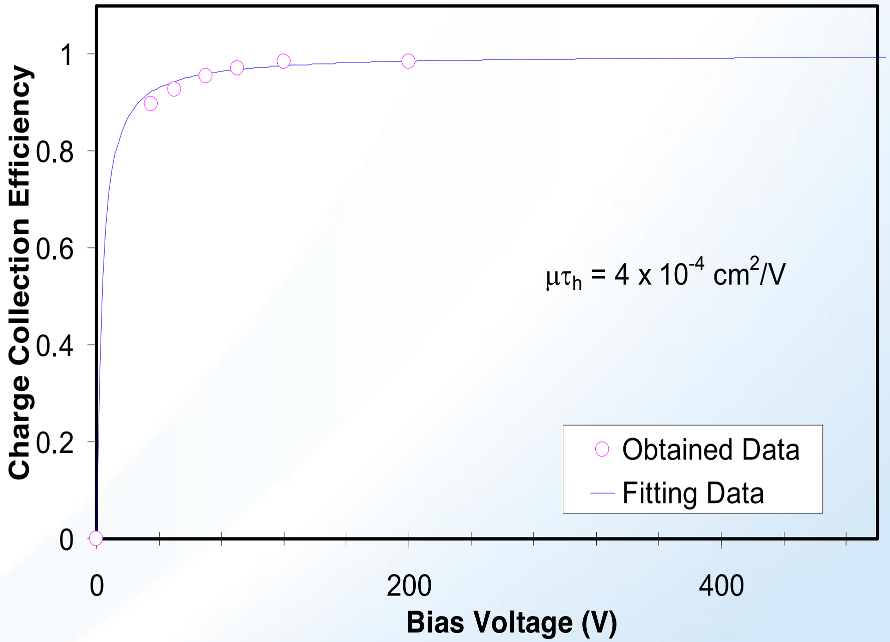

Progress in CdZnTe growth

Commercial producers: Endicott
Redlen

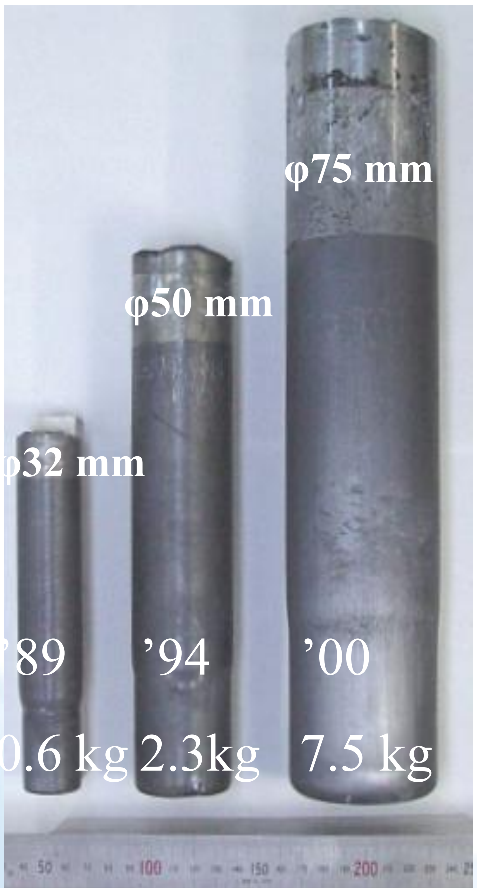

Strong Demand

- Lower cost
- Increase throughput
- Increase device size

Future

Up to 300-mm diameter

Ingot length: 2 m

Low- and high pressure Bridgman growth from melt

- Load charge and oriented seeds into growth ampoule

- Load growth ampoule into PMZF furnace (*Programmable Multi-Zone Furnace*)

    - 24 zone furnace built as NASA flight furnace
    - +/- 0.1˚C temperature control
    - Gradient = 1˚C/mm
    - Translation rate = 0.42 mm/hour (10 mm/day)

PMZF growth furnace

LPB is a bulk crystal growth method that directionally solidifies a molten charge

CZT 11-1 seed loading procedure

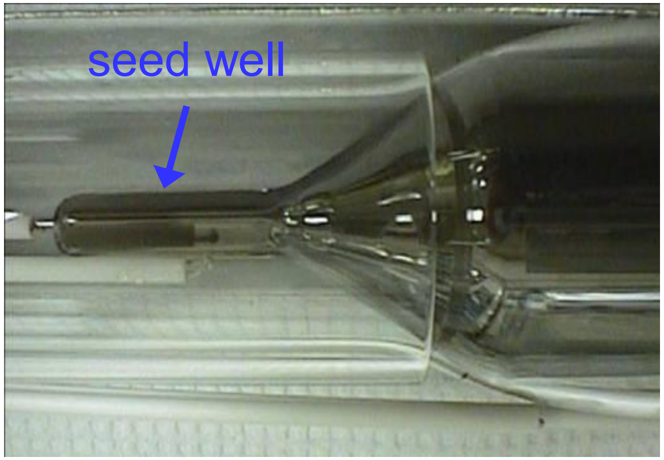

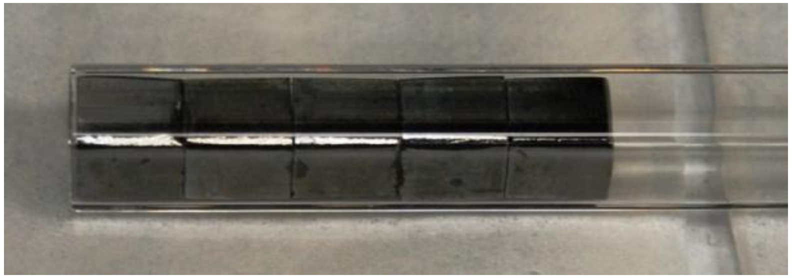

Seeds are carefully ground and etched to size, to prevent the melt from leaking past the seeds

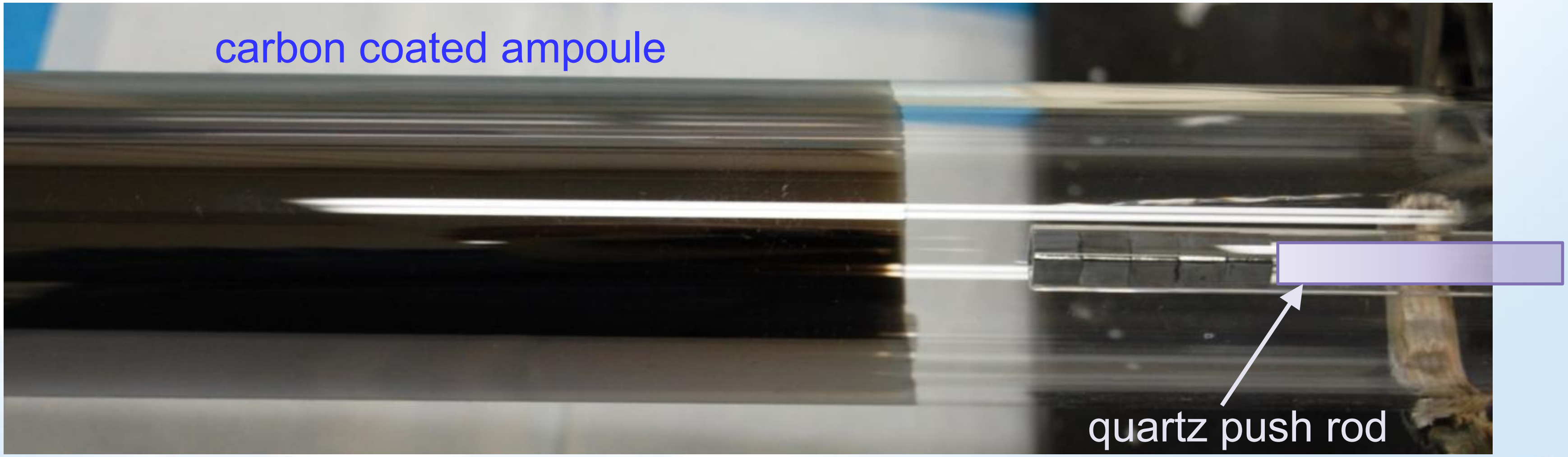

Seeds being loaded into growth ampoule

PMZF furnace before tilting to vertical growth orientation

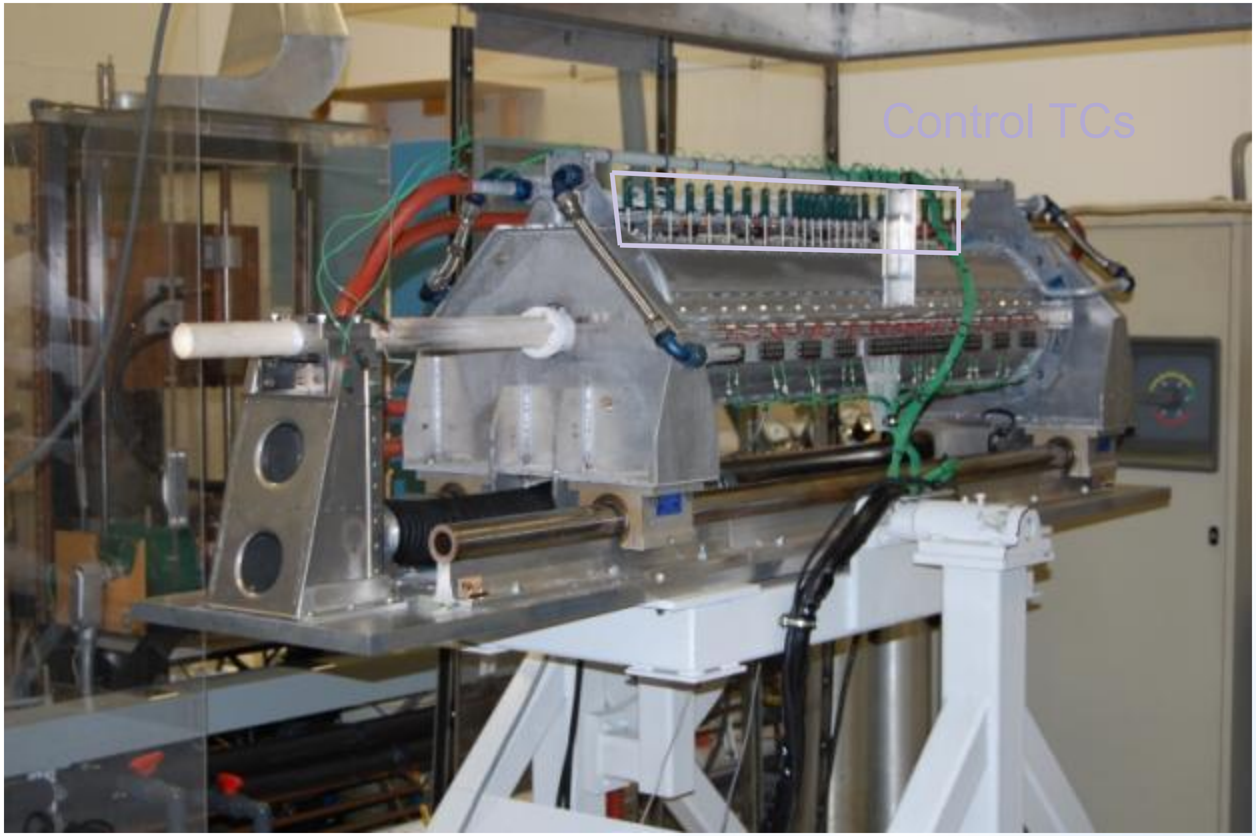

Close-up of PMZF furnace, loaded for growth
(crystal growth in vertical orientation)

CZT synthesis in rocking furnace

- Load elements and dopants into reaction ampoule
- React and melt charge in rocking furnace (>1100˚C, very exothermic)
- Mechanically rock ampoule to homogenize charge
- Quench charge (exothermic reaction)
- Melting points (˚C):

Cd – 321, Zn – 420, Te – 450, CdTe - 1092, ZnTe – 1290, CZT – 1102

Mellen rocking furnace

Rocking furnace ensures homogeneous charge

CZT 10-1 ingot

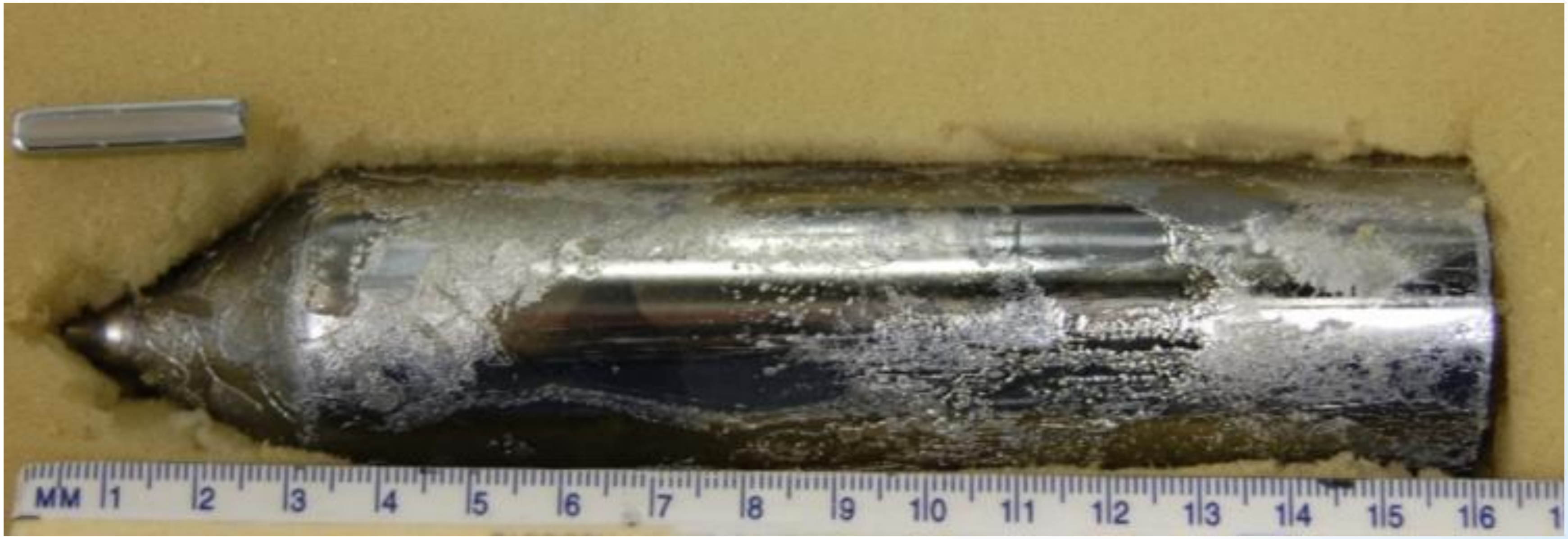

949 grams
38 mm OD
156 mm long
→18 wafers

CZT 10-1 CdZnTe ingot

CZT 10-1 results – grain structure of selected wafers

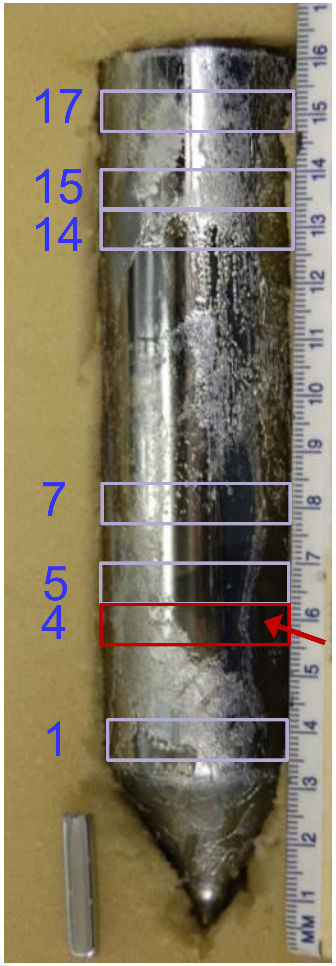

Seed
for 11-1

Wafer locations in ingot

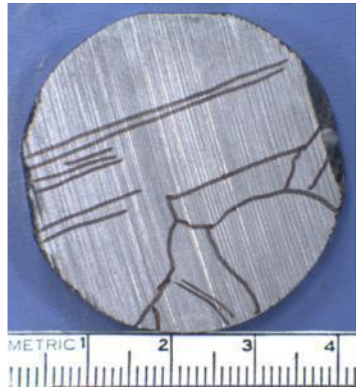

Wafer 1

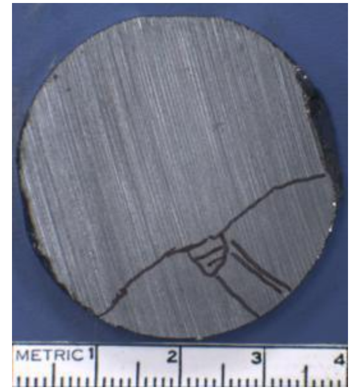

Wafer 5 to BNL

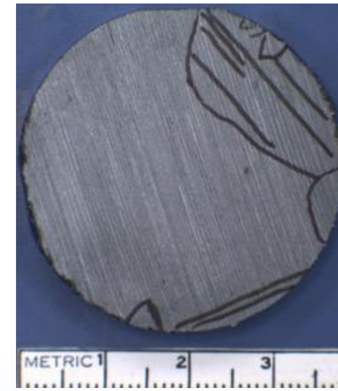

Wafer 7 to BNL

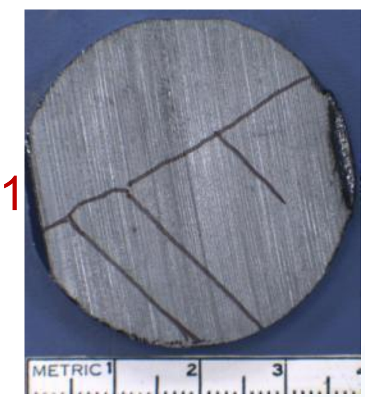

Wafer 14 to BNL

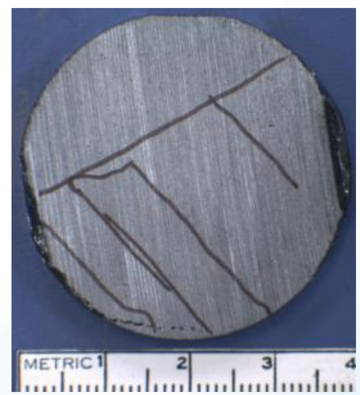

Wafer 15 to BNL

Wafer 17

Wire saw-cut CZT wafers have large grains

Recent advances of Redlen THM CZT

Crystal and detector volume expansion

Redlen's 50 mm dia. CZT ingot

75 mm dia.

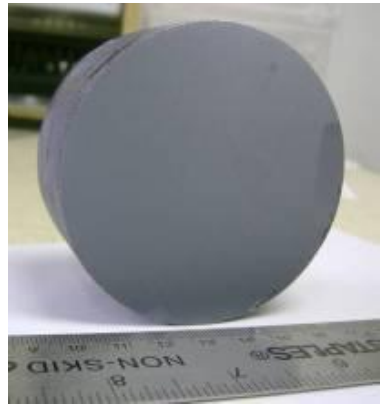

100 mm dia.

20x20x5 mm3
2006

20x20x10 mm3
2008

20x20x15 mm3
2010

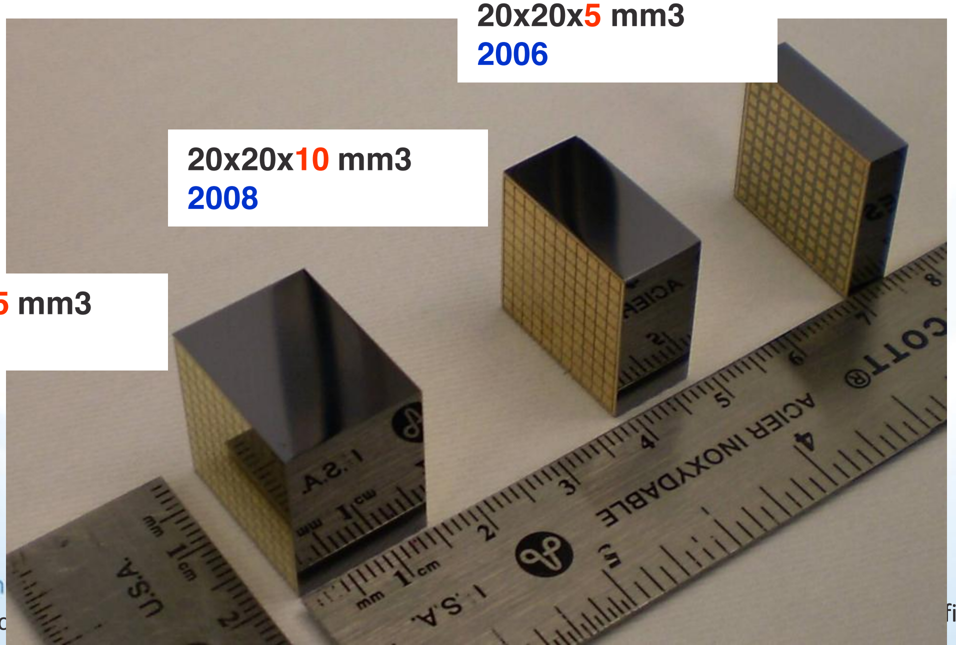

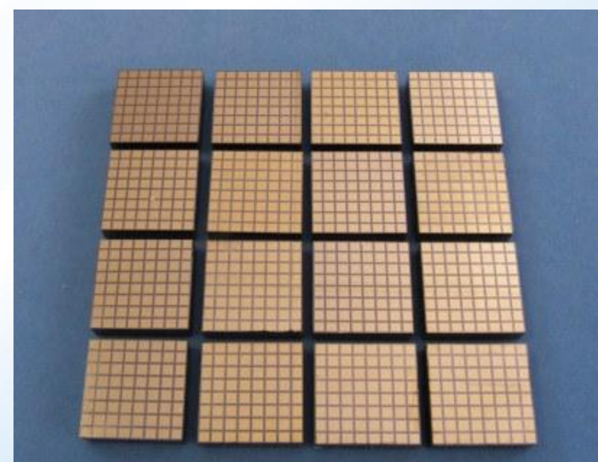

20x20x5 mm3 tiles

Redlen's more recent 100 mm diameter boule

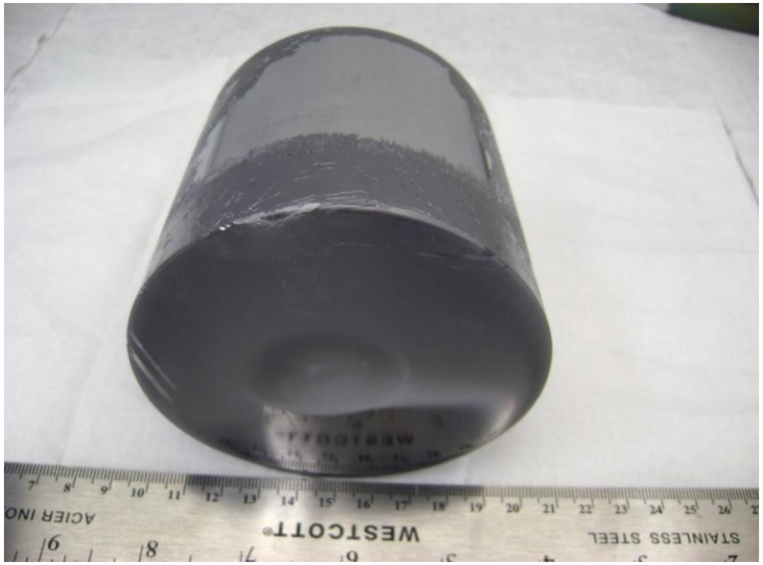

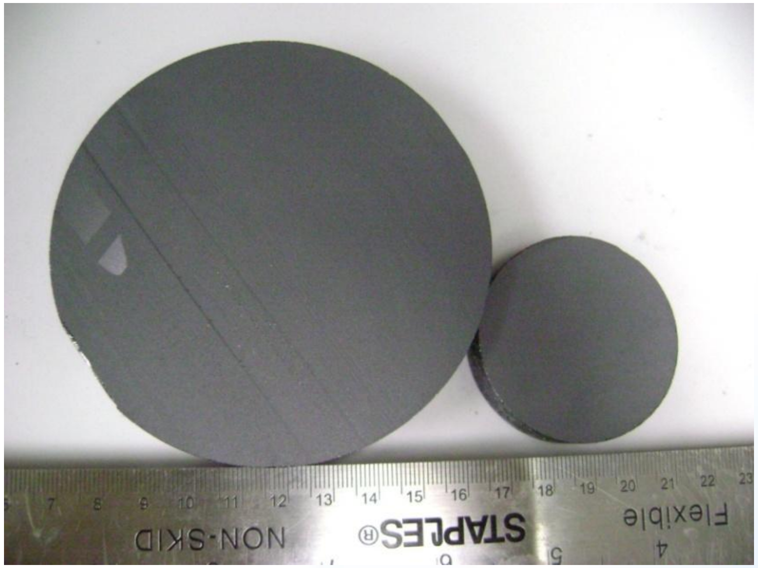

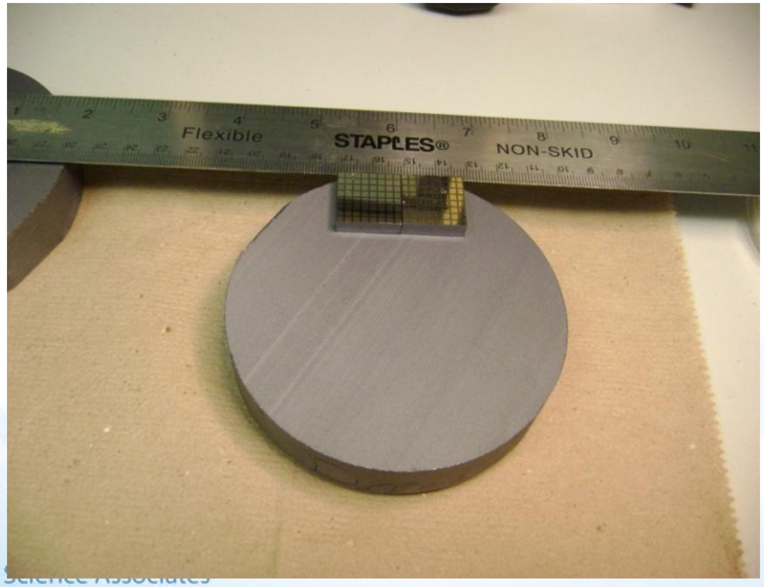

Conclusions 1

- Two growth method: Bridgman, THM, and floating zone
- THM is the most promising
- Grown crystals are far from perfect:
  - Te-reach secondary phases (inclusions and precipitates)
  - Twinning
  - Subgrain boundaries
- Difficult to grow in comparison to Ge and Si (Czochralski)

2. Operation principle of ionization detectors

- Low mobility of holes (single-charge carrier device)
- This makes CZT detectors different from HPGe

$$Q_{out} = Q_{col} - O_{ind}$$

Collected charge (mostly electrons)

Charge induced by trapped carriers (mostly holes). It is function of coordinates

Incident photon

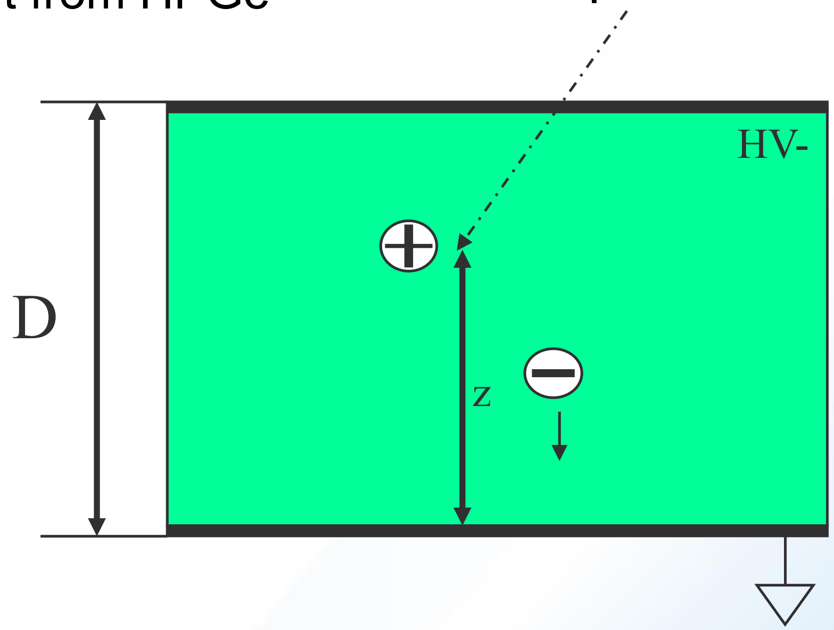

$$Q_{ind} = \frac{E_{ph}}{D} z$$

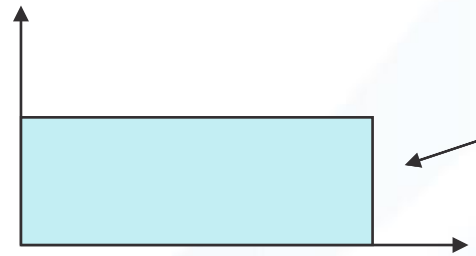

Spectral response to monoenergetic photons

A detector's design should provide efficient way for illuminating the effect of holes!

Elimination of the influence of the uncollected holes

Electron-only carrier device

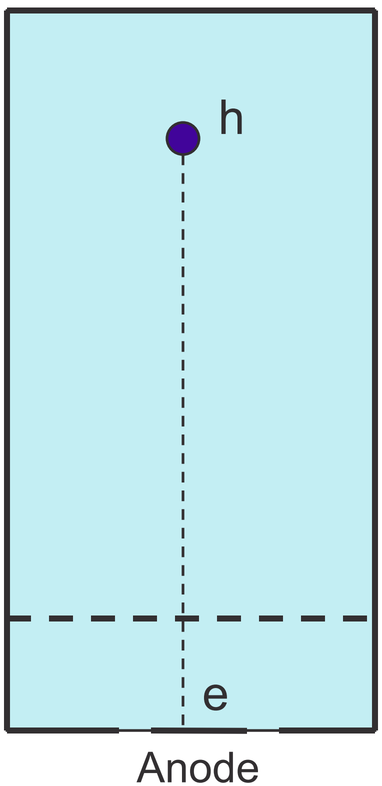

$$A \sim Q_{col}^{el} + \cancel{Q_{ind}^{hol}}$$

(1) Electrostatic shielding

- Frisch-grid ionization chambers
- Virtual Frisch-grid detectors
  - Spherical, Hemi-spherical, Three-terminal, CAPture, Frisch-ring, Capacitive Frisch-grid, Pixel detectors and their modifications

(2) Electronic subtraction

- Coplanar-grid detectors

Theoretically, all these designs should provide energy resolution close to its statistical limit determined by the Fano-factor (~0.5% at 662 keV)

3. Defects in commercial CZT material

- Yield of CZT crystals which provide energy resolution close to statistical limit is very low
- Several types of the extended defects that can be found in a average commercial CZT crystal:
  - twins,
  - sub-grain boundaries,
  - Te inclusions,
  - and dislocations which usually arranged in dislocation walls or mosaic strictures
- Most of these defects are not readily seen with visible or IR microscopes => they are often overlooked by vendors
- The extended defects are less important in thin detectors, but their critical roles increase with device thicknesses

Experimental techniques available in BNL

- Experimental techniques are used to identify the extended defect and to measure their effect:
  - IR microscopy
  - White X-ray beam diffraction topography
  - Micro-resolution X-ray beam mapping
  - Surface etching

IR microscopy

CCD camera

Objective lens (high field of view)

Motorized X-Y-Z translational stage, with custom slab holder. (not shown)

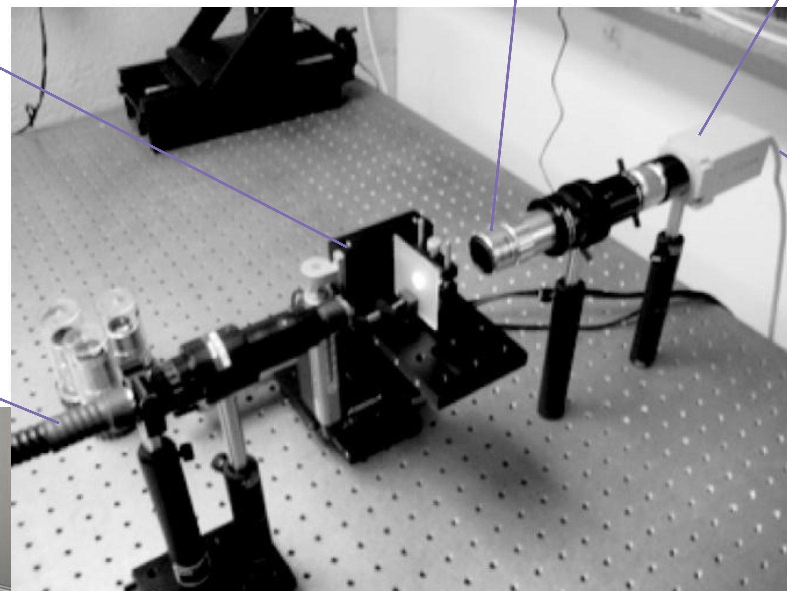

Light source

Connected to PC

Nikon microscope

- A stack of images is taken each position of a camera
- Background subtraction
- Locating individual inclusions

Te inclusions found to various degrees in all detector-grade CZT

- Te precipitates
  - Single crystals, dislocation fields (sub-grain boundaries), twin boundaries, grain boundaries

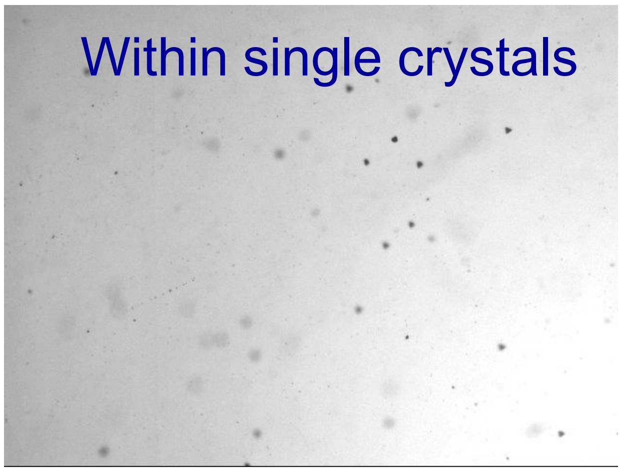

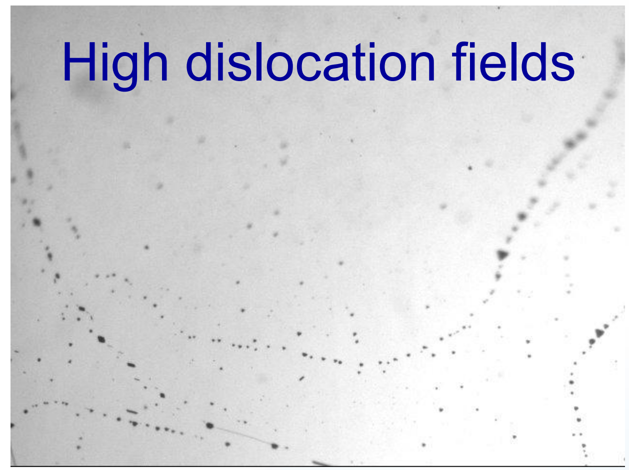

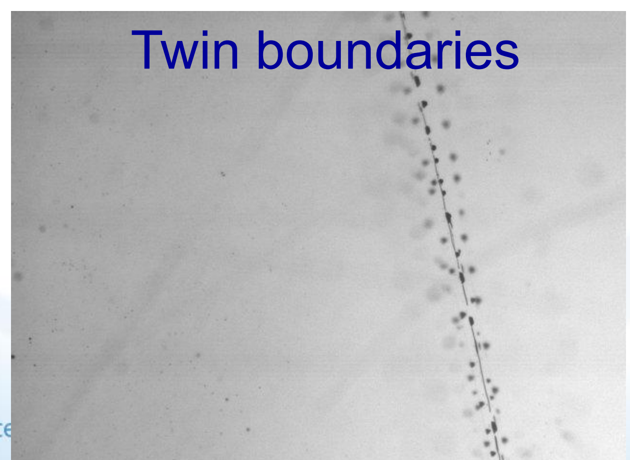

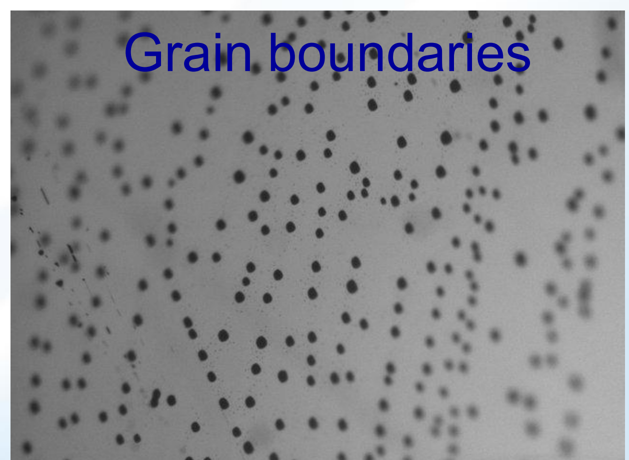

An example of a stack of 100 images projected on the one plane after background subtraction

Volume 1.1x1.5x10 mm^3

Te inclusions
"starry sky"

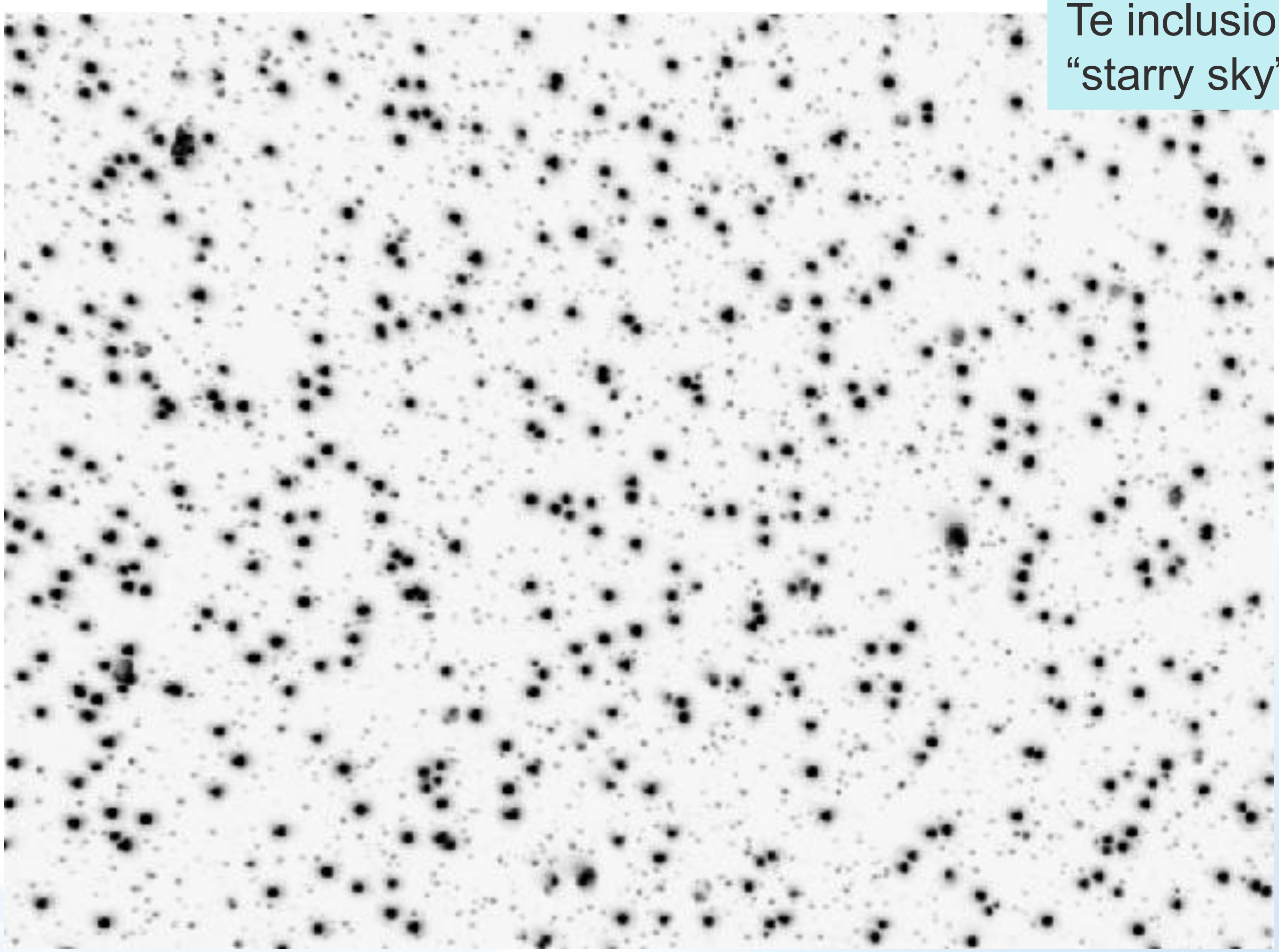

IR image analysis

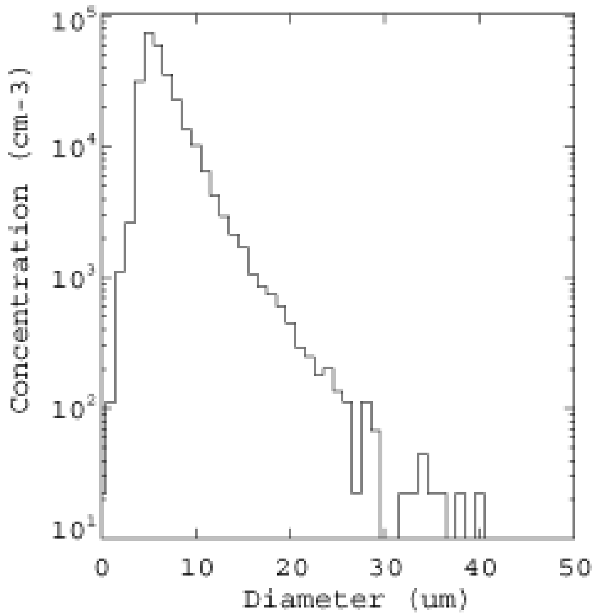

- Size distribution of Te inclusions
- Resolution is limited by the wavelength
- Min size is ~1 μm

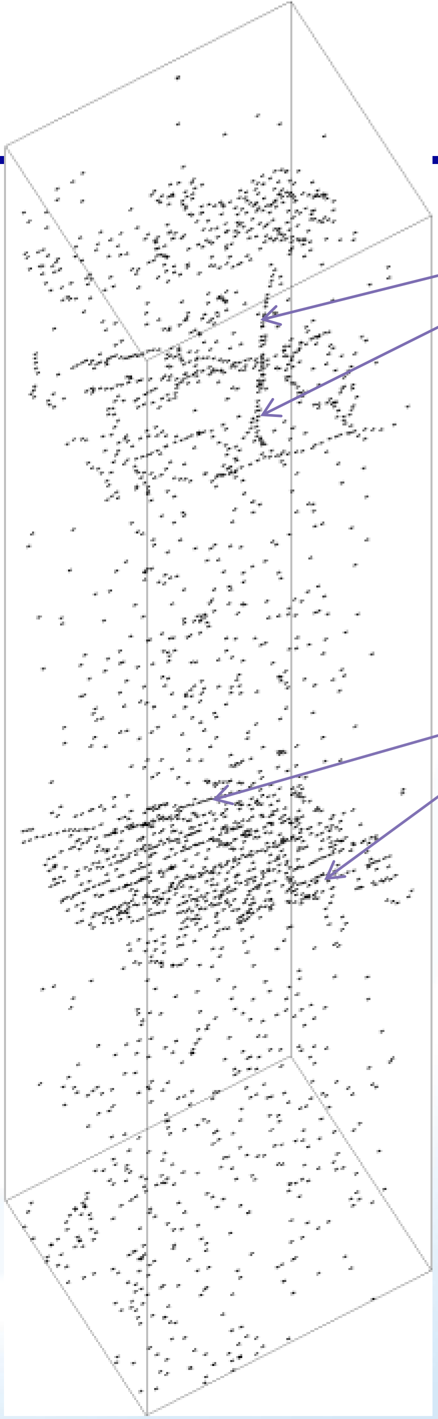

Twin boundaries decorated by Te inclusions

Volume: 1.1x1.5x6 mm^3
Four views rotated by 90^O

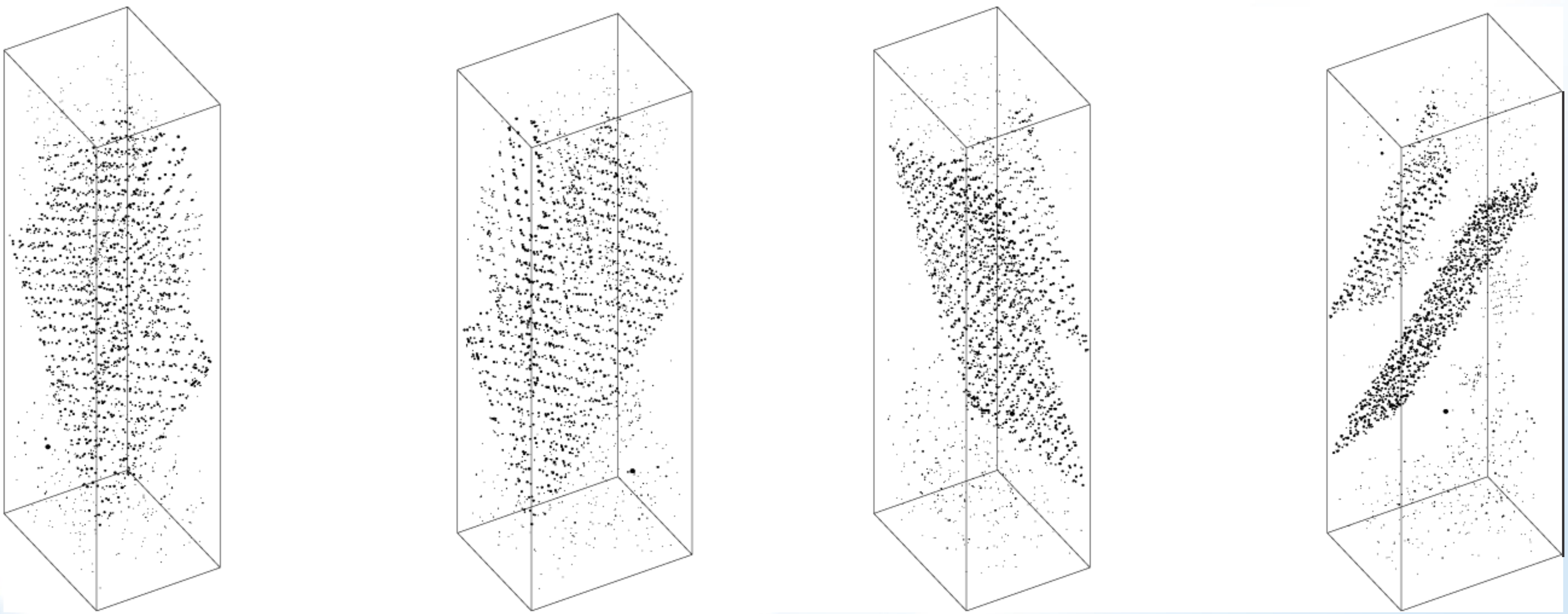

We note that inclusion-free regions were observed around decorated twin and subgrain boundaries

Synchrotron Radiation at NSLS

What is a synchrotron? It is a source of tiny beams of very bright x-rays, UV, visible and IR light

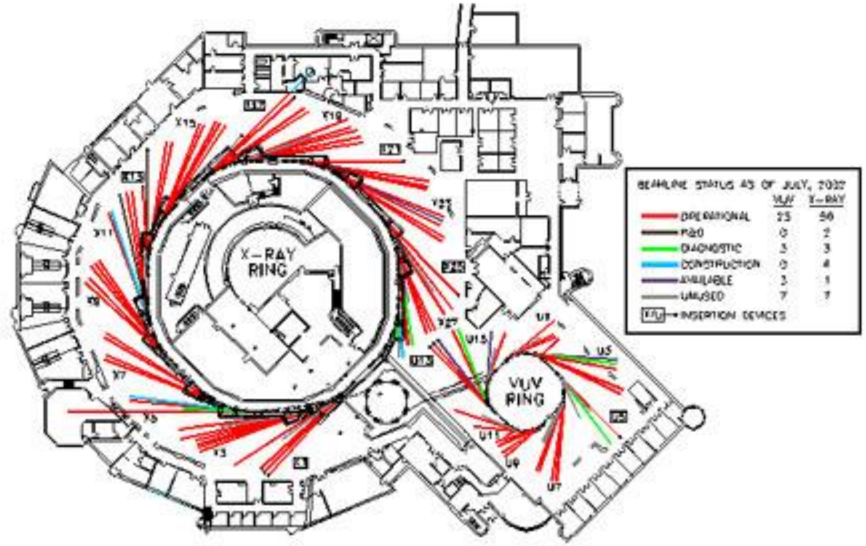

NSLS is a user facility

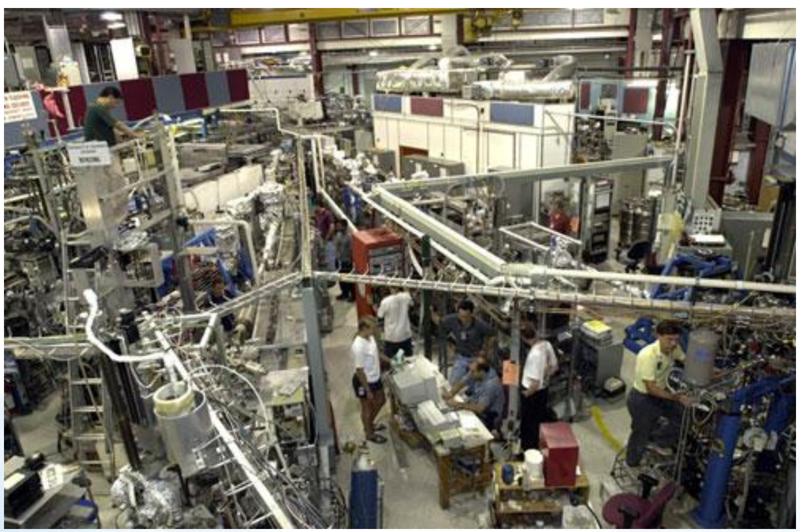

http://www.nsls.bnl.gov/users/usersguide/bt-gu.asp

Micro-scale X-ray mapping at BNL's NSLS

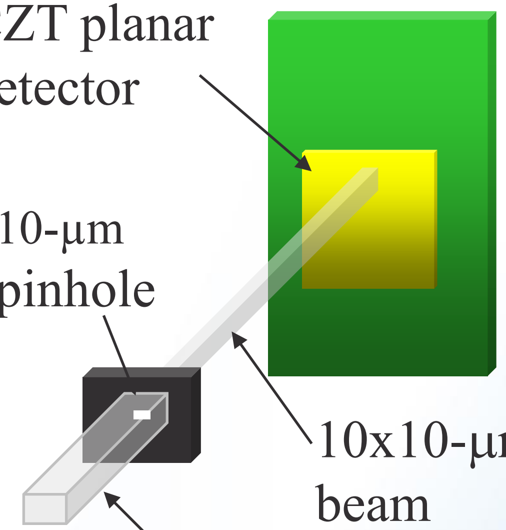

To investigate the role of precipitates and other non-uniformities in single-crystal CZT, we performed X-ray scans of CZT samples by using a highly-collimated X-ray beam.

Minimum beam size = 10 μm

Quasi-monochromatic beam 85 keV (bulk effects)
Monochromatic beam 30 keV
(surface effects & bulk).

For each location of X-ray beam, we collected a pulse-height spectrum and evaluated a peak position, which represents the device response from a small area illuminated by X-rays.

The results of scans were plotted as 2-D maps of device response versus beam position.

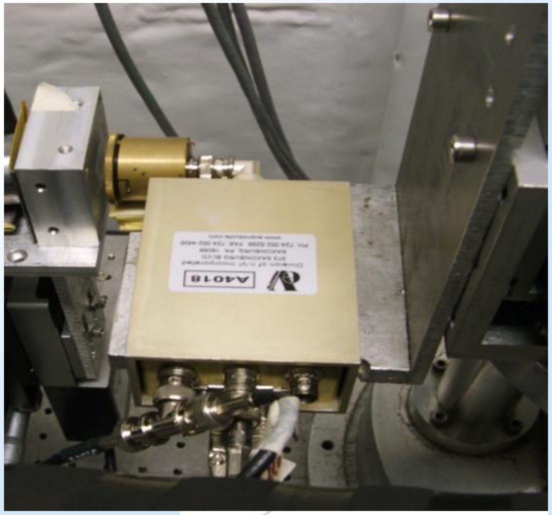

Brookhaven Science Associates

Correlations between x-ray response map & infrared transmission image

X-ray map shows the degraded regions precisely correspond to Te inclusions on the right

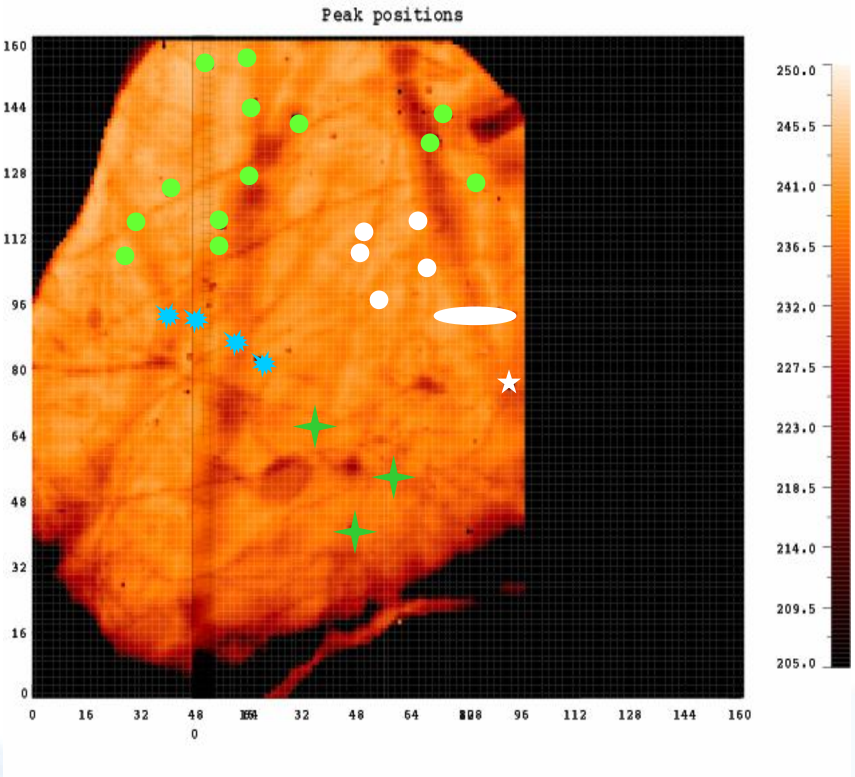

IR image shows Te inclusions, which could be identified by composition and shape

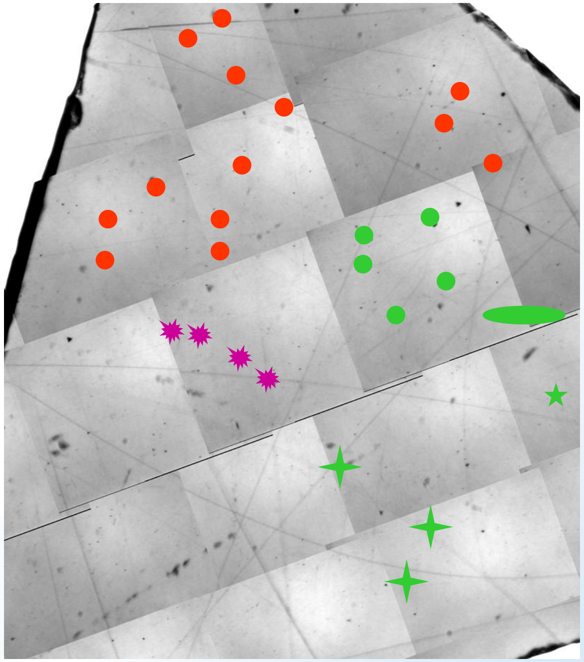

Very high correlation found for all CZT samples.

Spatial resolution and flux of Synchrotron Light Source required to understand the role of extended defects

In the past, small-scale non-uniformities caused by Te inclusions were overlooked because of the wide beams used

X-ray maps of a planar detector containing a grain boundary and Te inclusions measured with different beam sizes

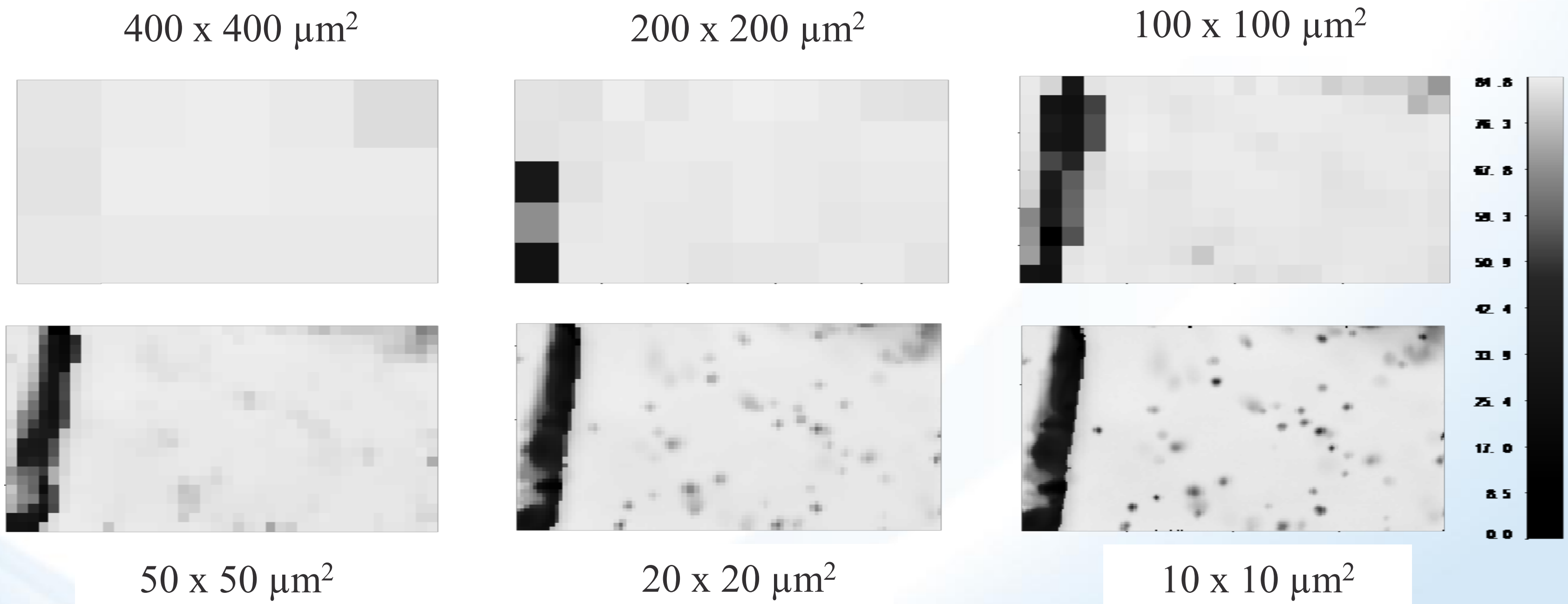

Modeling fluctuations caused by Te-inclusion

- Micro-scale resolution X-ray mapping clearly indicates that Te inclusions are opaque to electrons => charge losses are proportional to the geometrical areas of inclusions
- These effects can be easily simulated

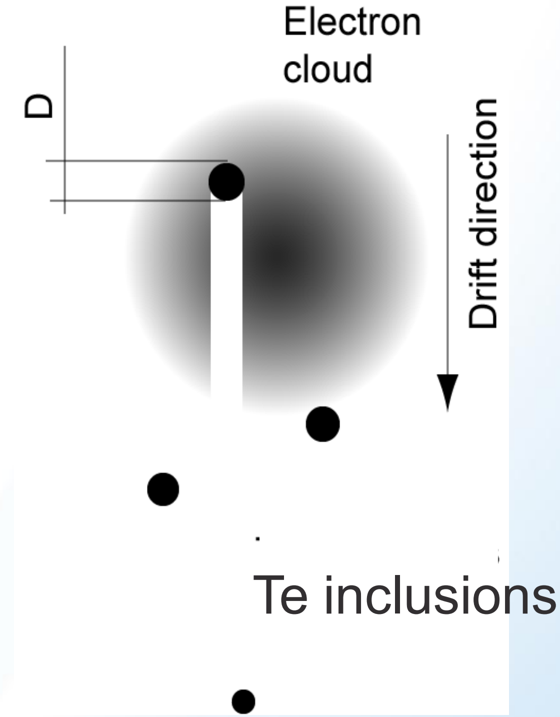

Inclusions < 3 μm can be neglected!

Inclusions >10 μm are the most harmful!

Confirmed experimentally!

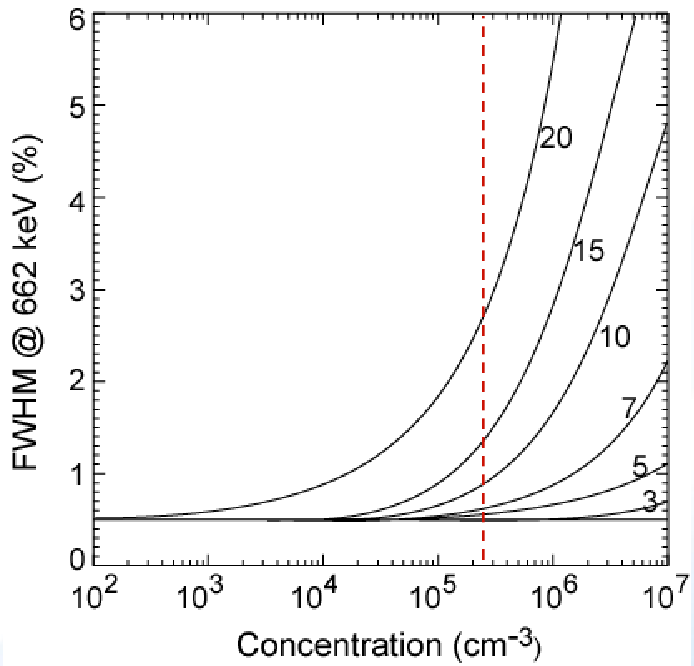

These results help vendors to improve CZT crystals!

Comparison between two detectors

Detector A
4x4x11 mm^3
Energy resolution 0.8% at 662 keV

Detector B
6x6x12 mm^3
Energy resolution 3.8% at 662 keV

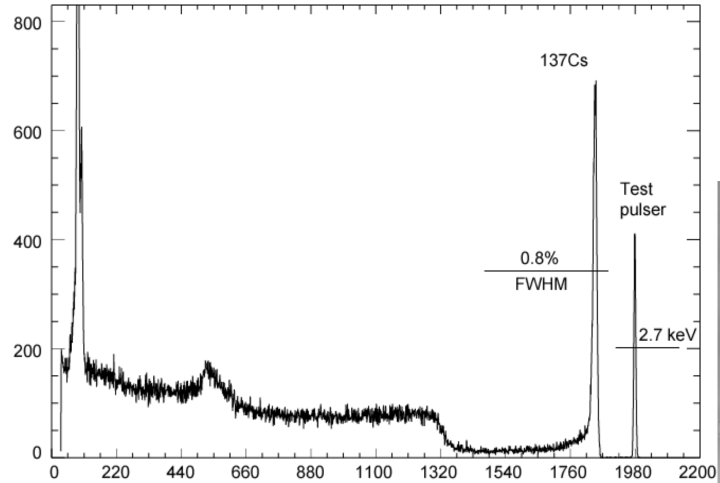

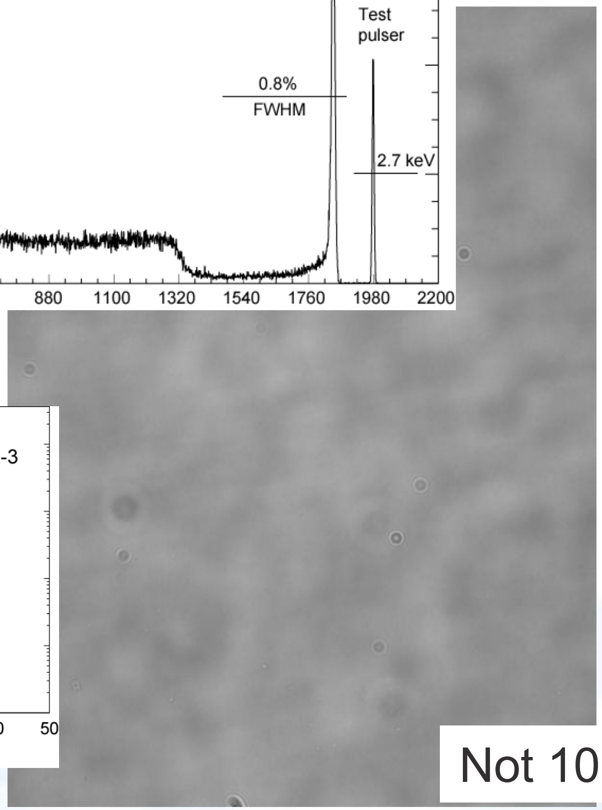

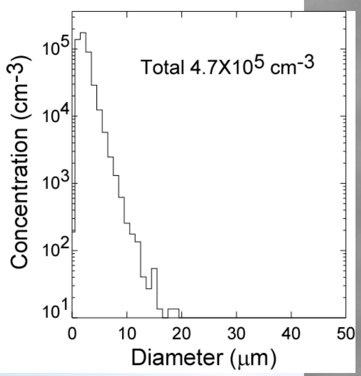

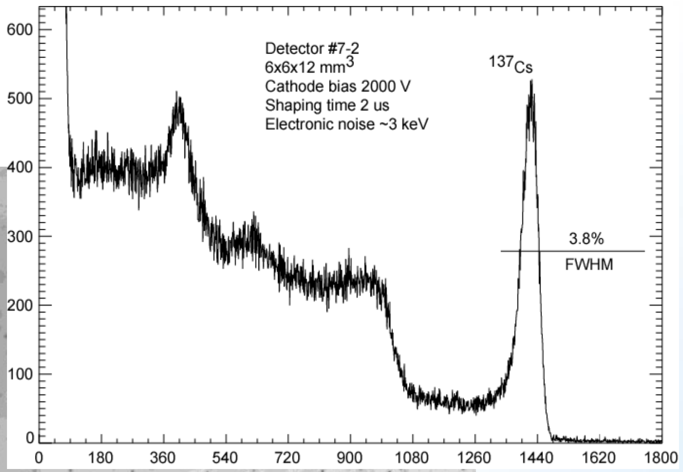

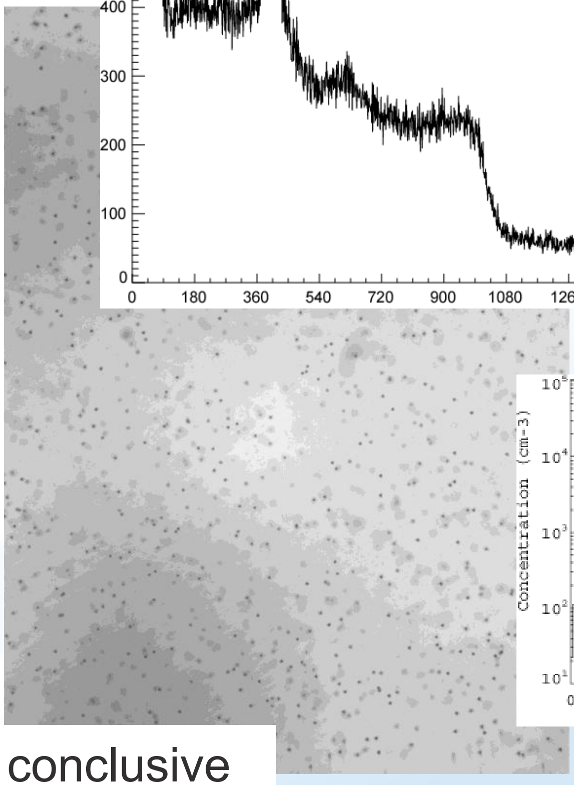

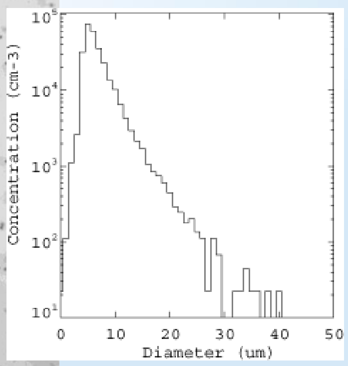

Not 100% conclusive

Electron trapping by Te inclusions in the case of thin detectors

X-ray scan of 10x10x1.2 mm^3
Cathode 200 V, 20 μm step

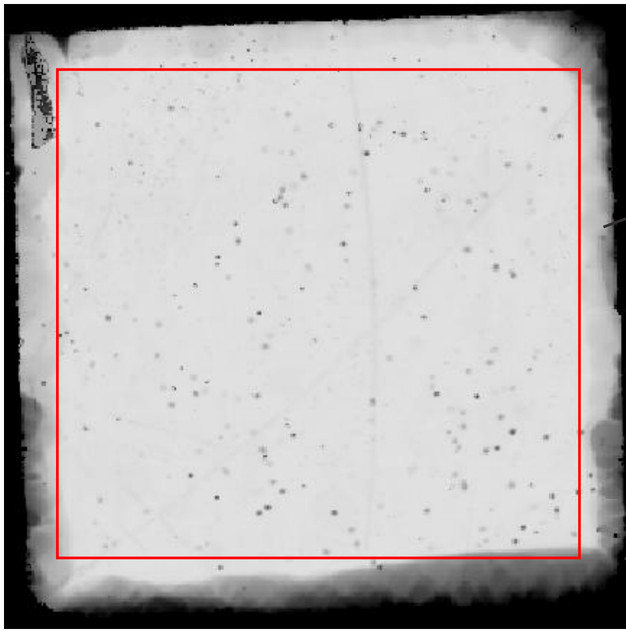

This X-ray map represents the intrinsic response of the detector without electronic noise contribution.

3-D representation of the response map

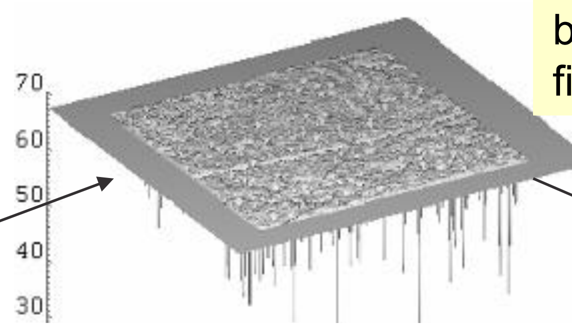

How important these peaks for the device spectral responce?

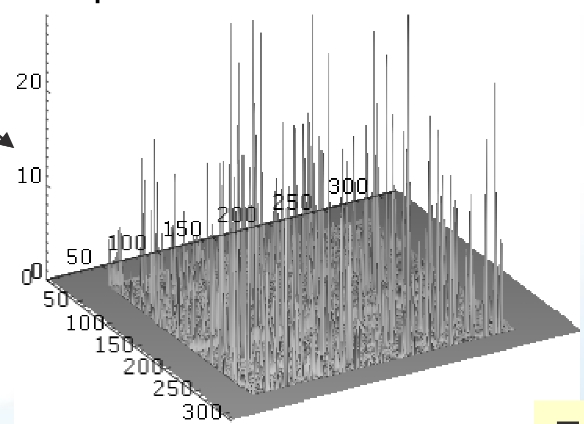

Histogram of the response map. Effect is negligible in thin detectors. 0.5% can be attributed to the peak fitting errors.

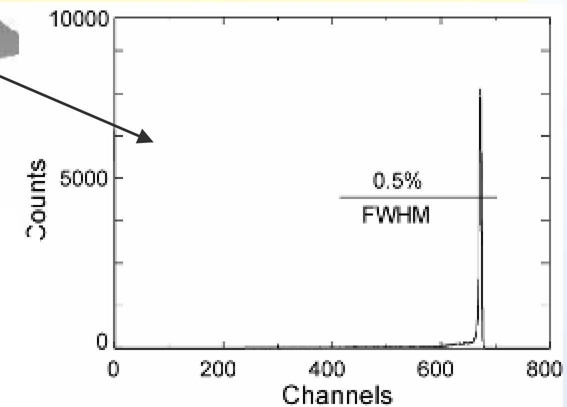

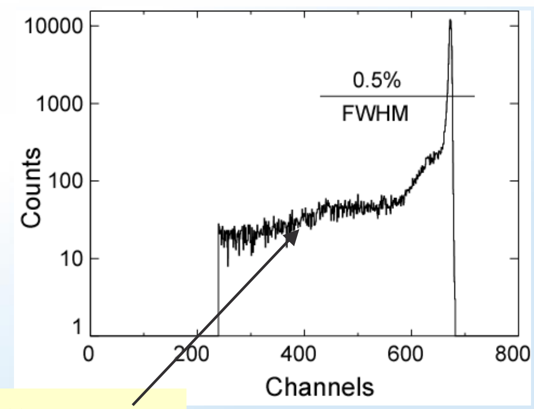

Efficiency loss

Response map in the case of a 10-mm thick detector

28 keV
1000 V,
50 μm step

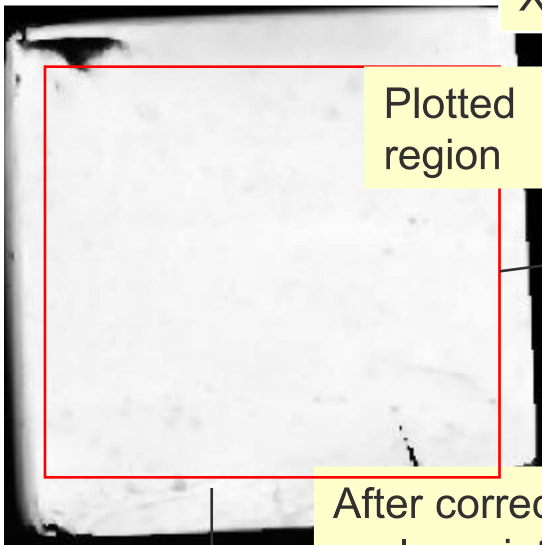

Plotted region

X-ray scan of 10x10x10 mm^3

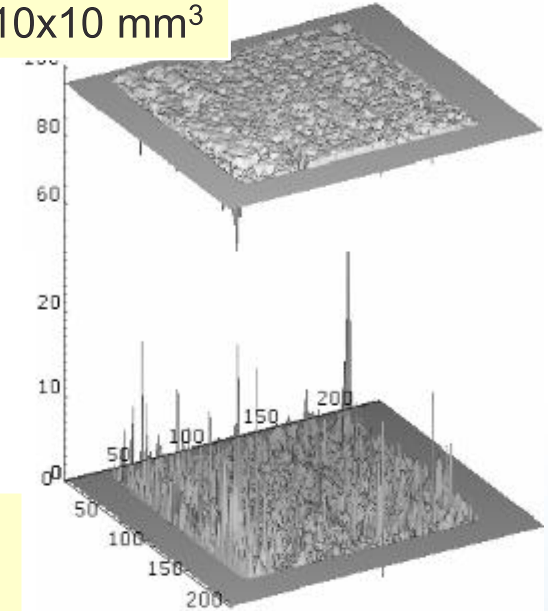

Histogram of the response map

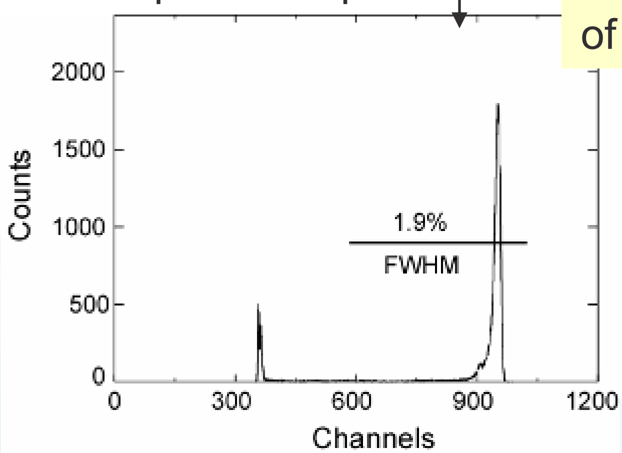

After correction for large–scale variations, which is equivalent to the response from a pixel detector made of this crystal, 1x1 mm^2.

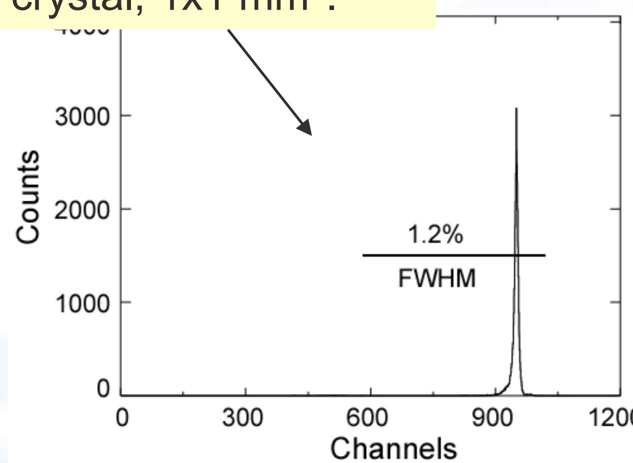

Fluctuations is ~1.2%, compared to 0.5%.

The fluctuations are primary attributed to Te inclusions.

Detector response degrades with device thickness.

1x1x1 cm^3 detector with high concentration of inclusion

X-ray scan of 10x10x10 mm^3
28 keV, 1000 V, 50 μm step

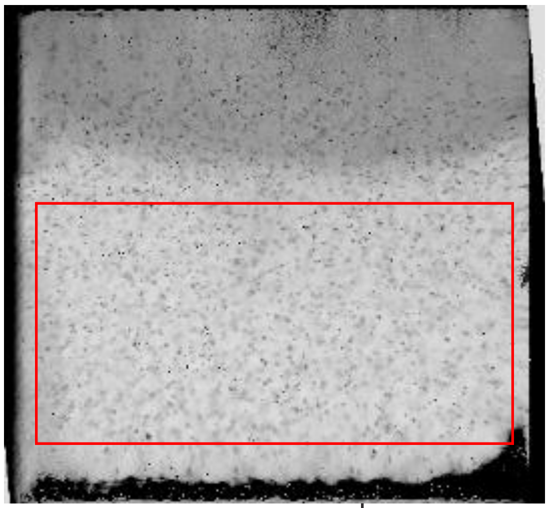

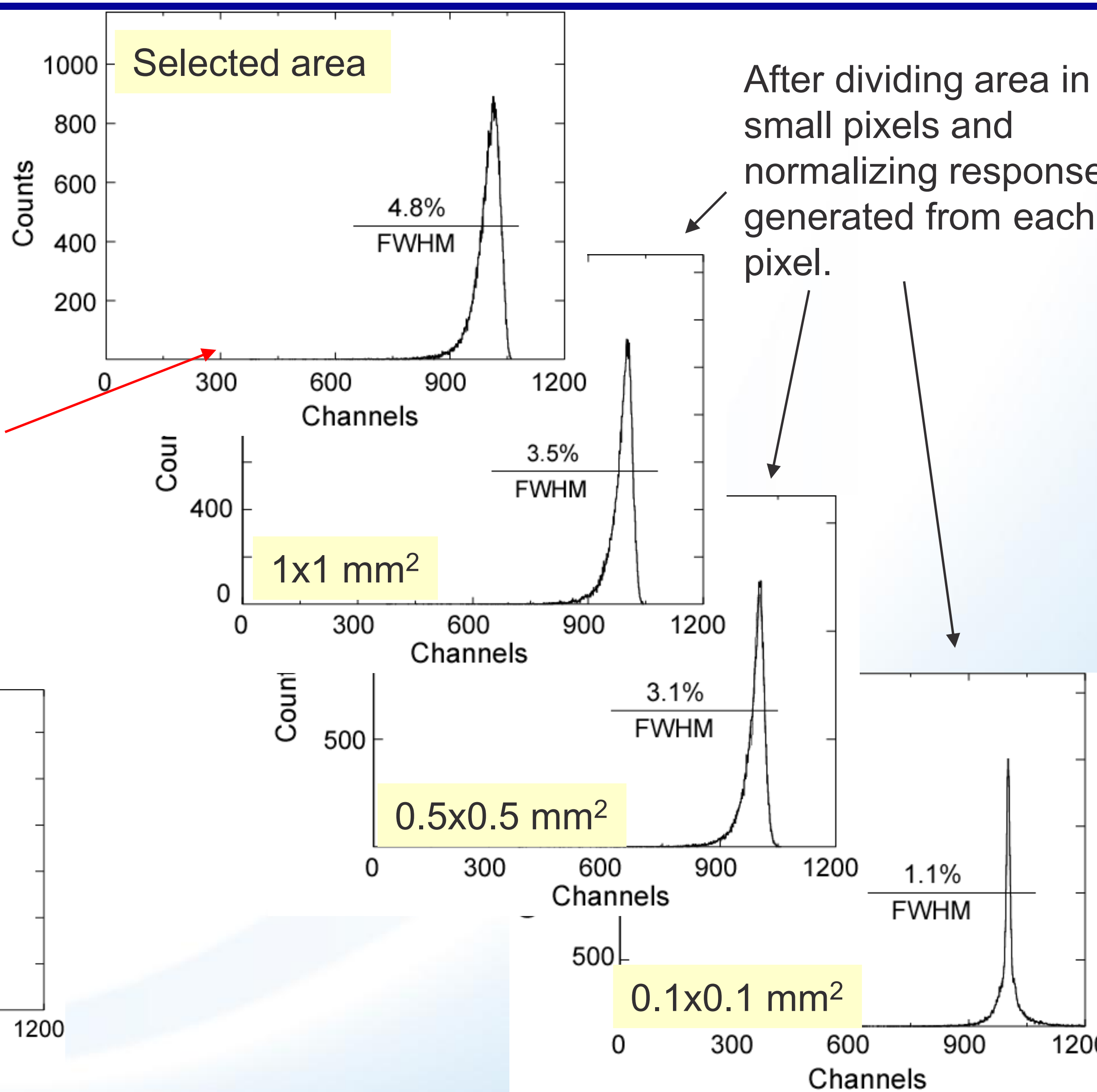

After dividing area in small pixels and normalizing responses generated from each pixel.

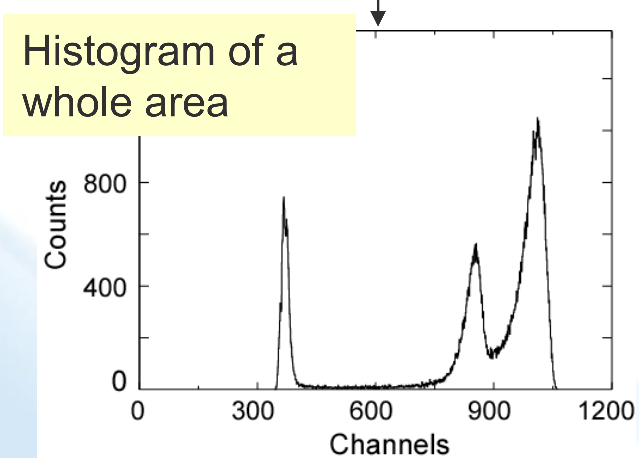

Prismatic punching dislocation patterns

Photograph of the etched surface of a 5x5x12 mm^3

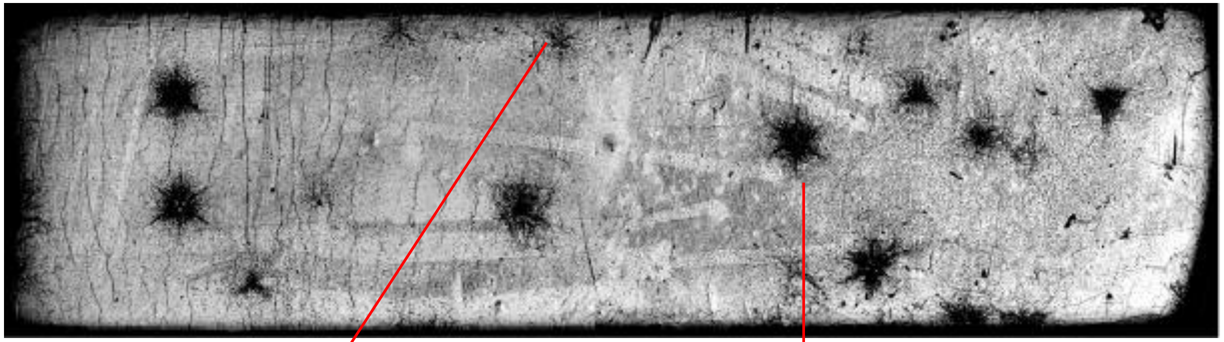

5x magnification

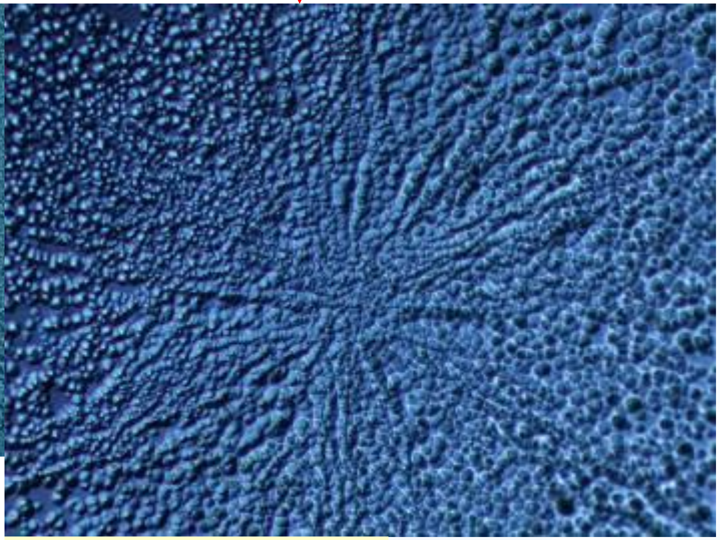

50x magnification

The origin of such defects is unclear. Two mechanisms are discussed in the literature: 1) caused by high pressure built inside inclusions (R. D. S.Yadava et al., J. Electron. Mater 21, p. 1001, 1992); 2) moving dislocations interact with inclusions or precipitates (P.B. Hirsh, J. Inst. Metals 86, p. 7, 1957).

Not remnants of inclusions or precipitates are seen inside the "stars".

Prismatic punching defects

2x2 mm^2

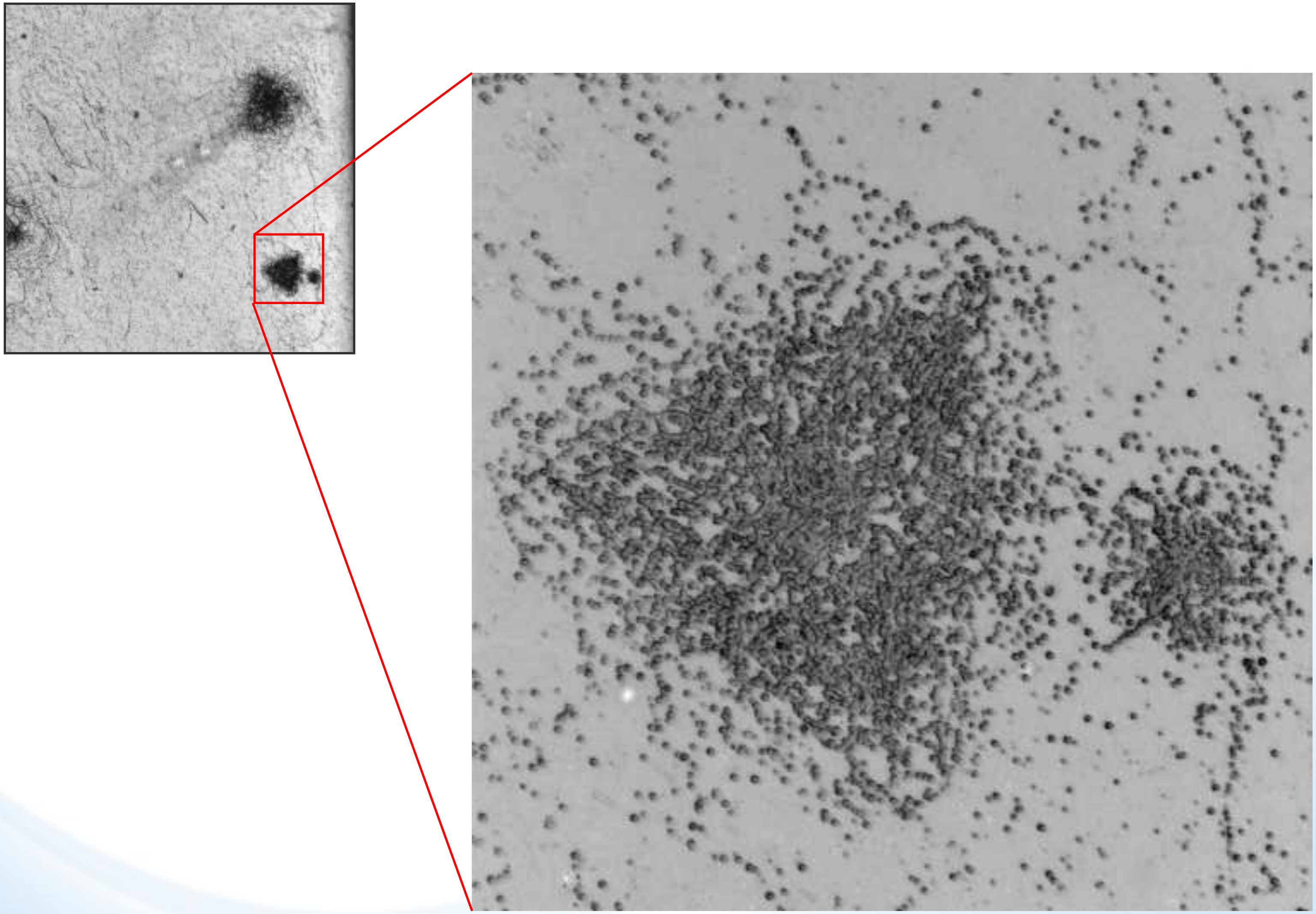

Photograph of the etched surface

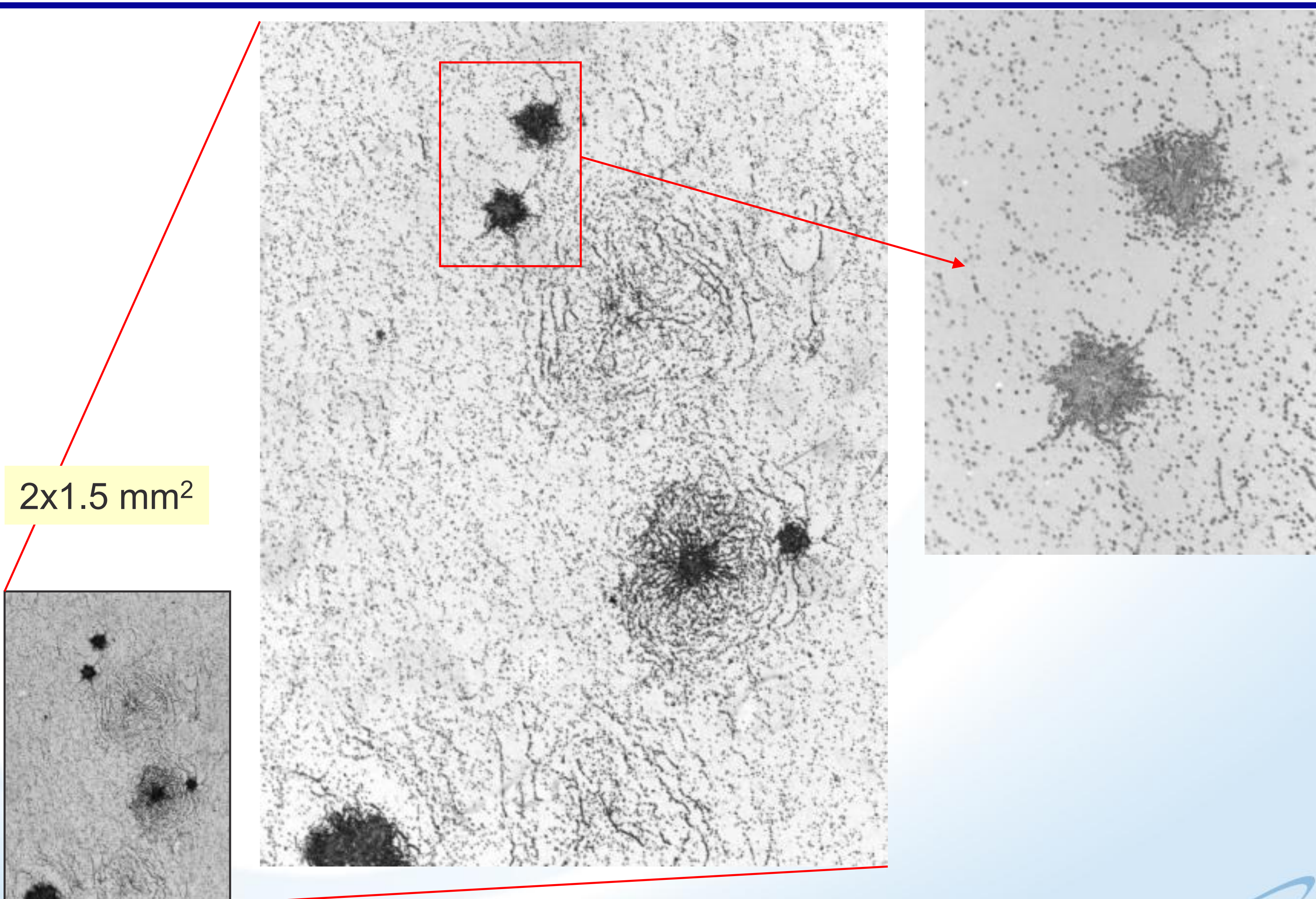

White beam X-ray diffraction topography

Beam-size: 200 μm x 22 mm

White beam up to 200 keV

Scan in z and 2θ

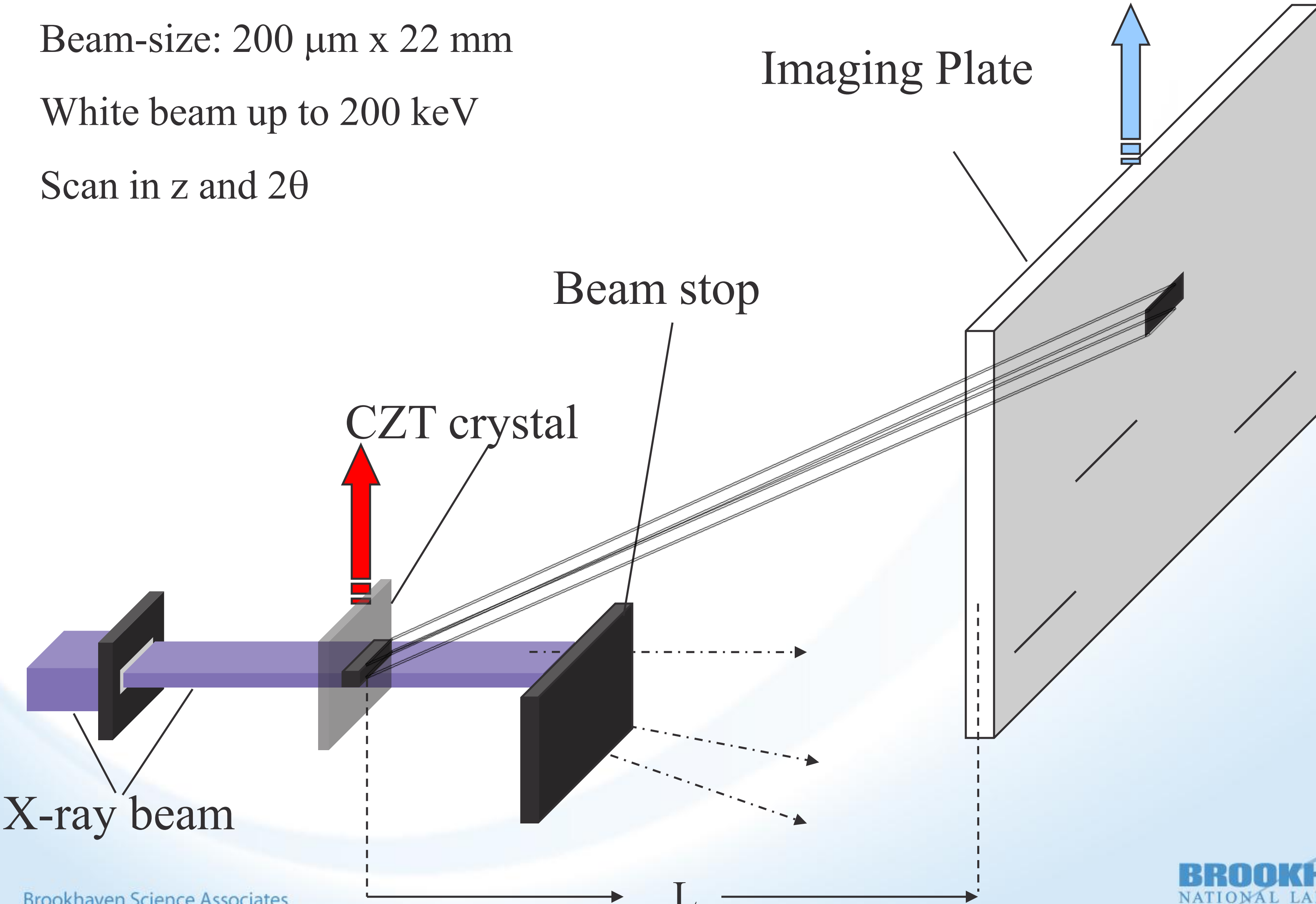

Two types of contrast: geometrical and dynamic

Example of geometrical contrasts

- Image can be explained based on geometrical optics
- Twins, grains and subgrains

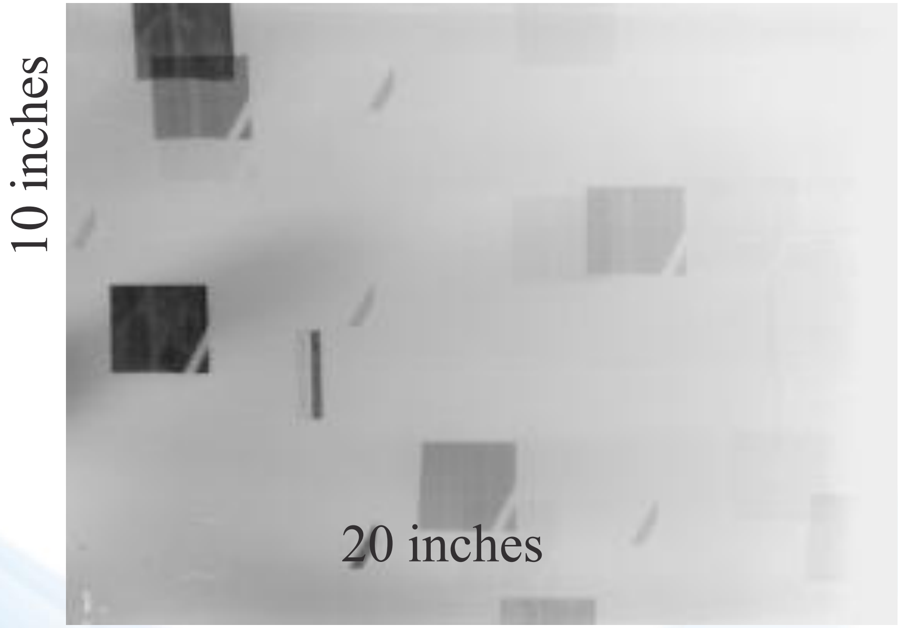

Example of dynamic contrast

- Features can be explained based on the dynamic diffraction theory which takes into account interaction of the beam with a crystal
- Difficult to reconstruct images
- Crystal strains and dislocations patterns

Examples of diffraction topography images

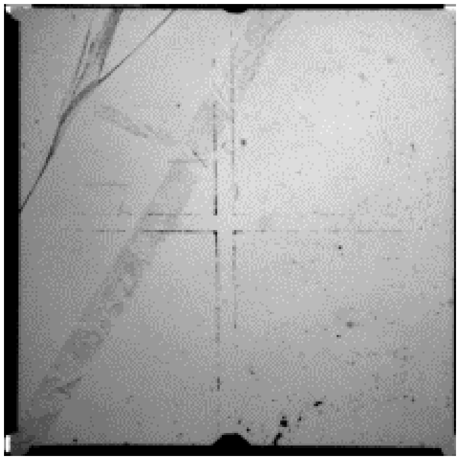

IR Transmission Map

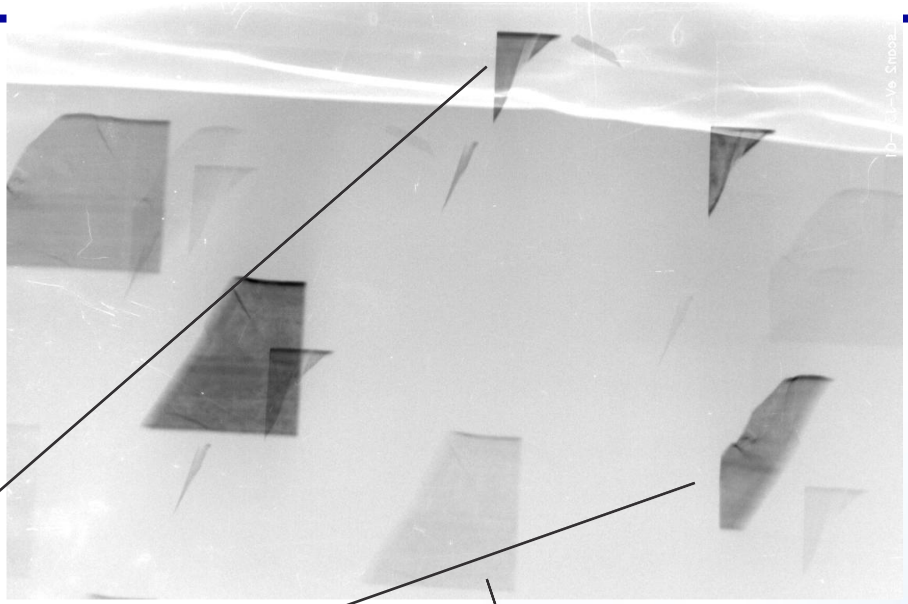

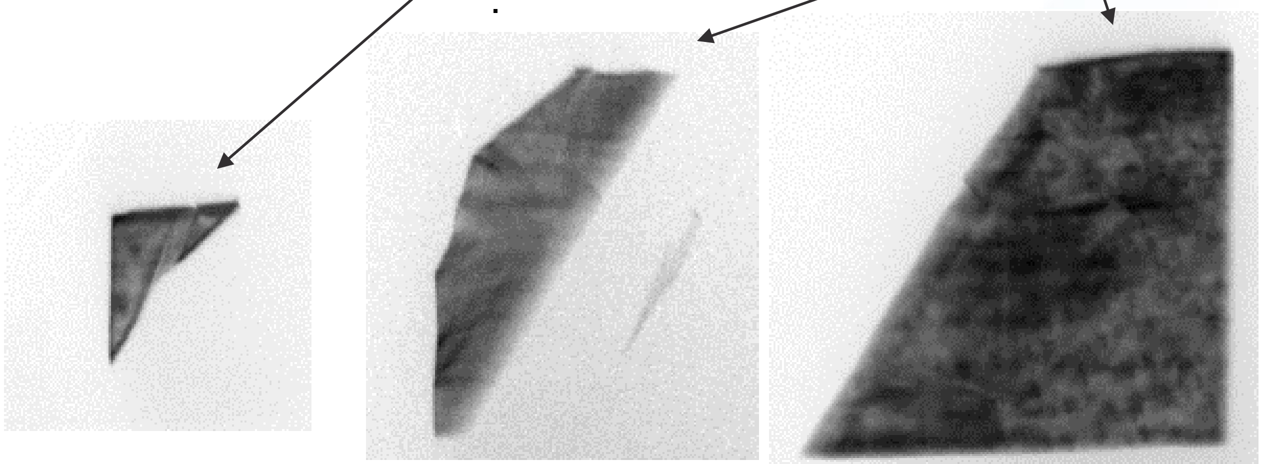

White beam diffraction topography

Subgrain boundaries exist in all commercial CZT regardless of growth techniques or vendors

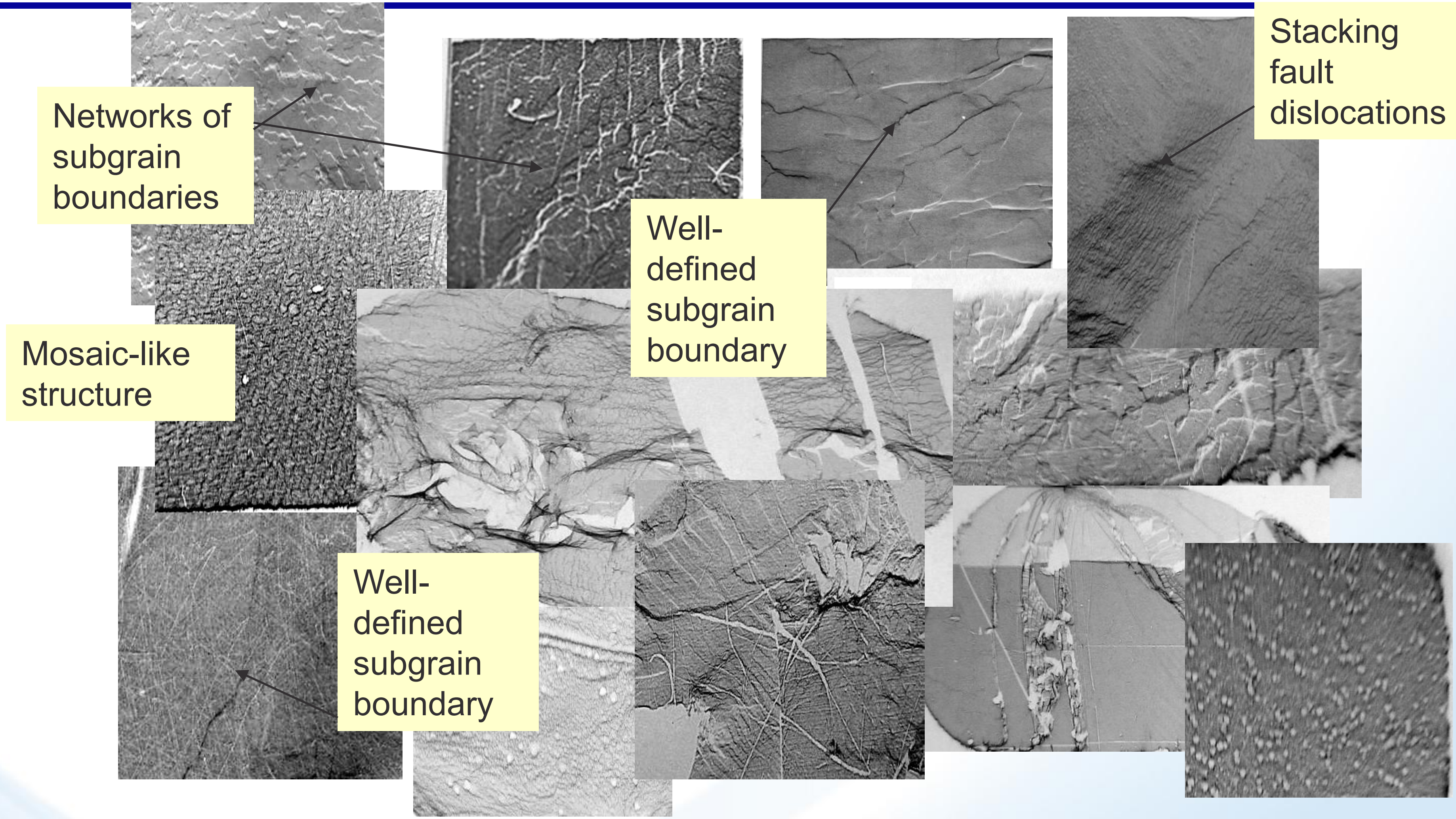

There are large varieties of subgrain boundaries in commercial CZT material
It is important to find the extent to which they can be neglected

Correlations of subgrain boundaries and X-ray response maps for a 2-mm thin detector

Impurities and secondary phases accumulated within subgrain boundaries are primary cases for carries trapping (known from other semiconductors)

Diffraction topograph
~10x15 mm^2 area, 2-mm thick

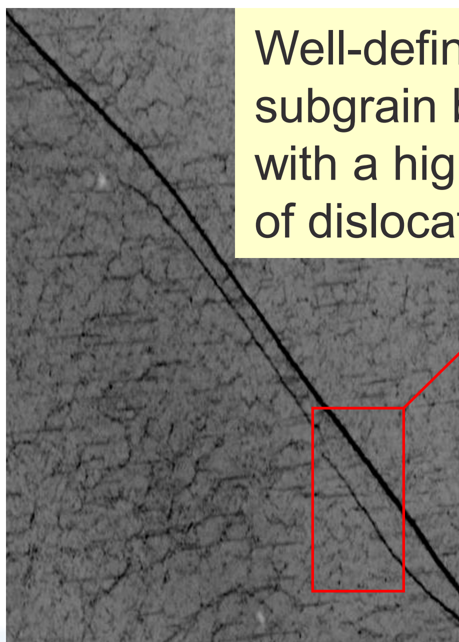

Well-defined subgrain boundary with a high density of dislocations

High-resolution X-ray response map, 10 μm

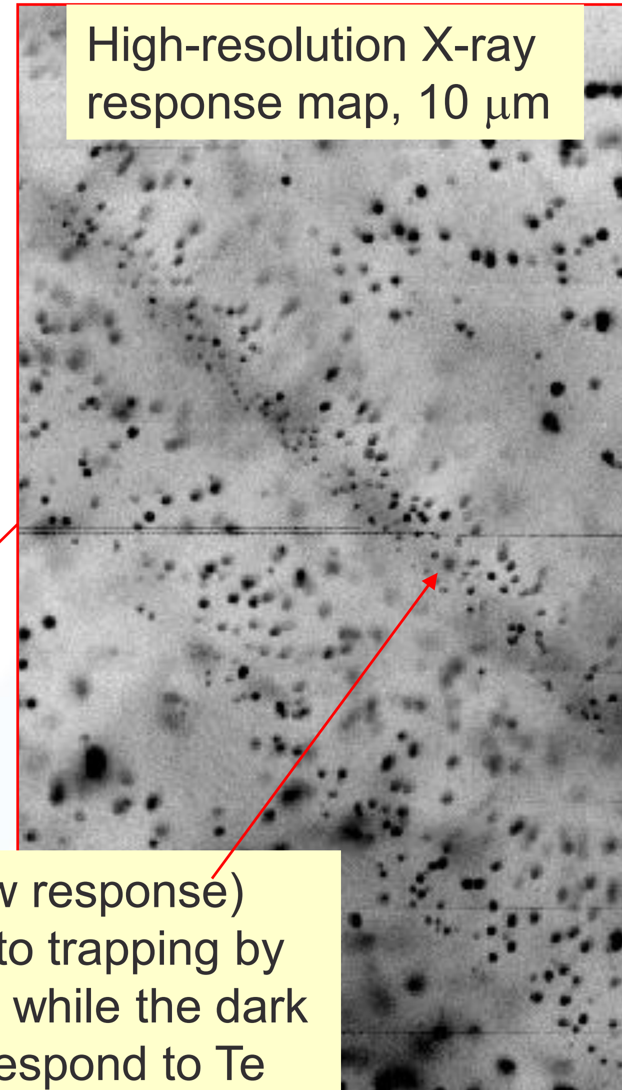

A dark (low response) band due to trapping by impurities, while the dark spots correspond to Te inclusions

X-ray response mapping of the network of subgrain boundaries in a 2-mm thick sample

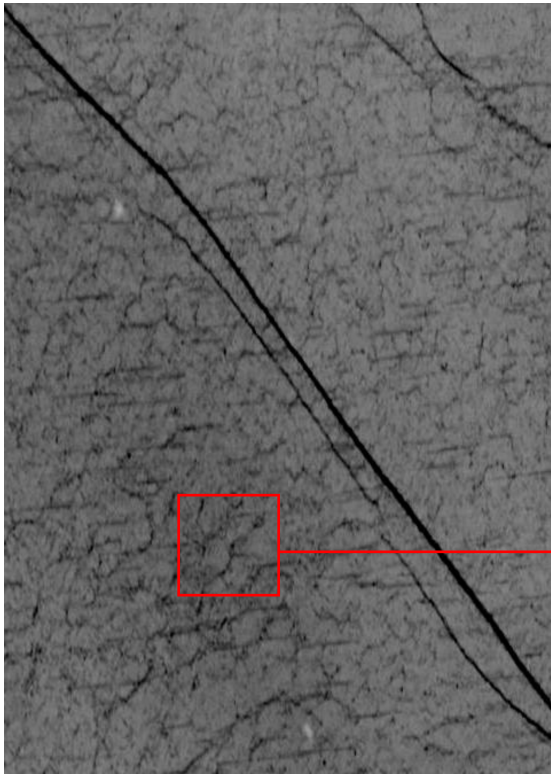

2x2 mm^2 area,
5-μm step size

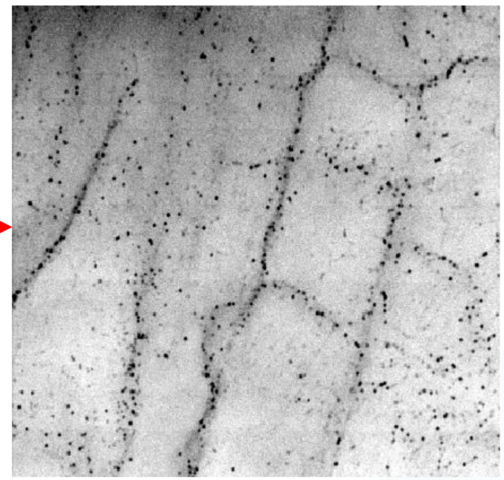

Isometric plot illustrating a small scale of charge losses

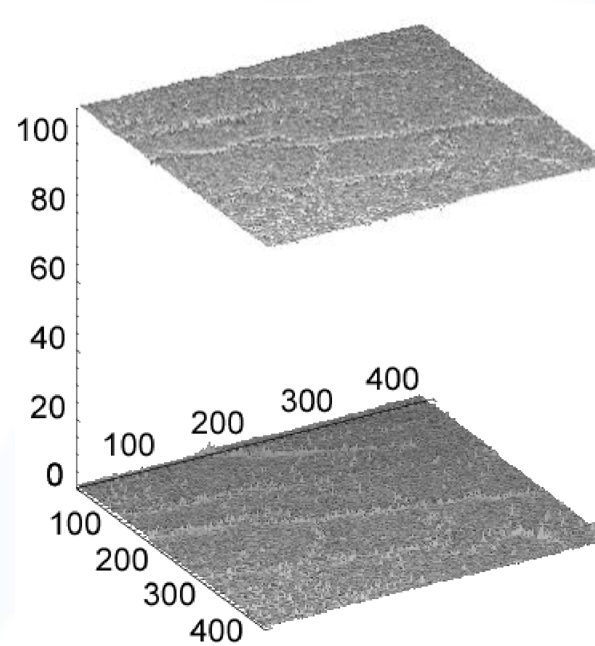

Charge losses are small (~1%) → less important in thin detectors

But they could cause significant fluctuations of the collected charge that would affect energy resolution in thick detectors?

Effects of the subgrain boundaries with high dislocation density (previously reposted)

Contact pattern "chessboard"

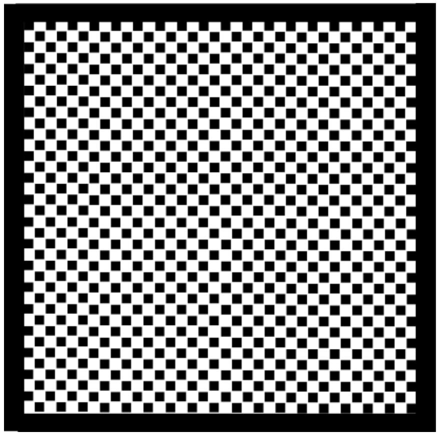

X-ray response map of a 2-mm thick pixel detector illustrating variations of pixel sizes

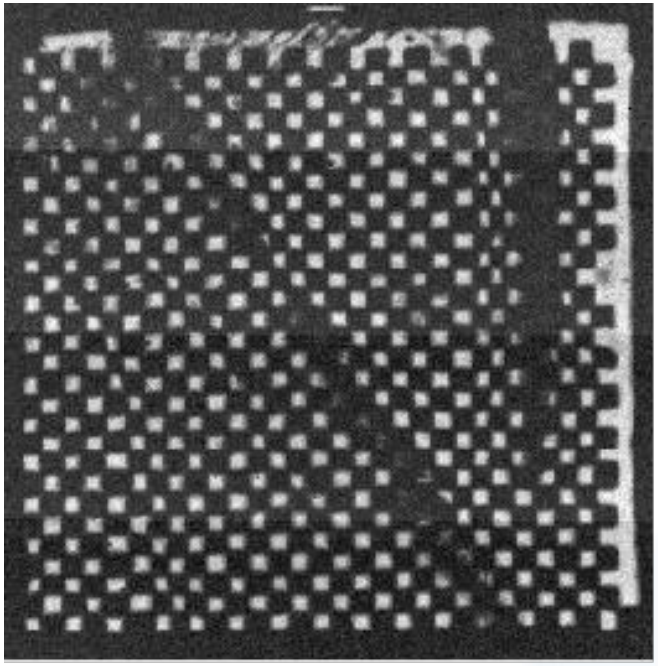

X-ray diffraction topography image of the subgrain boundaries with high dislocation density

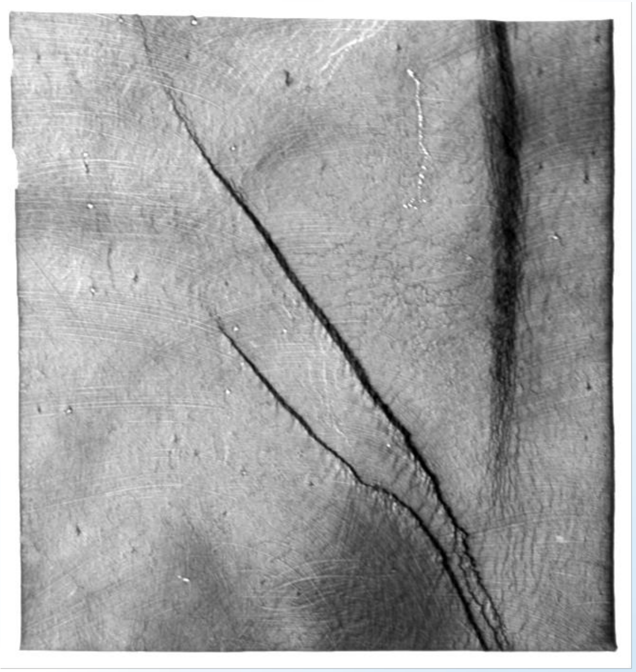

Such subgrain boundaries with high dislocation density are very detrimental and cannot be tolerated in CZT detectors

X-ray maps of CPG

Illuminating from the grid-electrode side

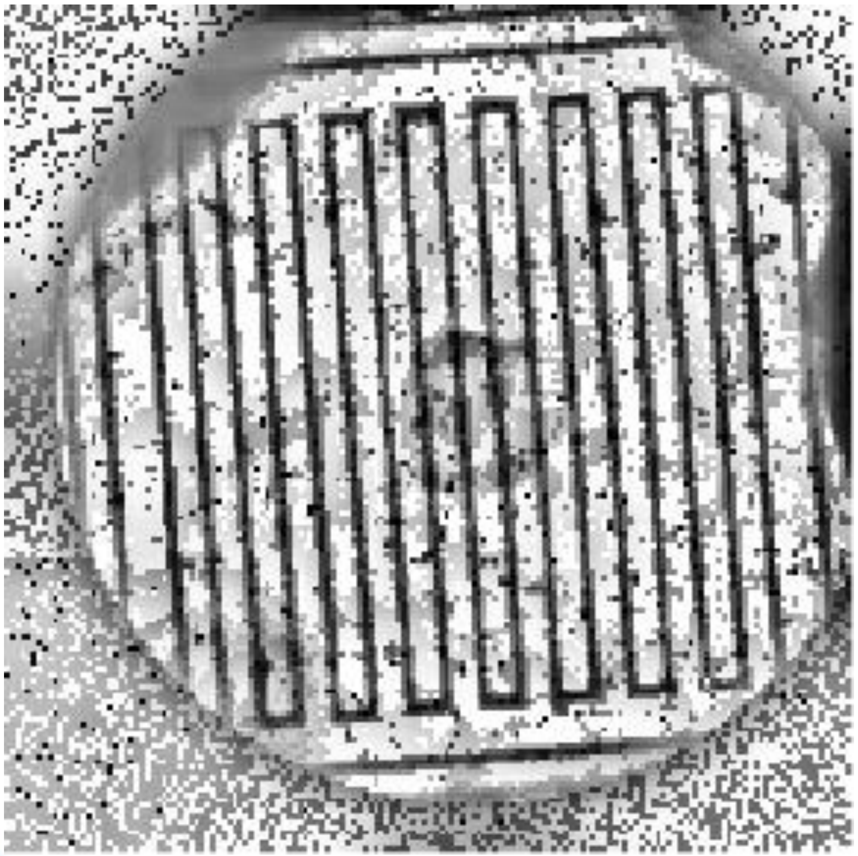

Raster scan area: 15.5mm x15.5mm
Step size: 100 μm; 600 V; 18keV

Illuminating from the planar-electrode side

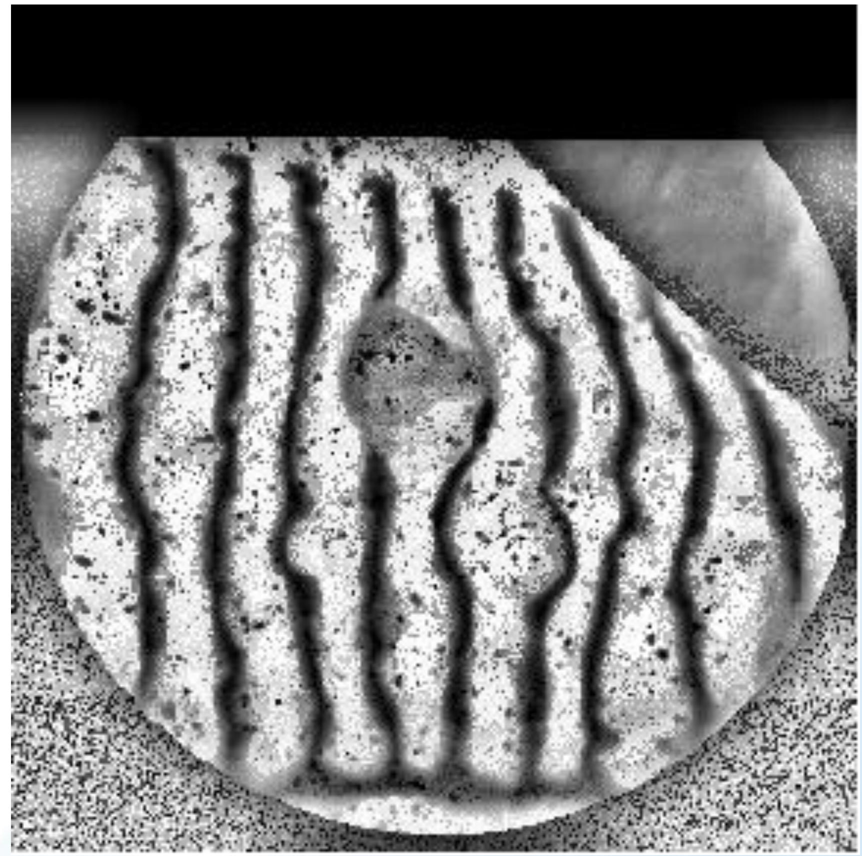

Raster scan area: 15.5mm x 15.5mm
Step size: 50 μm; 600 V; 18keV

Conclusions 2

- Defects is the main problem:
  - Point defects (impurities) -> electron lifetime, can be electronically corrected
  - Extended defects (secondary phases, subgrain boundaries, dislocations) -> non-uniformities in spatial distribution of trapping centers, cannot be corrected
- Solutions:
  - Purification of starting materials (Cd, Te, Zn)
  - Improving crystal growth techniques
  - Electronic corrections and rejecting incomplete charge collection events

Rejection of the incomplete charge collection events (ICC)

- Charge signals readout from the cathode and anode in generalized spectroscopic detector (e.g., Frisch-grid ionization chamber)

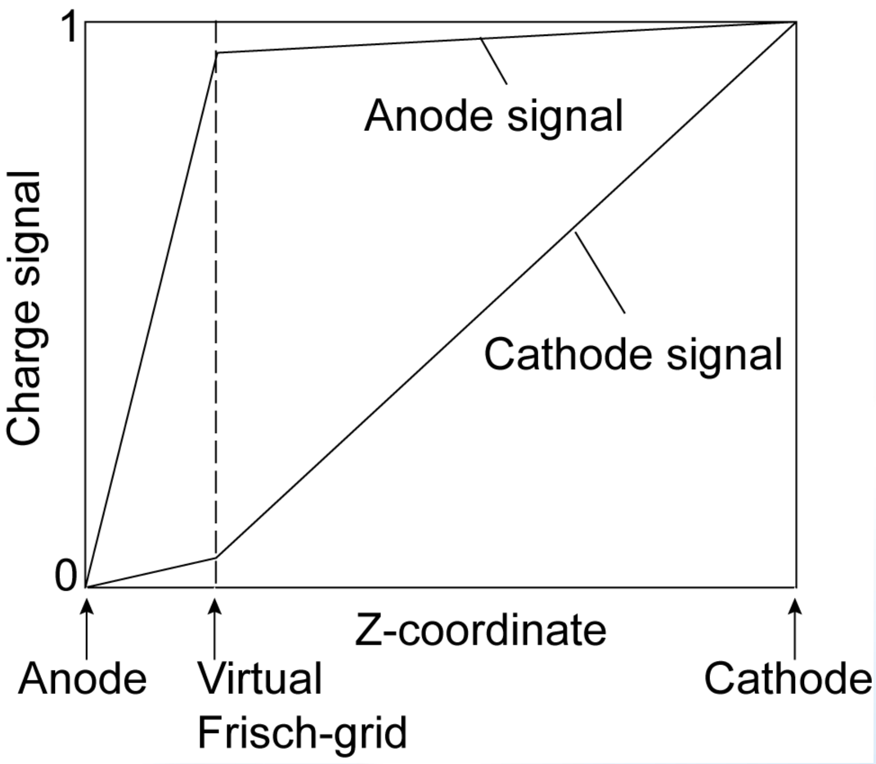

Example of the virtual Frisch-grid detector

15-mm long virtual Frisch-grid detector

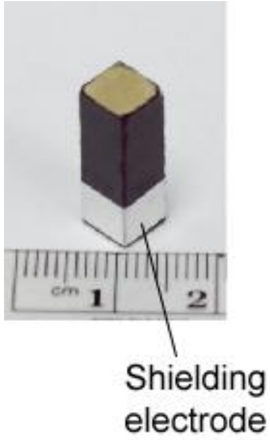

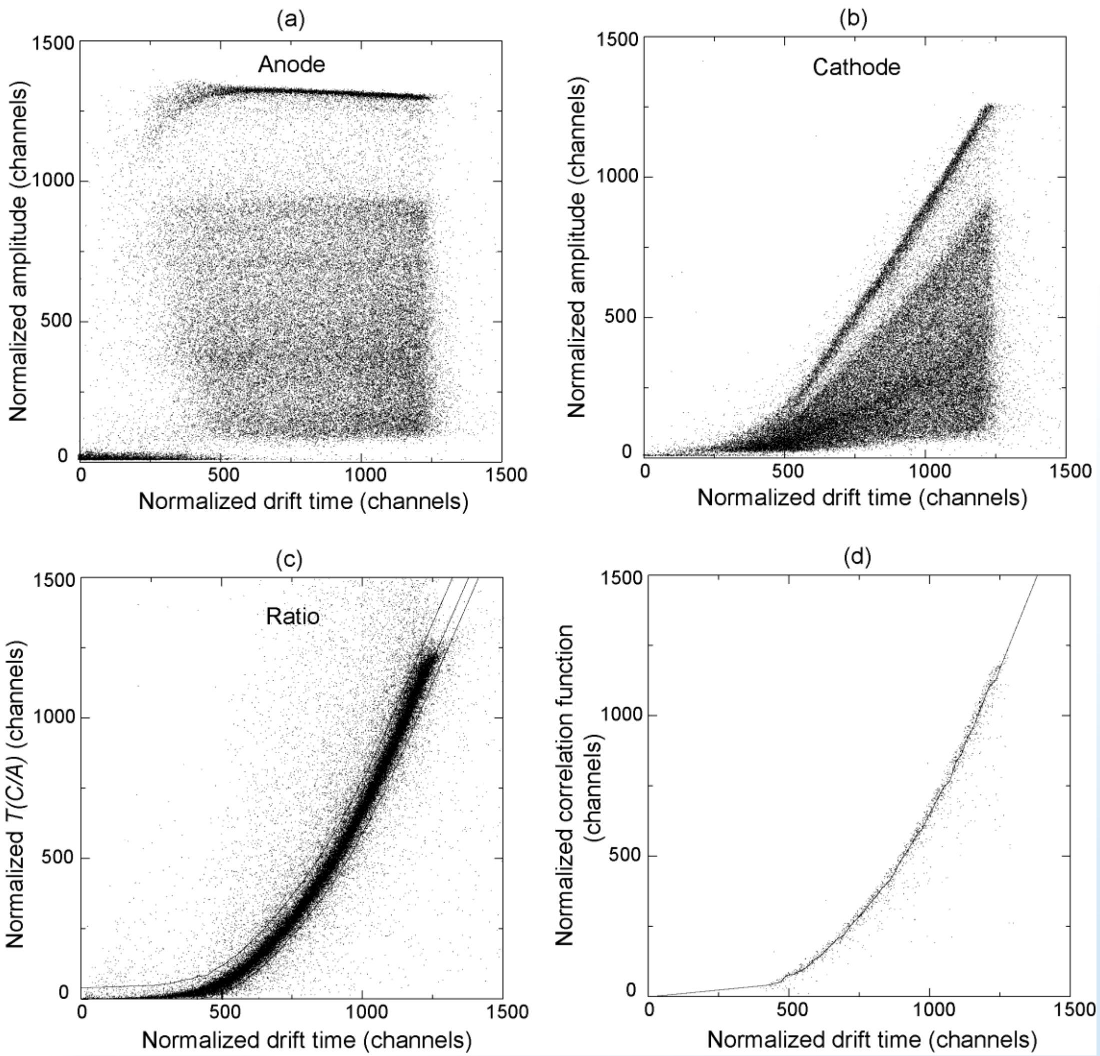

Rejection of ICC

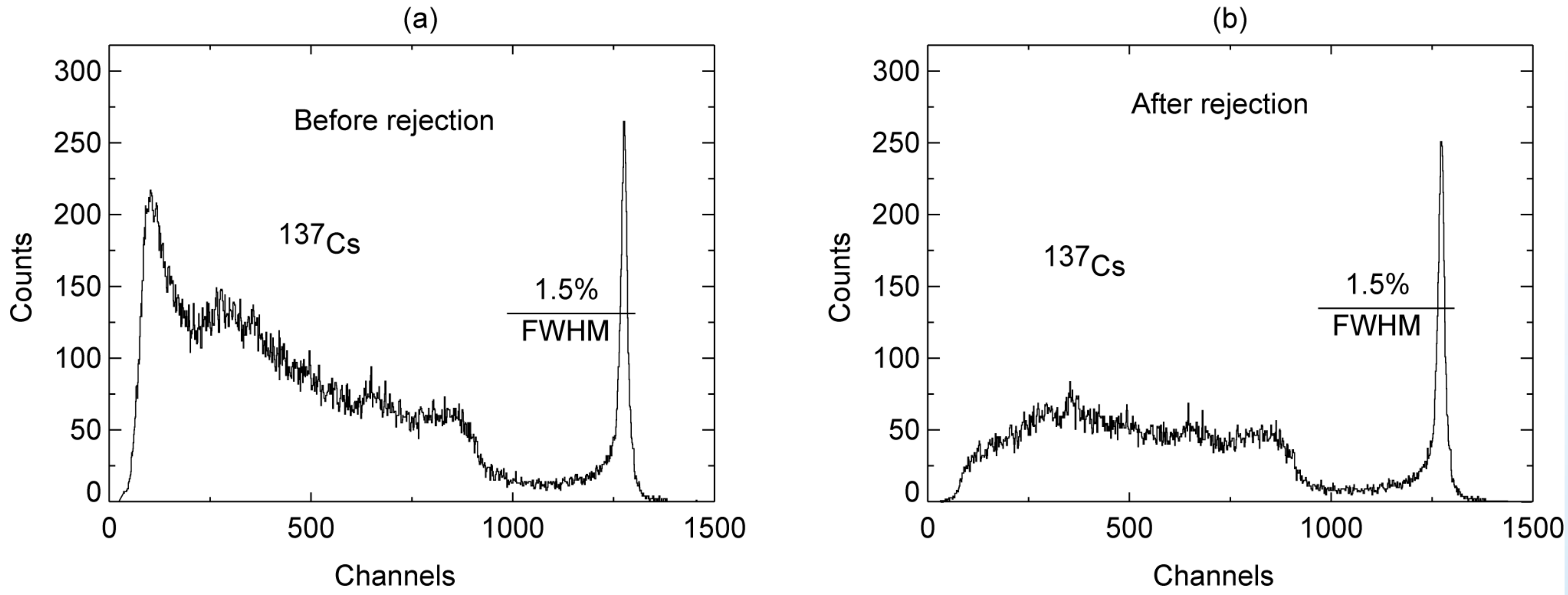

Rejection of ICC events

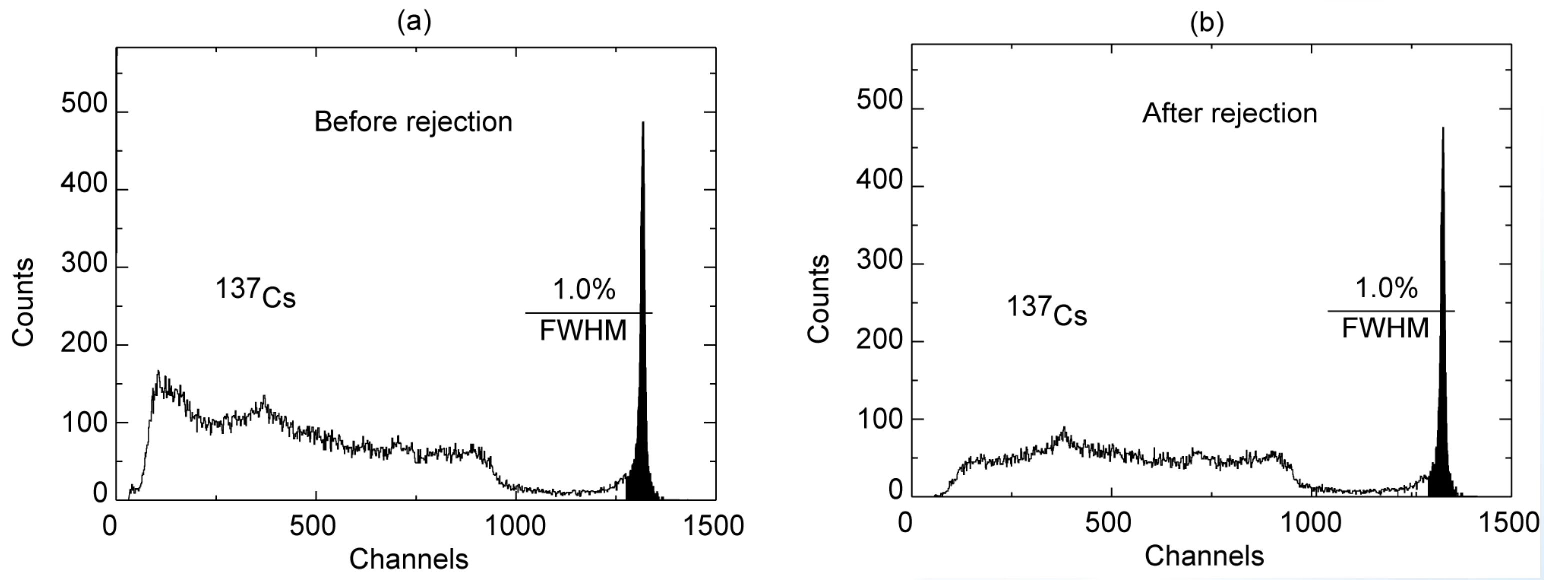

^{133}Ba source

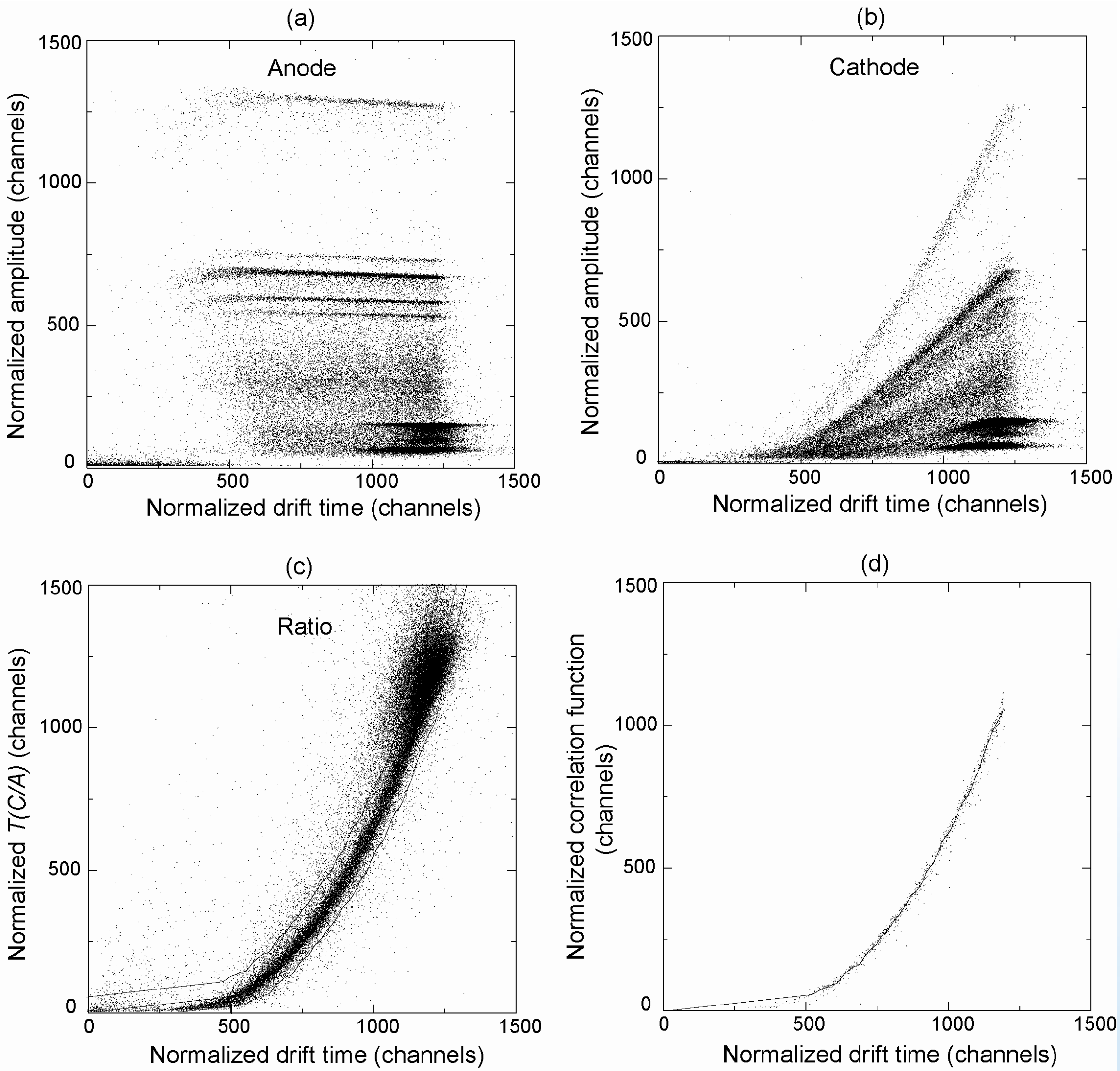

Corrections and rejections of ICC events

Raw data spectrum

After rejecting the events interacting close to the anode

After charge-loss correction

After rejecting the ICC events

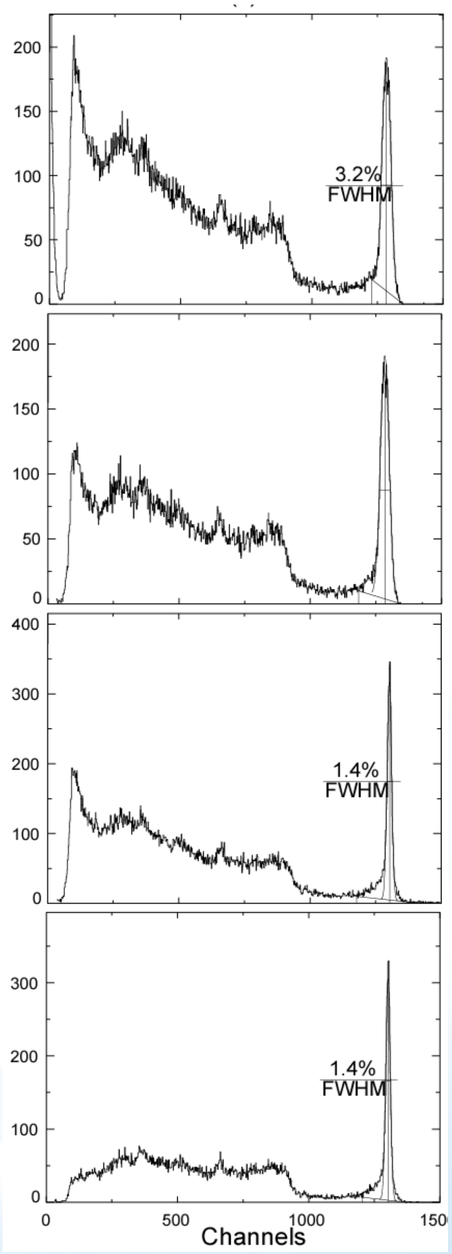

A 6x6x15 mm^3 virtual Frisch-grid detector readout with two hybrid preamplifiers

Applications

Arrays of virtual Frisch-grid detectors

- Selected 4 representative detectors (out 30 tested detectors)
- Mounted detectors on the substrate with connectors matching a plug-in board for the 3D readout system
- Collected the data stream from ^{137}Cs at 2000 V bias (amplitudes and drift times for each event)
- Use cooling (dry ice) to stabilize the temperature just below 17 C (without cooling the temperature quickly rises > 40 C)

Test box containing readout electronics and CZT array plugged into detector board

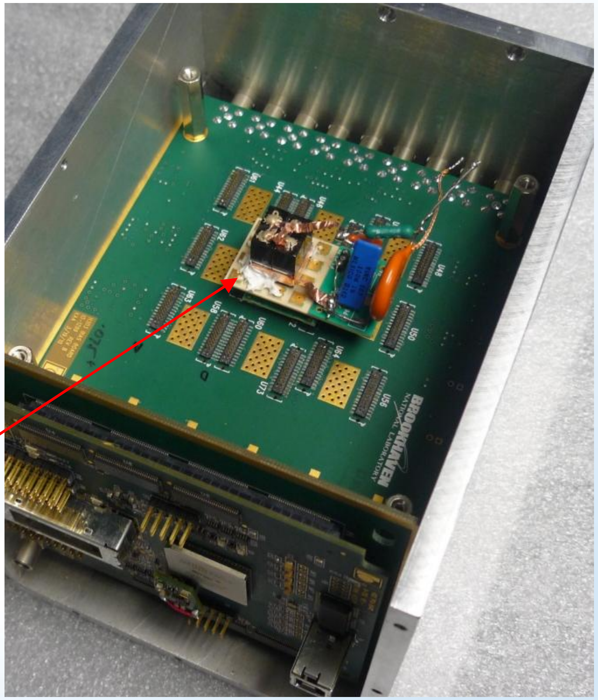

2x2 array of 6x6x15 mm^3 virtual Frisch-grid detectors with the common cathode

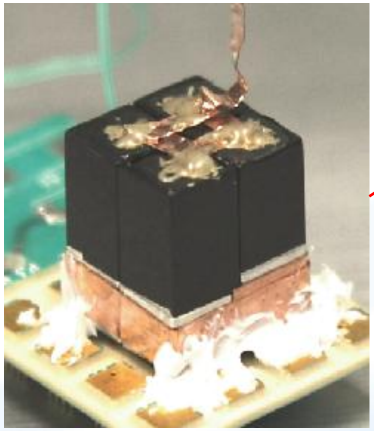

Testing the array: raw data

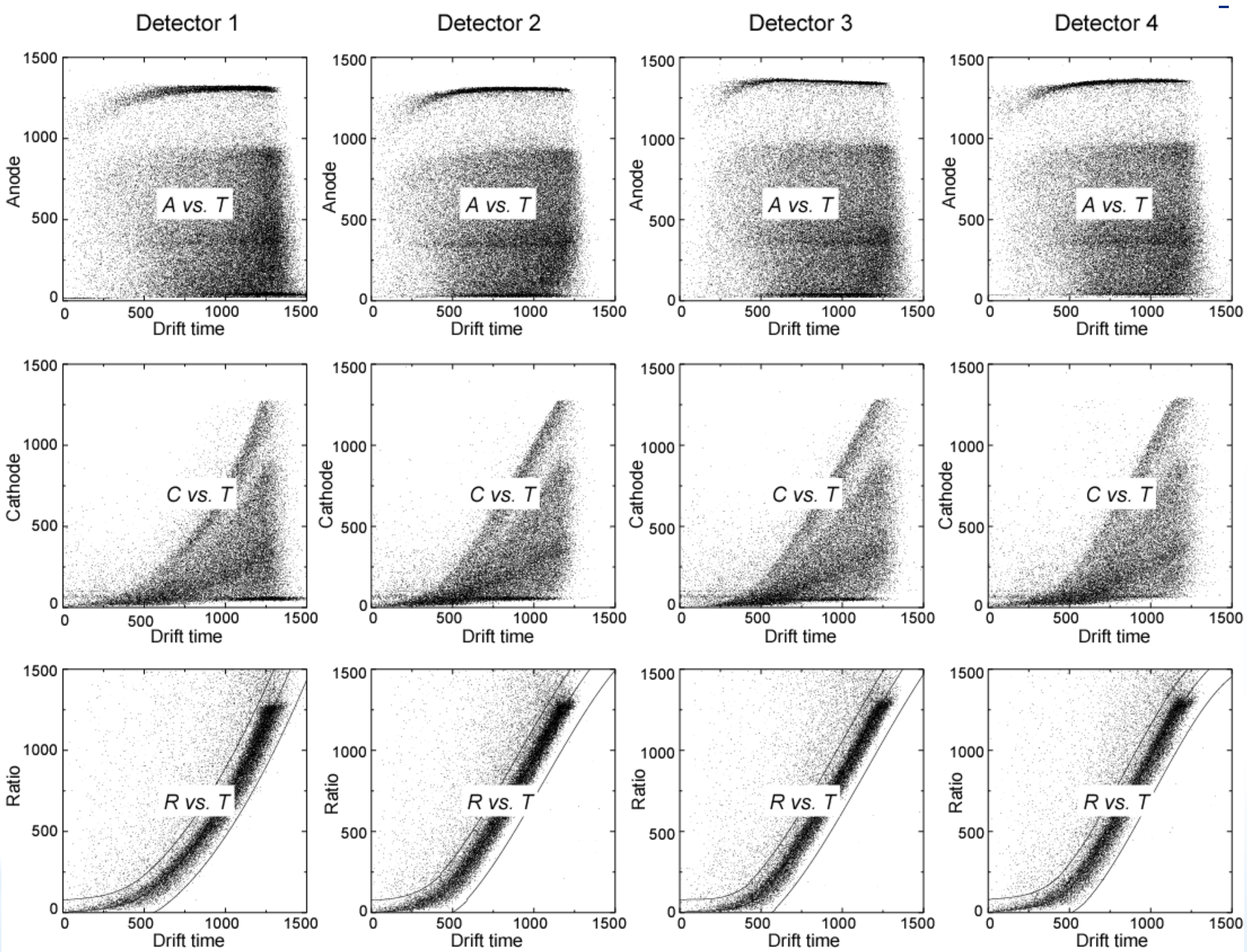

Use the raw data to plot the following distributions

Amplitude vs. Drift time were used to correct for charge trapping and reject events taking place in the collection region

Cathode-to-Anode ratio vs. Drift time was used to reject the ICC events

Detector 1 shows poor performance!

R vs. T is too broad due to systematic error in drift time detection→ ASIC needs to be optimized for the array!

Pulse-height spectra measured from 4 detectors

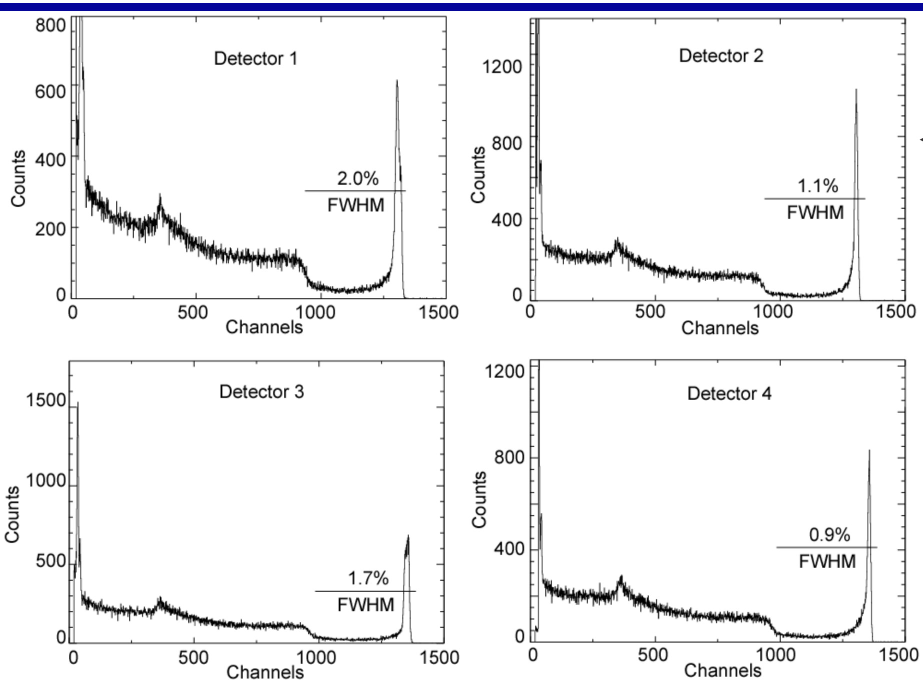

Raw spectra

Spectra after the charge-loss correction and rejecting the events interacting inside the collection region near the anode

Good energy resolution
Large peak-to-Compton ratio

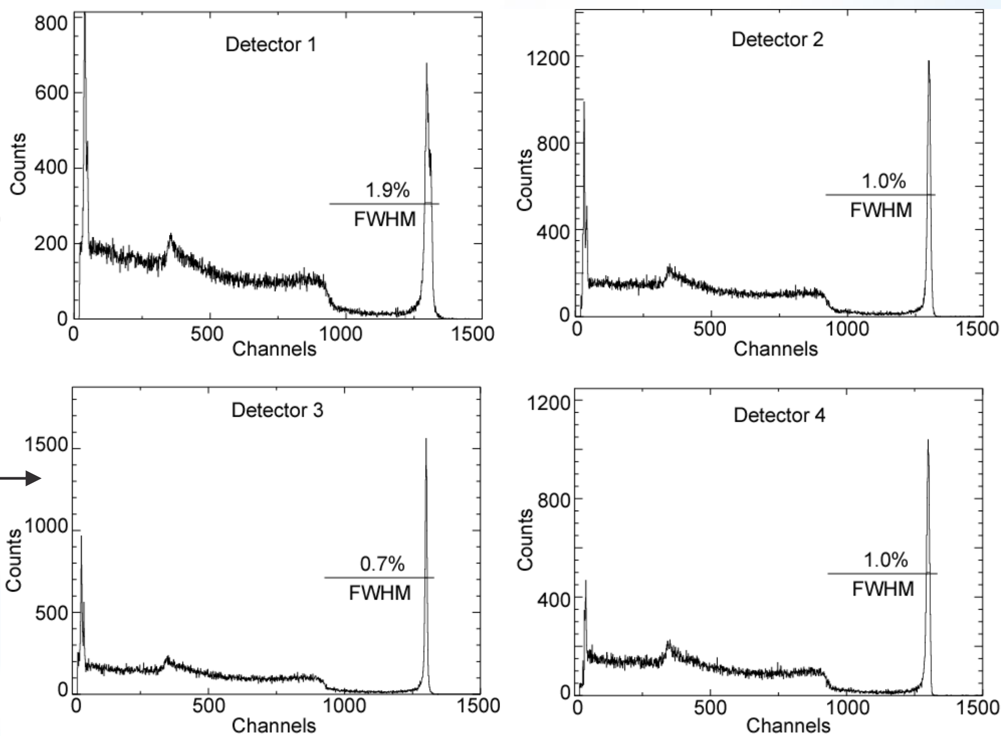

BNL develops camera for prostate cancer detection

- ❖ High spatial resolution images (10x better than current gamma cameras)
- ❖ High specificity for cancerous tumors (based on pharmaceutical tracers)
- ❖ Compact design (capable of trans-rectal measurements)
- ❖ Low cost (less than 1/3 of conventional imaging devices)

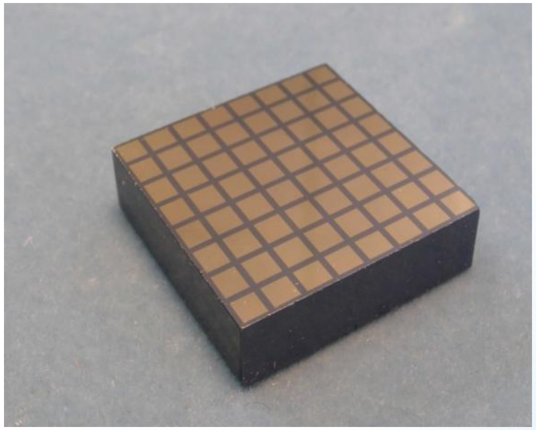

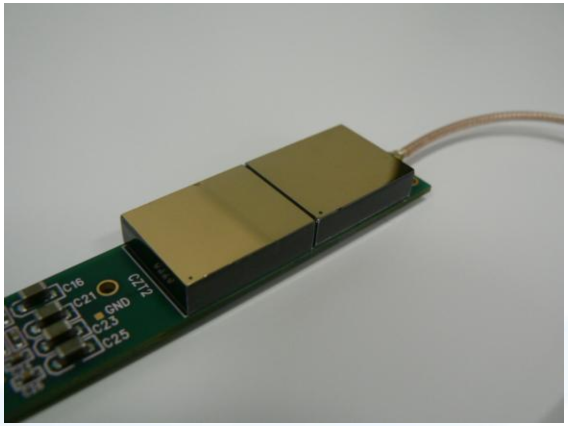

ProxiScan™

Medical

Redlen NM module for Spectrum Dynamic

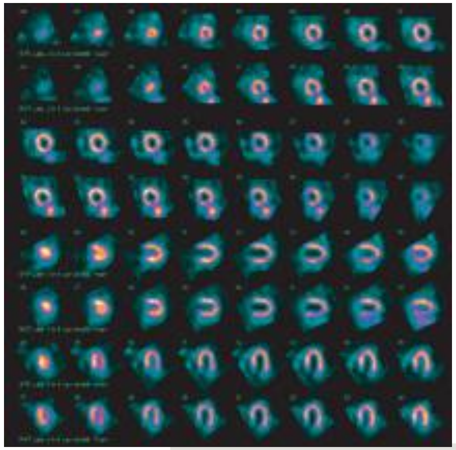

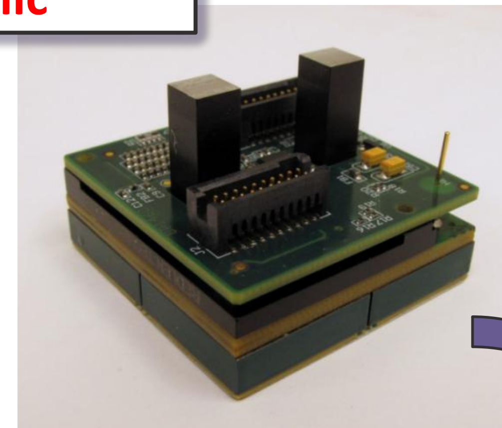

Molecular Imaging… Redefined

SPECTRUM DYNAMICS

Though nuclear cardiology has grown significantly in the past 25 years, supporting detector technology has not improved.

Sodium iodide and vacuum tubes continue to be the dominant technology in the nuclear equipment marketplace. The lack of industry investment in new technologies has placed severe constraints on clinical workflow and the development of new applications. With exciting new molecular imaging radiopharmaceuticals on the horizon and tremendous gains being made routinely in computing horsepower and applications, the limiting factor necessary to unlock the true potential of molecular imaging will be data collection.

Spectrum Dynamics redefines SPECT Imaging with the innovative D-SPECT™ Cardiac Imaging System.

10x The Sensitivity

For New Clinical Applications

Larger Radiation Collection Angles.

Unique Scan Pattern.

2x The Resolution

For Sharper, Enhanced Images

Novel Design of Scanning Solid State Detectors.

Unique Reconstruction Algorithms.

10x The Speed

For Unprecedented Throughput

Gated SPECT can be Completed in as Little as 2 Minutes.

Breaking the Paradigm

Spectrum Dynamics provides technology that allows medical professionals to experience a true breakthrough in Nuclear Imaging. Now we no longer have to choose between speed and image quality.

Dramatic improvements in both clinical workflow and image quality are now possible with the D-SPECT™ Cardiac Imaging System, powered by Spectrum Dynamics' unique BroadView™ Technology. This new technology represents a breakthrough in almost every component of nuclear cardiology imaging diagnostics and workflow, including up to a 50% improvement in energy resolution, which will provide the capability to image multiple isotopes simultaneously.

These dramatic gains in detector performance, combined with proprietary high resolution reconstruction algorithms, allow medical professionals to enhance clinical results while drastically reducing acquisition time, thereby improving overall clinical workflow. With these improvements, the D-SPECT™ Cardiac Imaging System revolutionizes the entire molecular imaging process.

Medical - Future

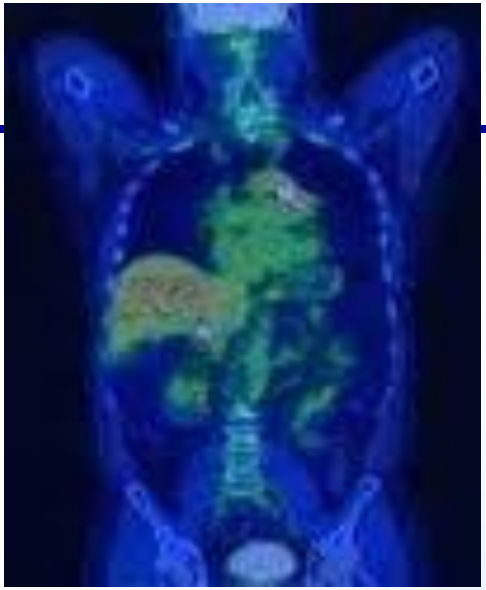

- $B/Yr market – Biggest driver
- Full body scanning in nuclear medicine
- CZT for X-ray Computed Tomography
  (high flux X-ray CT)
- CZT for Positron Emission Tomography (PET)
  (See *Gu et al. Phys. Med Biol.* ***56*** *(2011) 1563* for instance)

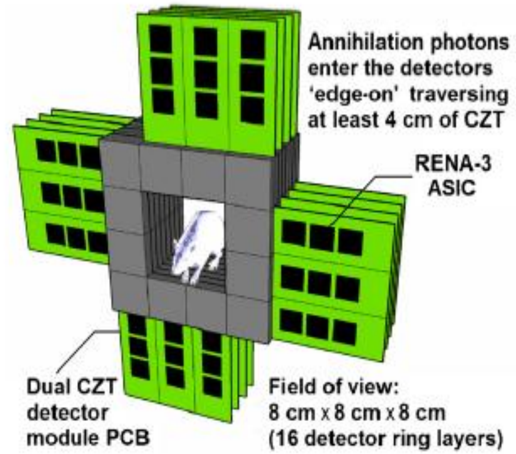

Figure 1. CZT high-resolution small animal PET system under development.

High-Resolution Digital Radiography Enabled

• Single-Photon Emission Computed Tomography (SPECT) + (CT) Imaging

• Position Emission Tomography (PET) also demonstrated

GE and Gamma Medica-Ideas

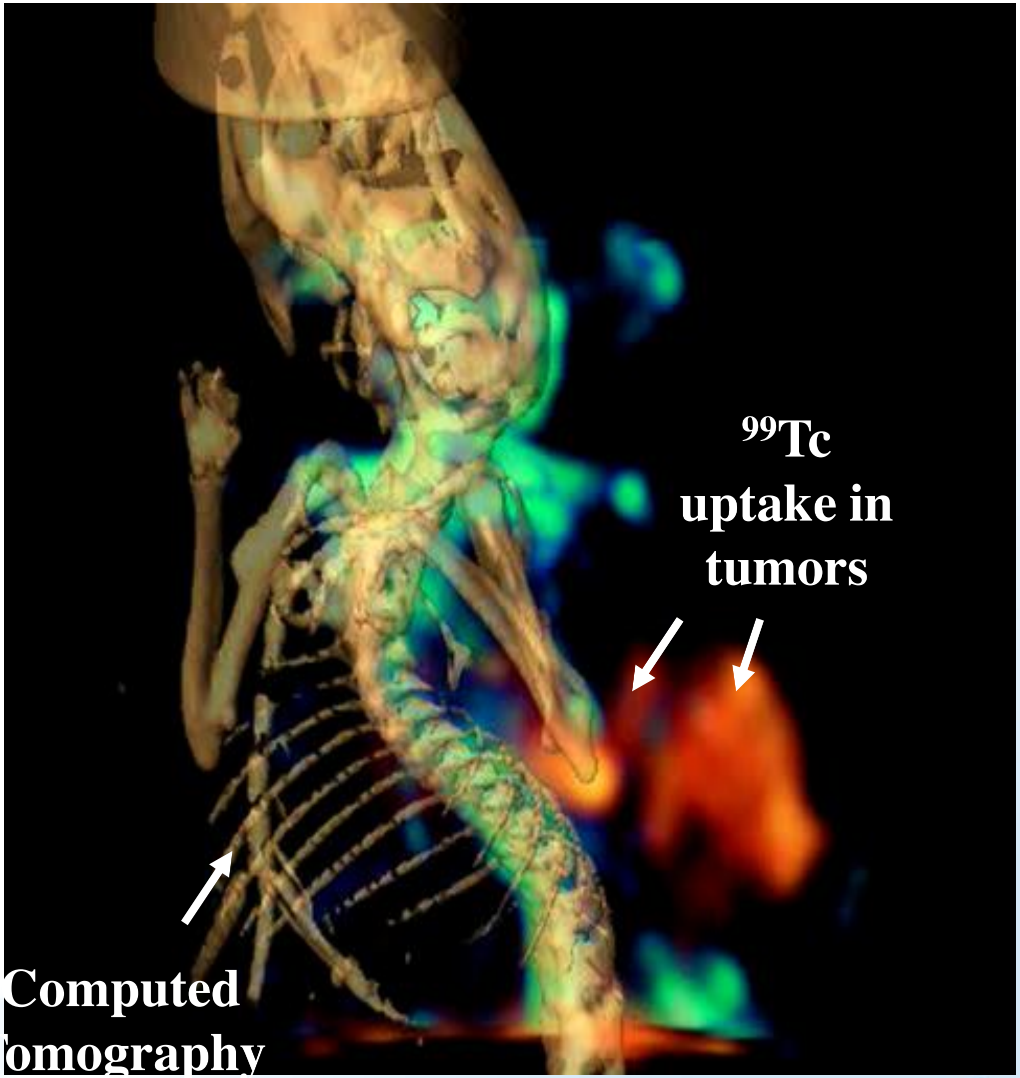

A High-Resolution MRI-Compatible SPECT System

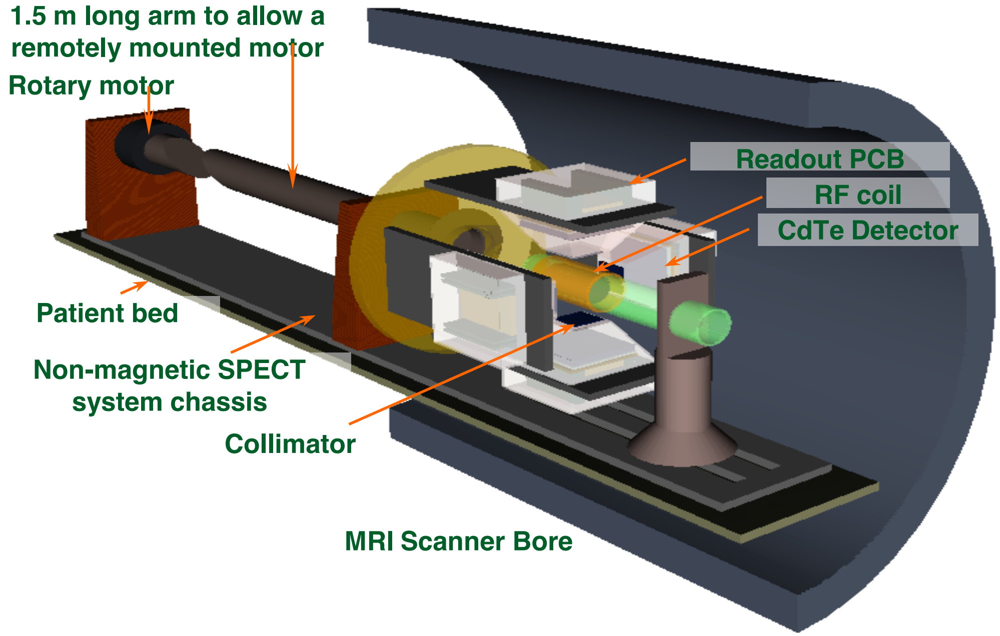

The Siemens Allegra 3 T MRI scanner at BIC that will be used in the combined SPECT/MRI System.

- We are developing a MRI-compatible SPECT system with four heads installed on a rotational gantry.
- Two key objectives: (a) demonstrate the capability of achieving an sub-500 µm SPECT resolution inside MRI scanner (b) provide a flexible platform for testing different detector and system designs

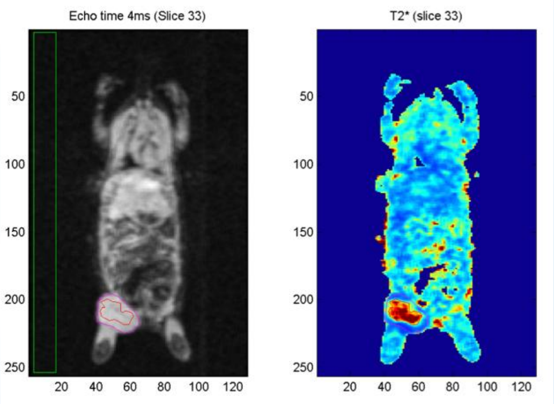

Left: A 3-D whole-body image of a rat acquired with the 3 T Allegra scanner. Right: T2* relaxation of the tissues. The images were obtained with a multiecho fast low angle shot (FLASH) sequence written by Professor Brad Sutton of UIUC. It resulted in 0.5 mm isotropic resolution from an 8 minutes whole body scan.

NCI, R21/R33CA004940, R21CA135736-01A1.

Meng et al, 2011 IEEE NSS/MIC/RTSD, Valencia

Energy-Resolved Photon Counting Detector – Design Concept and Considerations

Basic design target: generic, high performance and flexible.

- Hybrid photon detector concept with highly pixelated (pixel size: 350 μm) CdTe or CZT bump-bonded to 2-D readout ASIC – compact, high resolution.
- ADC on each channel – all digital output, amplitude, time stamp, pixel address for each hit.
- Flexible sparse logic – allowing signals from adjacent pixels to be summed together.

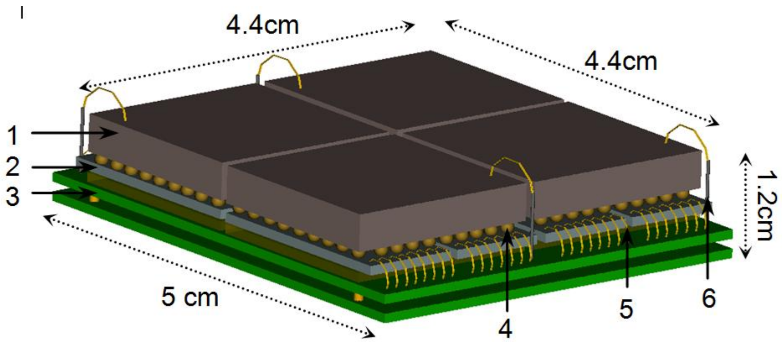

The proposed ERPC detector. (1) CZT crystals of 4.4cm × 4.5 cm × 2-4 mm in size, (2) ERPC ASICs, (3) Readout PCBs, (4) indium bump-bonding between CZT detector to the ASIC, (5) wire-bonds between the ASIC and the PCBs and (6) Cathode signal out.

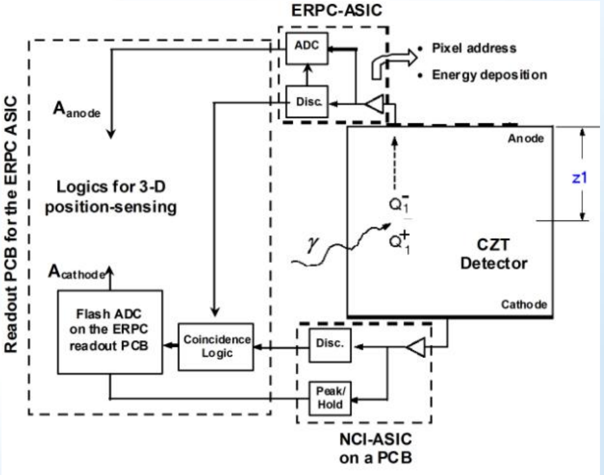

Z. He et al, NIM A380 (1996) 228, NIM A388 (1997) 180.

Meng et al, 2011 IEEE NSS/MIC/RTSD, Valencia

A Sub-500 μm Resolution PET Insert

A

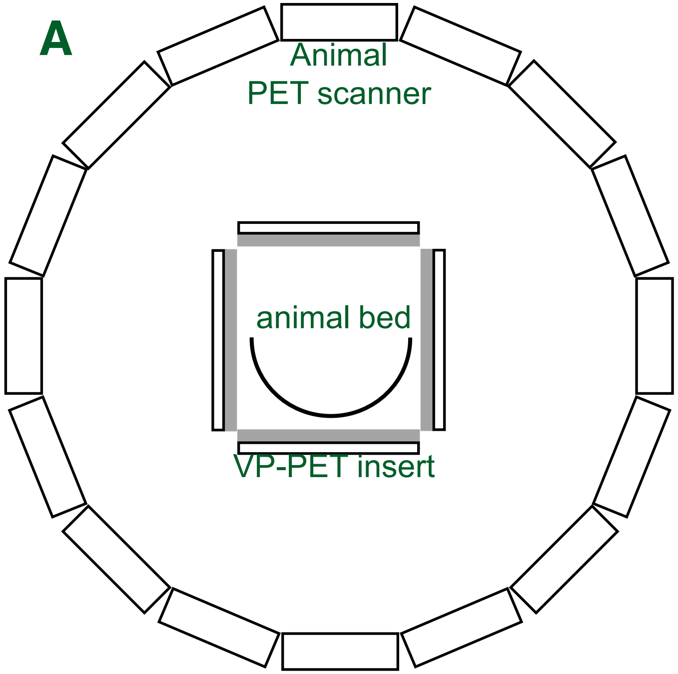

B

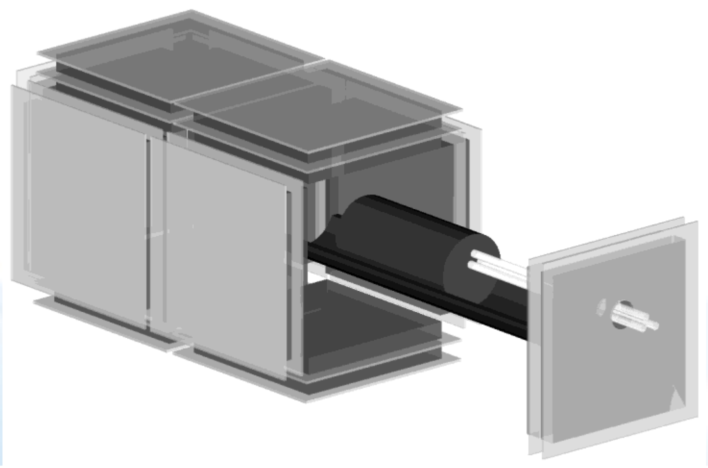

(A) Geometry of a potential 4-panel VP-PET insert device inside an animal PET scanner.

(B) A potential implementation of the detector technology proposed in this work.

(C) A prototype PET detector developed for the PET application.

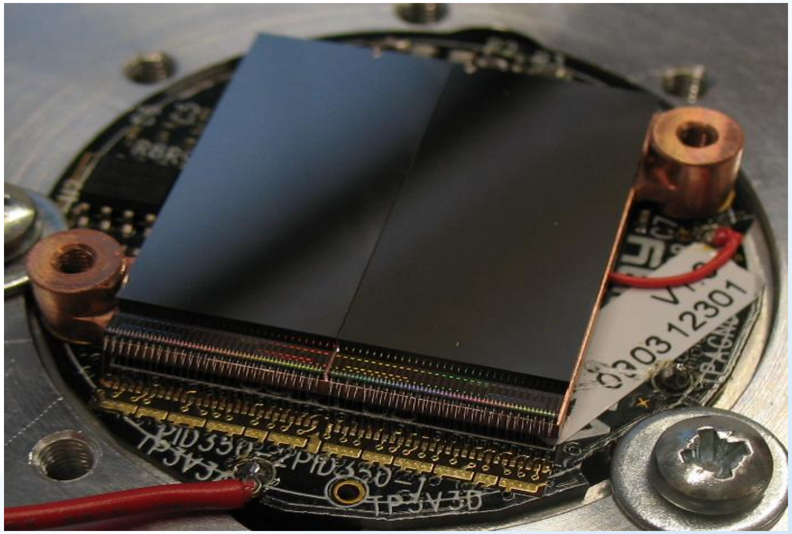

DOE, Office of Biological and Environmental Research (DE-FG2-08ER6481).

Meng et al, 2011 IEEE NSS/MIC/RTSD, Valencia

Pixelated CdTe Detectors

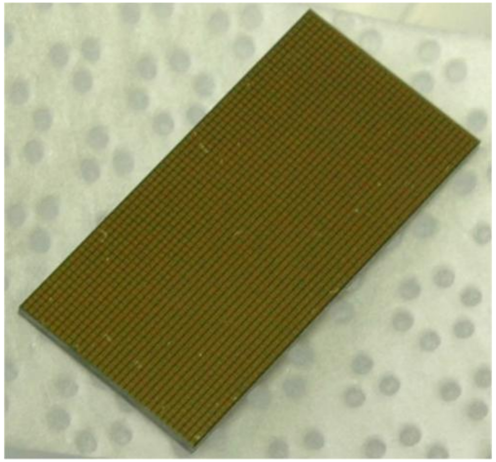

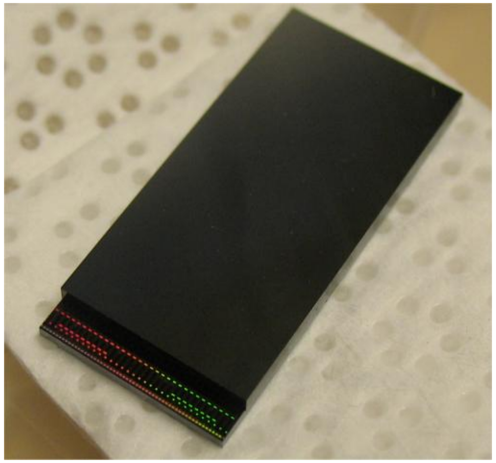

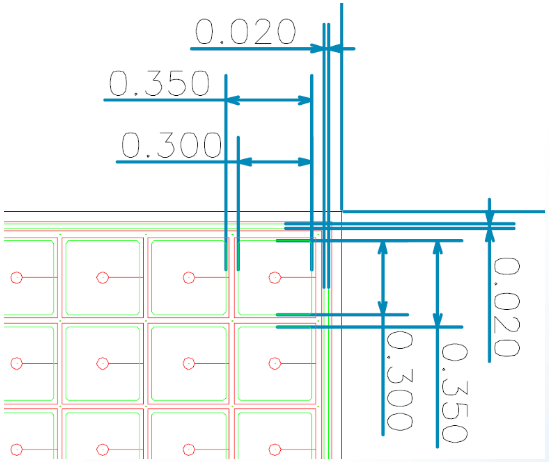

- A pixelated CdTe detector of 11mm × 22mm × 1 or 2 mm in size and having 32×64 350 μm × 350 μm pixels.
- ERPC detectors with 2 mm thick CdTe detectors will be used in the prototype system.
- Other pixel sizes – 515 um, 700 um read out with the same ASIC?

CdZnTe/CdTe Detectors for Use in Strong M-Field

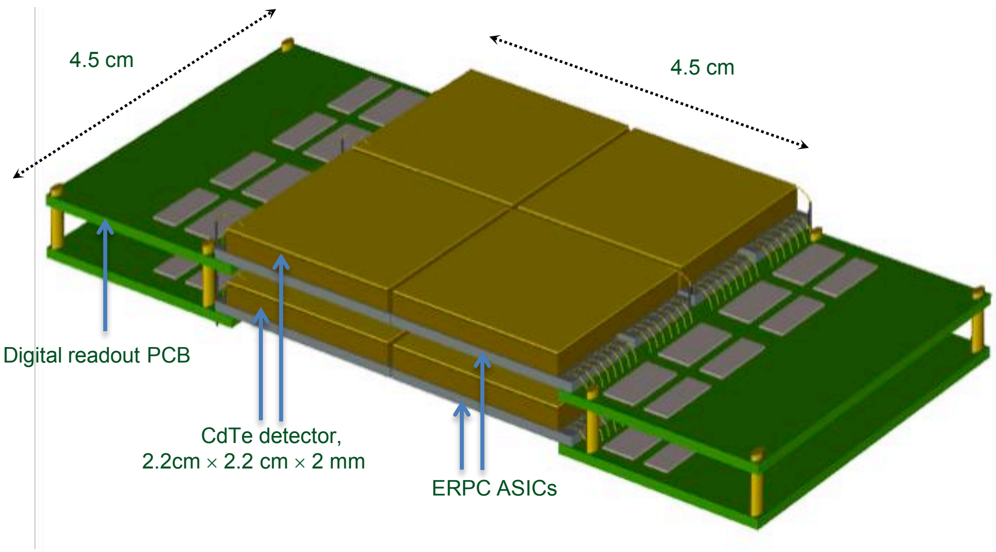

1.9cm×1.9cm×5mm CZT detector, cathode side

Anode side

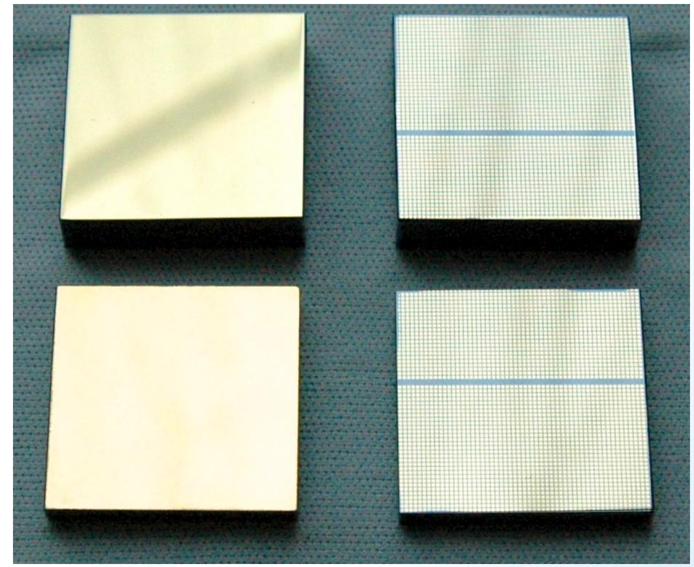

2mm thick CZT detector, cathode side

Anode side

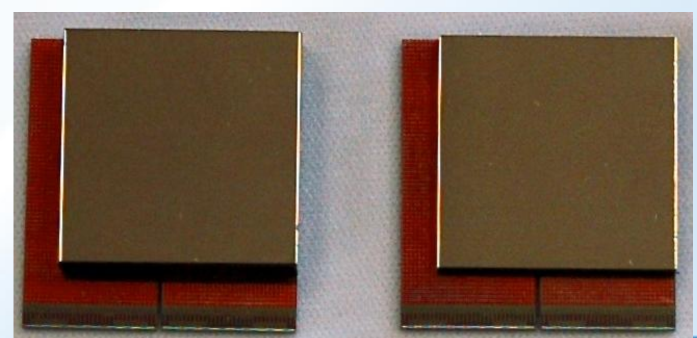

- We are exploring the use of CZT detectors of 2 mm and 5 mm thicknesses with the ERPC ASIC (fabricated by Creative Electron Ltd.).
- Two different CZT-ASIC bonding techniques (SnBI bump-bonding and Ag/Cu conductive epoxy bonding) are under evaluation.

Meng et al, 2011 IEEE NSS/MIC/RTSD, Valencia

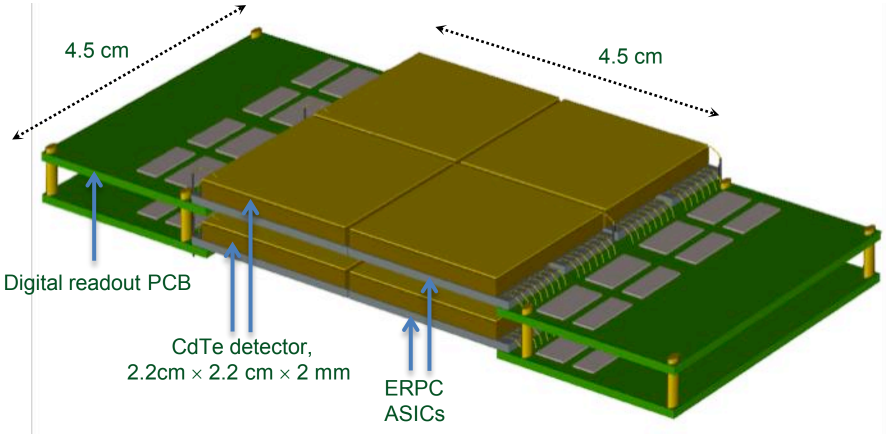

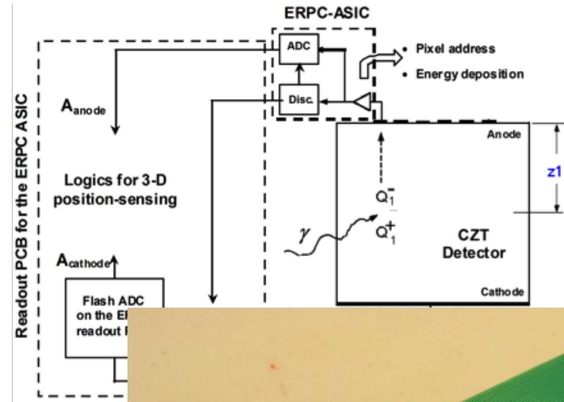

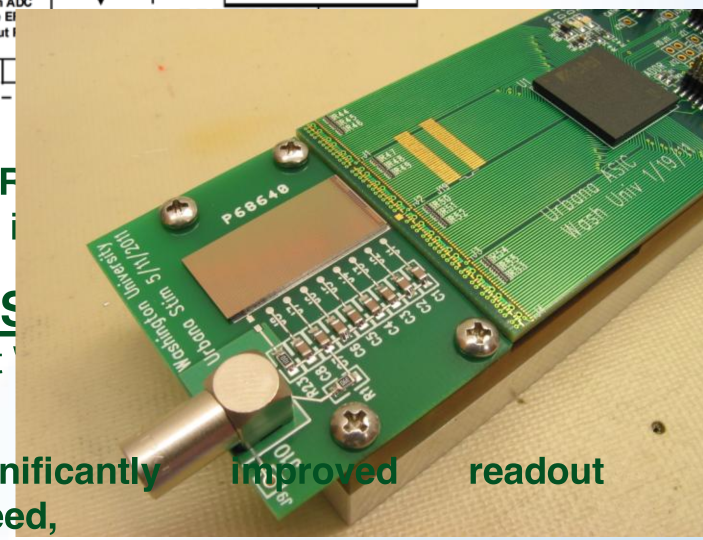

Left: The proposed MRI-compatible ERPC CdTe detector. F
the cathode-to-anode ratio to derive the depth-of-interaction i

A New Digital Readout System for the S

developed by Dr. H. Krawczynski's group at

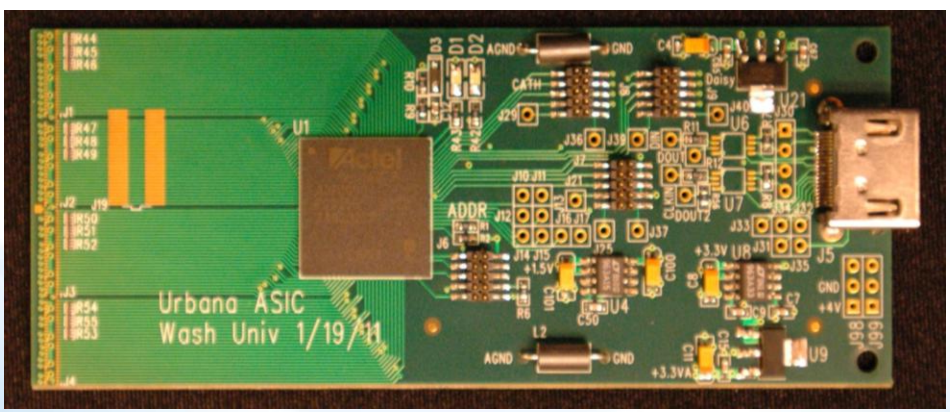

- **Significantly improved readout speed,**
- **Relatively compact**, width of the readout PCB is equal to the width of the CZT/CdTe detectors (4.5 cm), allowing a compact ring geometry.
- Cathode readout system is under development

Meng et al, 2011 IEEE NSS/MIC/RTSD, Valencia

Applications: tomography

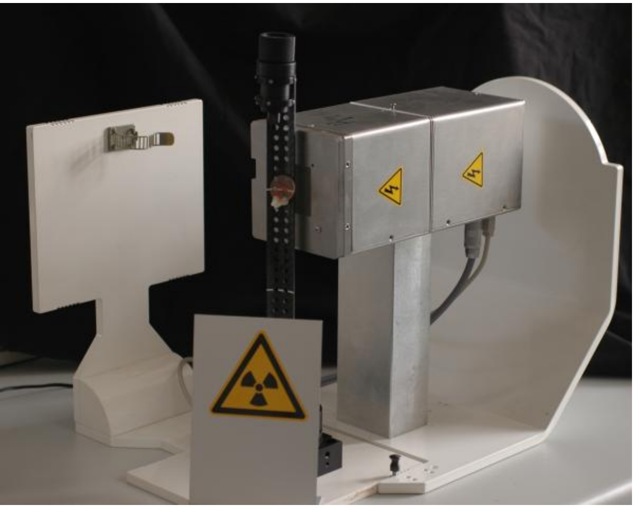

Tomographic acquisition setup

Radius of rotation=22.5 mm

(Courtesy of Biospacelab)

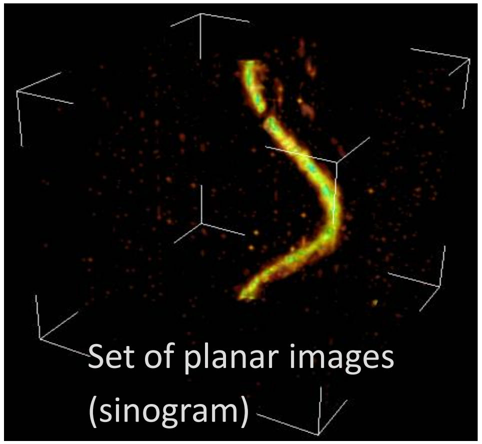

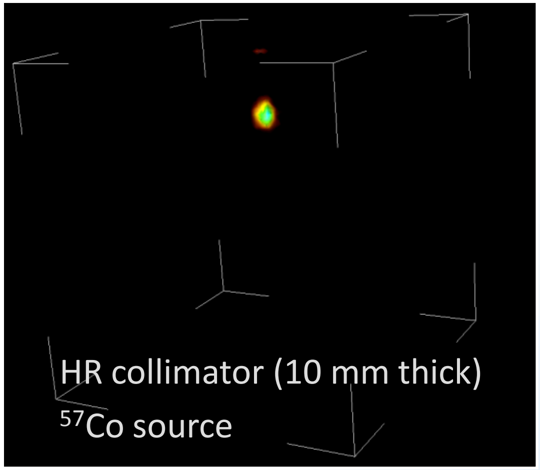

1.6 mm FWHM resolution

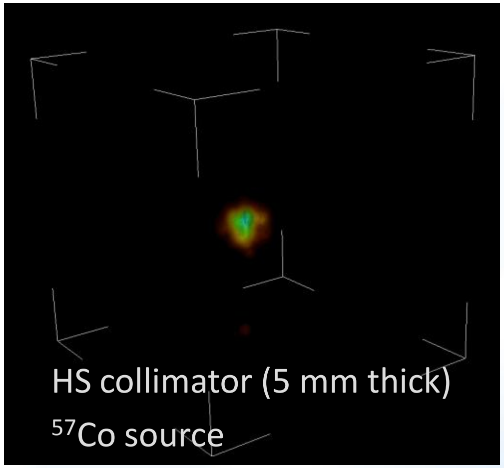

3.3mm FWHM resolution

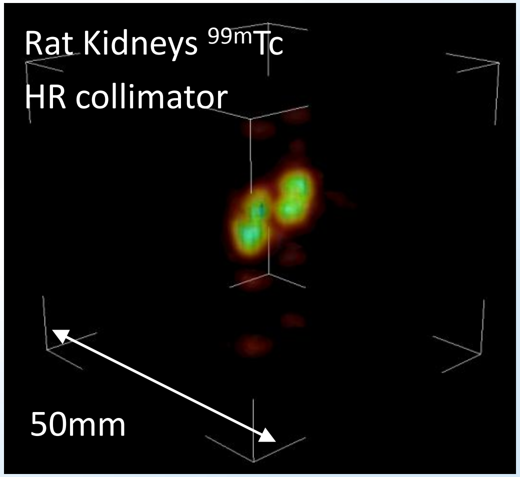

Courtesy of L. Riou (INSERM U877), ANR project SIGAHRS

Instruments for space applications use CZT detectors

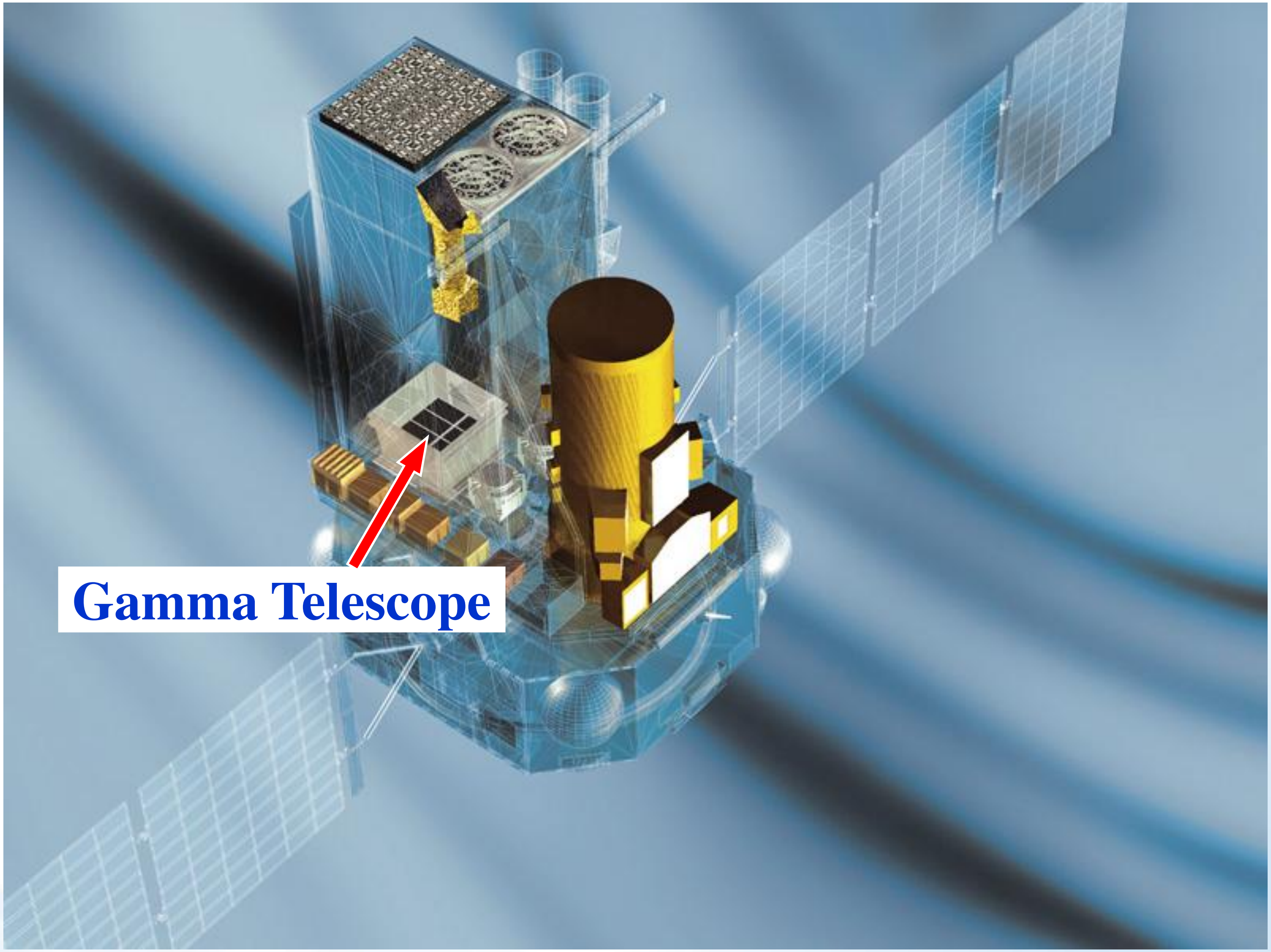

Integral

Scientific Research

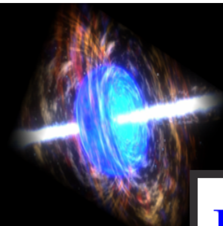

EXIST: Surveying the birth and evolution of Black Holes

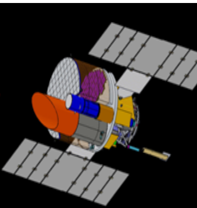

Harvard-Smithsonian/NASA

- **Astrophysics - NASA driven**
  - **Current: Single focal plan array detectors in conjunction with a focusing optic.**
  - **Future: Space-flight gamma burst instrument; high-energy x-ray astronomy.**

- **High Energy Physics (Future)**

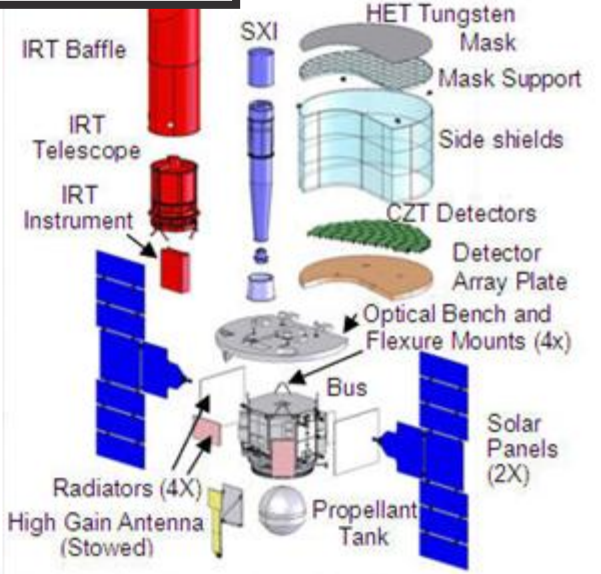

EXIST exploded view; the Observatory uses a modular instrument/bus design.

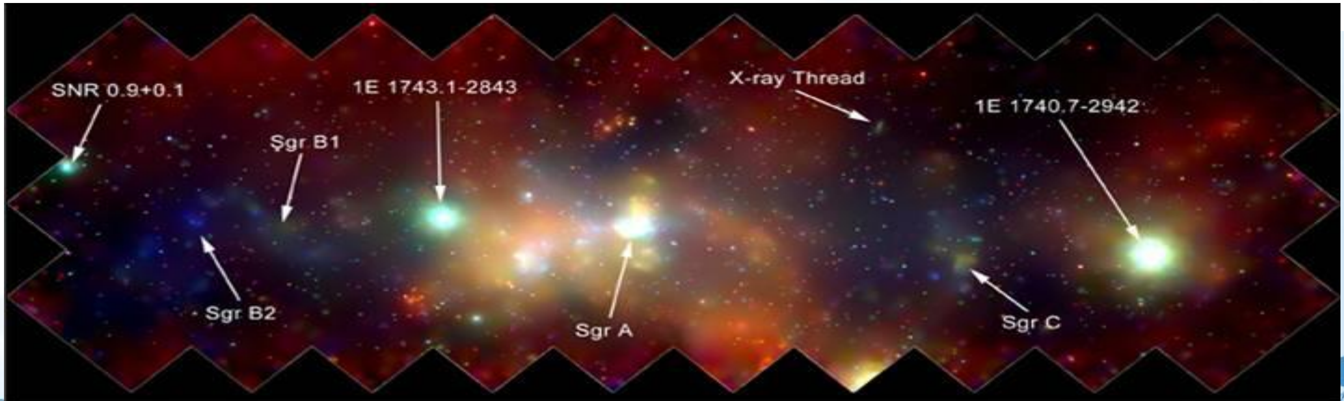

Applications of CZT detectors in basic science

- Burst Alert Telescope (BAT) for detecting gamma-ray bursts and other transient cosmic events, e.g., supernovas (launched in 2004)
  - Detection plane 30,000 5x5x2 mm^3 CZT crystals
  - Total area of 2 m^2
  - A coded aperture mask
  - Locate bright sources within 4 arcmin
  - Wide field-of-view.

Swift instrument

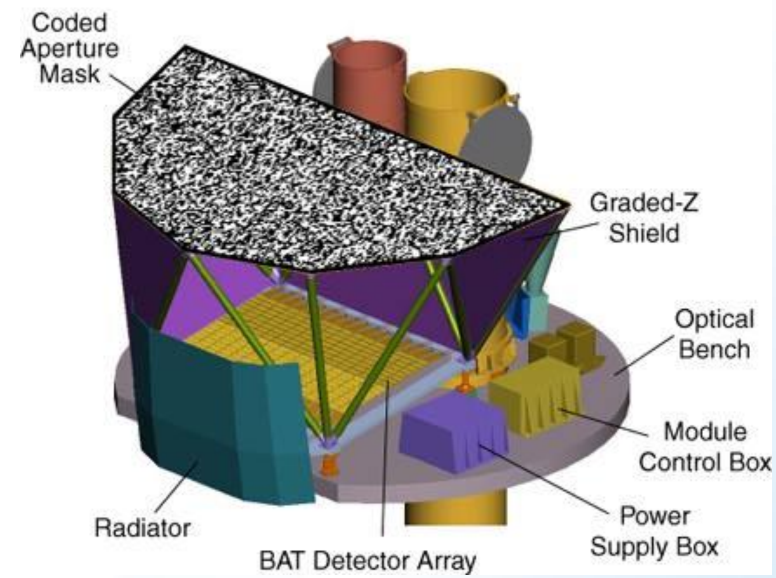

From NASA website

Swift relays a burst's location to other telescopes around the world.

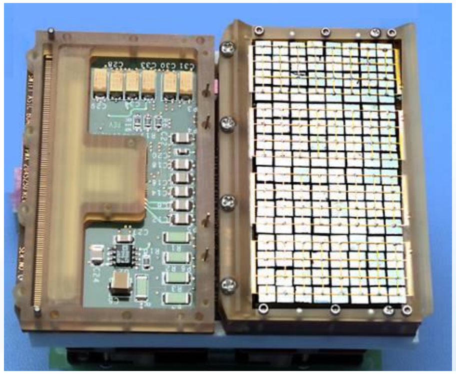

One of CZT modules

CZT-based Gamma Camera

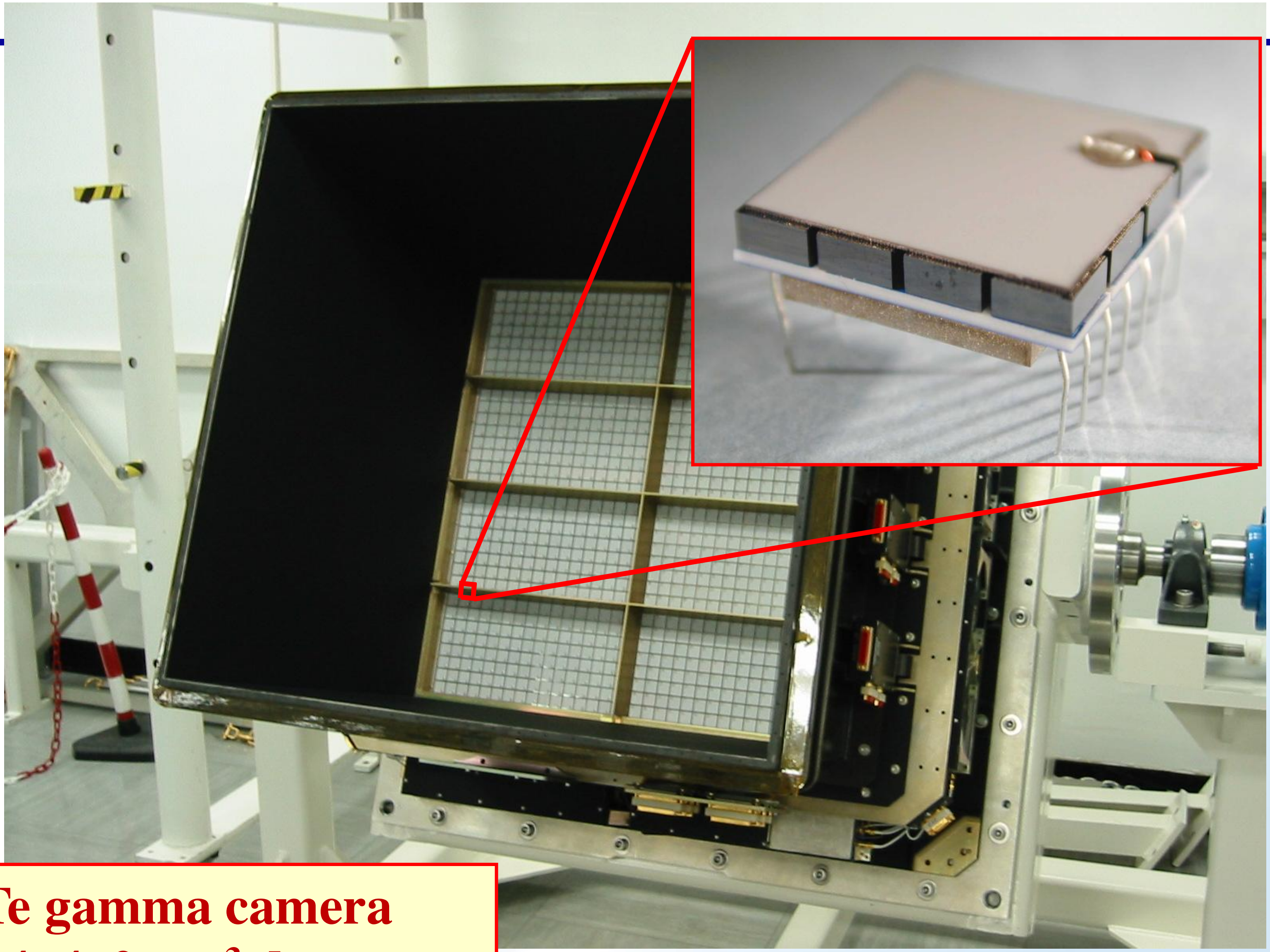

CdZnTe gamma camera
32,000 4x4x2mm^3 detectors
250 modules

NuStar X-ray Satellite Mission, Caltech/JPL

NuSTAR Focal Plane Detector
(focusing multilayer, deep studies of single objects)

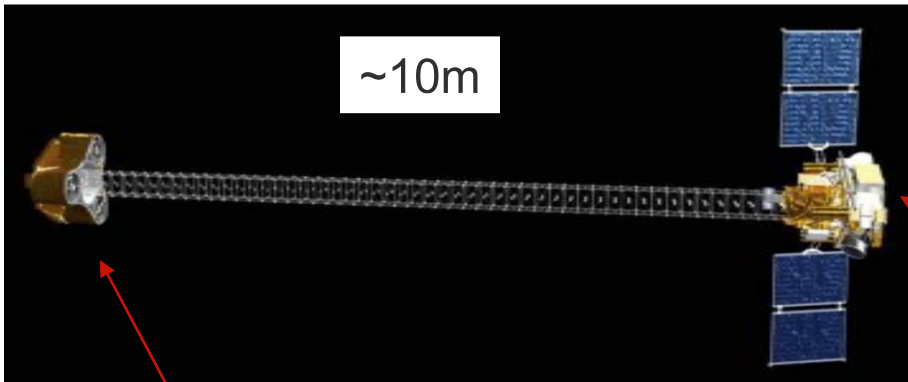

Focal plane detector

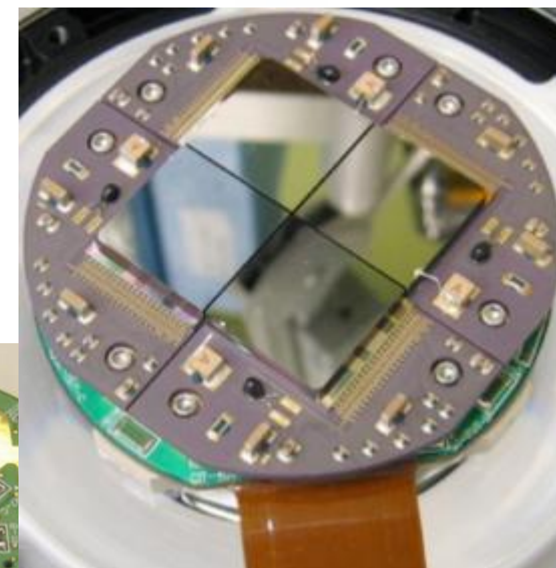

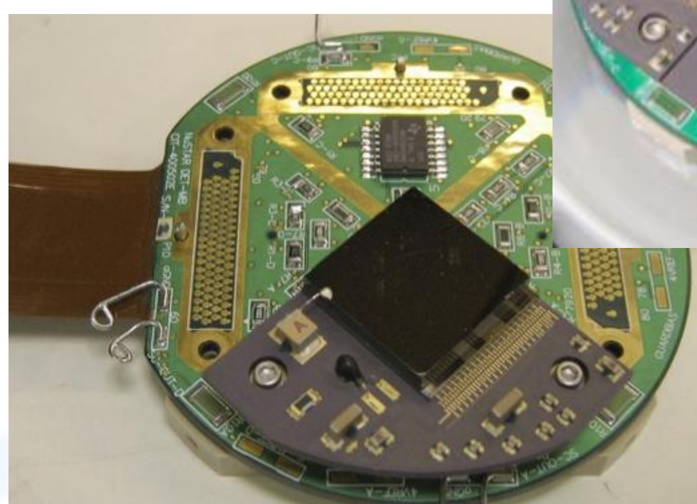

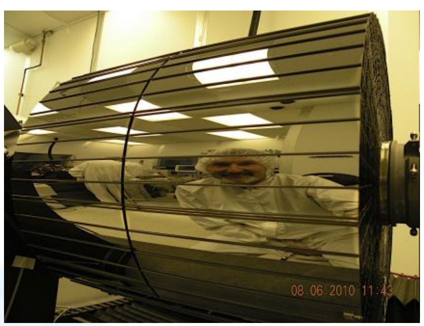

X-ray focusing optics

Motivation for ProtoEXIST

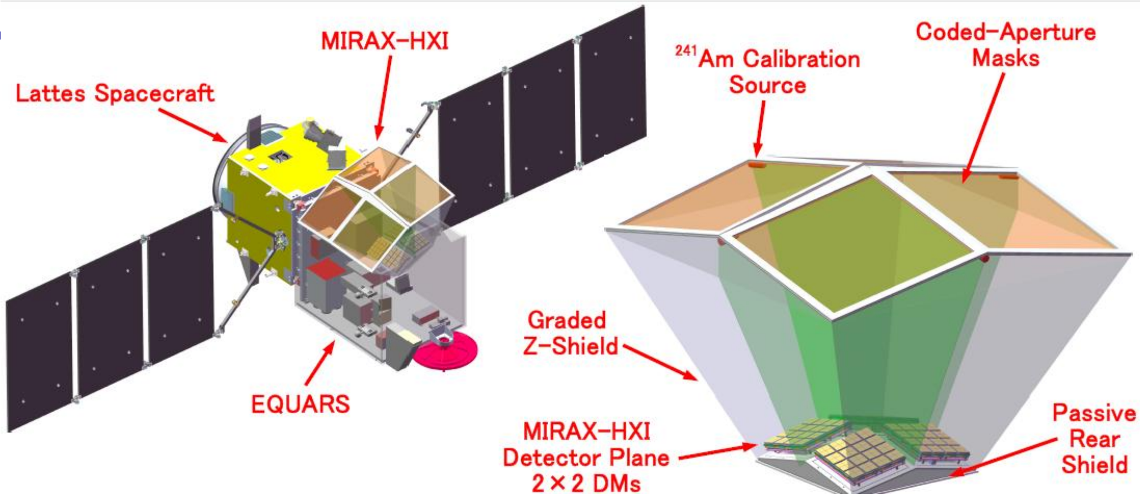

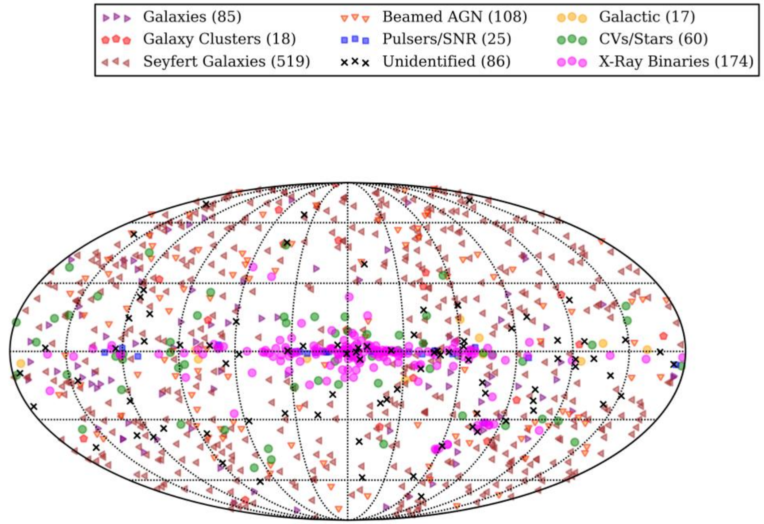

Swift–BAT 58–Month catalog.

Implementation of a wide–field Hard X–Ray Telescope using CZT with:

- Sensitivity between 5 keV and 600 keV
- Wide FOV for all sky transient monitoring.
- Good (~5 arcmin) angular resolution.
- Low power consumption for implementation of large high sensitivity missions (4.5–5.0 m^2 total active area)

The MIRAX–HXI was proposed US contribution to the Brazilian Cesar Lattes Program:

- Would carry out monitoring of the southern sky approx. every 90 min.
- 70° × 70° FWHM FOV
- 5 arcmin angular resolution in a compact package.
- Provide contemporaneous observations with Advanced LIGO, next generation TeV observatories, and next generation radio optical transient monitors.

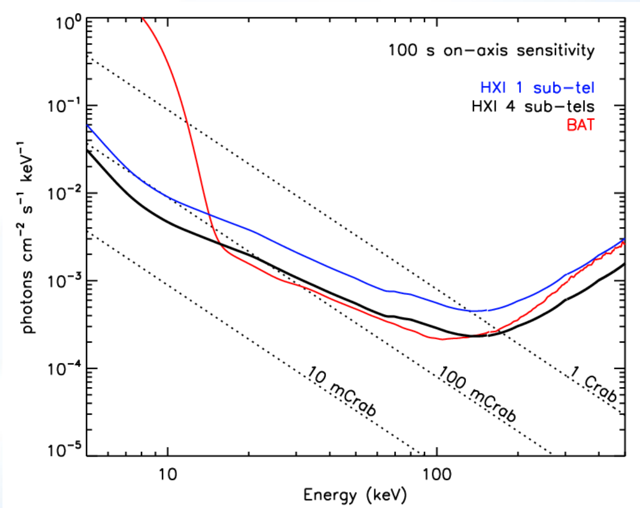

Sensitivity of the Mirax–HXI compare with the Swift–BAT

ProtoEXIST Program

ProtoEXIST:
- Dedicated to the production of a modular and highly scalable CZT detector plane architecture.
- ProtoEXIST1 successfully integrated and completed a successful 7 hour balloon flight
- ProtoEXIST2 development ongoing.

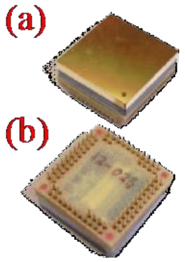

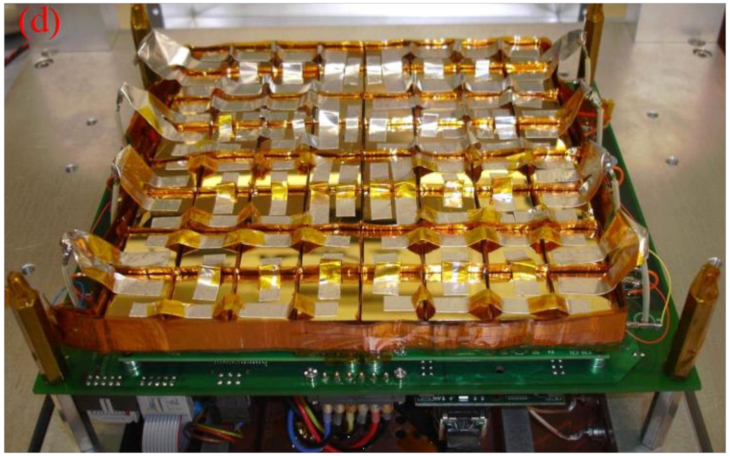

ProtoEXIST1:
- Composed of 64 individual CZT detectors readout using a RadNET ASIC via an interposer board.
- 2.5 mm pixel pitch.
- Detectors are grouped into modular 4×2 sub-arrays called detector crystal array (DCAs)
- Full detector plane composed of a 2×4 array of DCAs mounted to a flight control board.

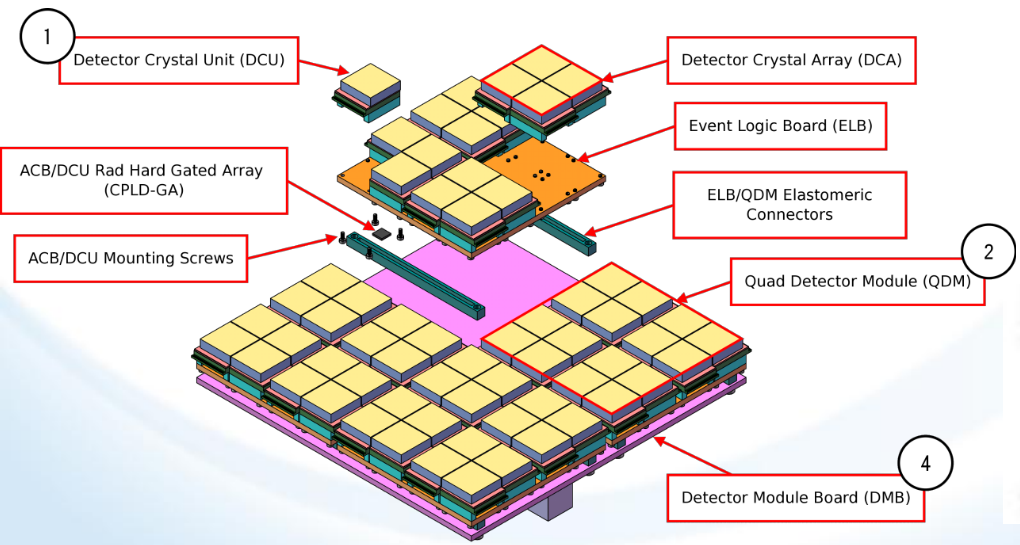

ProtoEXIST2:
- Individual detectors now utilize the NuASIC originally developed for NuSTAR (to launch in early 2012).
- 604.8 μm pixel pitch.
- Detectors now grouped in 4×4 sub-arrays, Quad Detector Modules (QDMs).

Detector (ASIC)	Pix. Pitch [mm]	N_{ch}	Power [mW/ch.]
INTEGRAL-ISGRI	4	4	2.8
Swift-BAT (XA)	4	128	3.3
ProtoEXIST1 (RadNET)	2.5	64	0.25
ProtoEXIST2 (NuASIC)	0.6048	1024	0.05
ProtoEXIST3 (ExASIC)	0.6048	1024	0.01

ProtoEXIST2 Detectors Crystal Units (DCU)

The RadNET ASIC attached to the ProtoEXIST1 IPB. ASIC anode inputs were mapped to a 8×8 array of inputs on the upper surface of the IPB for bonding to CZT.

Development of the ProtoEXIST 2 detectors continues in collaboration with Creative Electron Inc. (hybridization), Caltech and GSFC. 20 mm × 20 mm, 5 mm thick Redlen CZT are utilized at the detector medium.

Current Status:

- Front-end electronics for ASIC control validated and successfully demonstrated in a test board implementation.
- 2 bonding methods utilizing a conductive epoxy bond + anode pad gold studs, and conductive epoxy bond + metallized anode pads.
- 5 hybridized detectors completed to date:

3× bonded to test boards (upper right), 2× complete prototype DCUs (lower right)

- Full production of 80 detectors to commence shortly in preparation for flight of a test detector in September 2012.

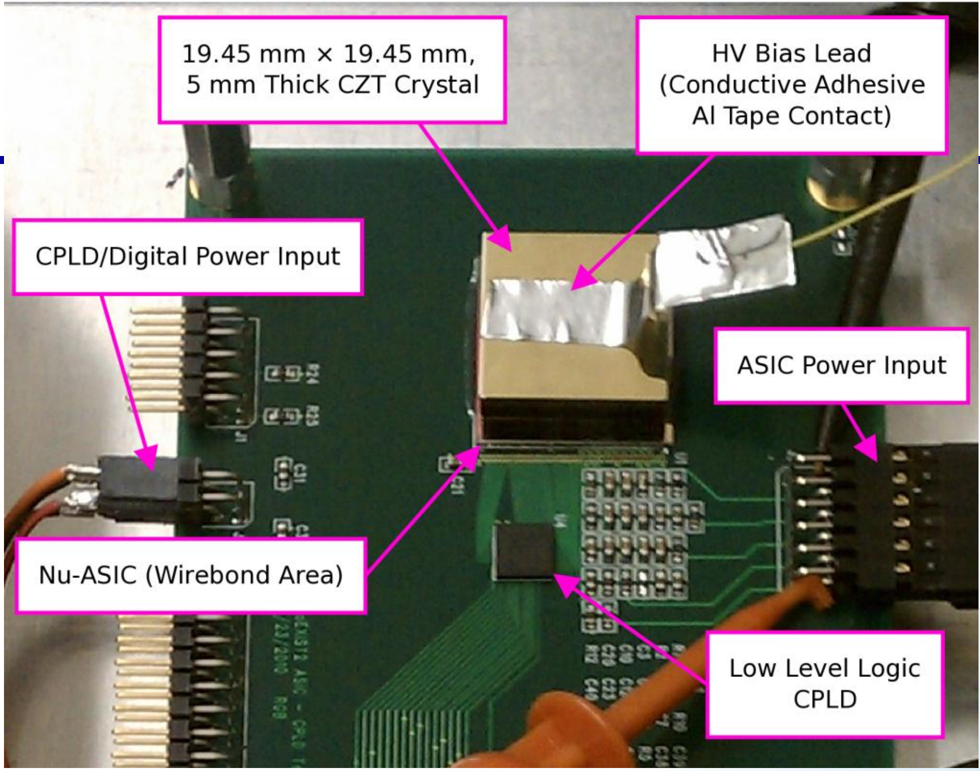

D001– The First Prototype ProtoEXIST 2 Detector.

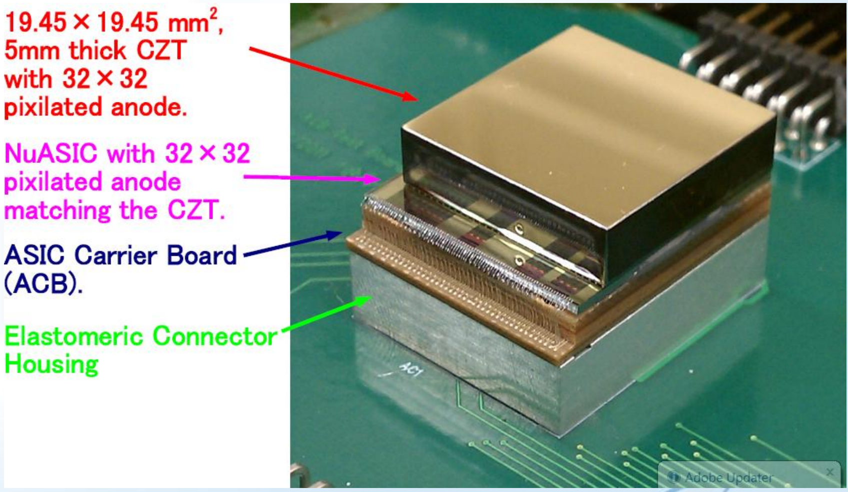

D004– The First Prototype ProtoEXIST 2 DCU

Detectors for homeland security applications currently under development

J. Matteson et al., University of California in San Diego

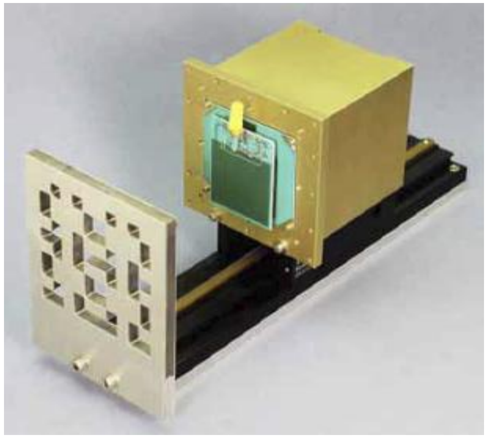

Consists of 25x25x5 mm^3 orthogonal strip detector detectors

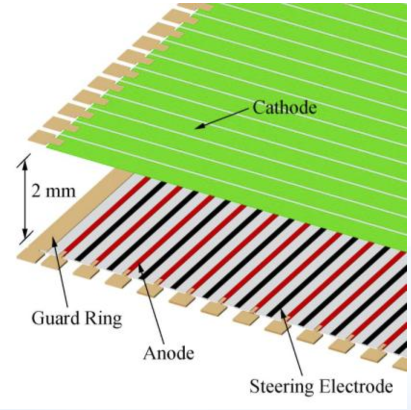

Z. He et al., University of Michigan

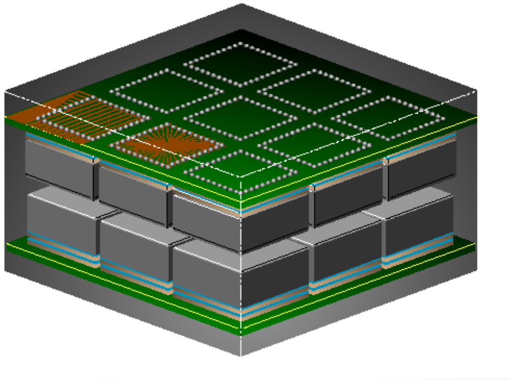

Consists of 18 20x20x15 mm^3 pixel detectors

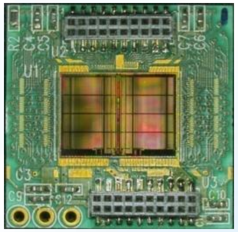

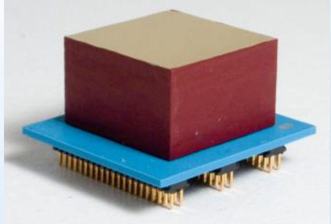

Security & Surveillance

- **Nuclear spectroscopy application of CZT moving from traditional small detector based nuclear instrumentation (past) to very compact prototype imaging system (current) and eventually mobil type imaging system (Future)**

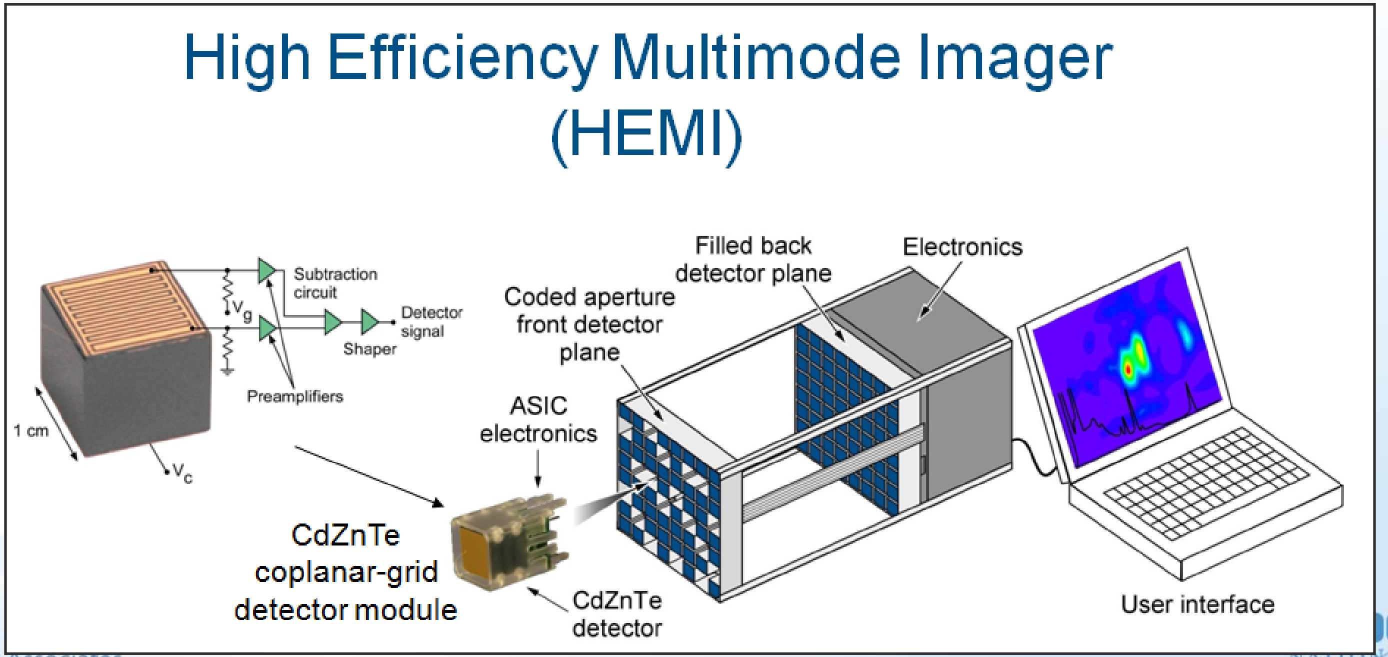

Myriagami: system architecture

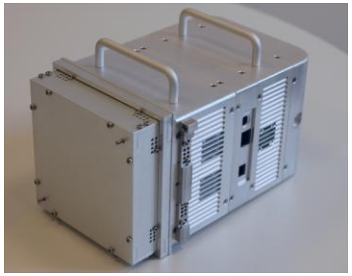

Power board with HV supply

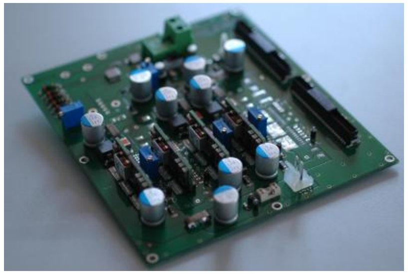

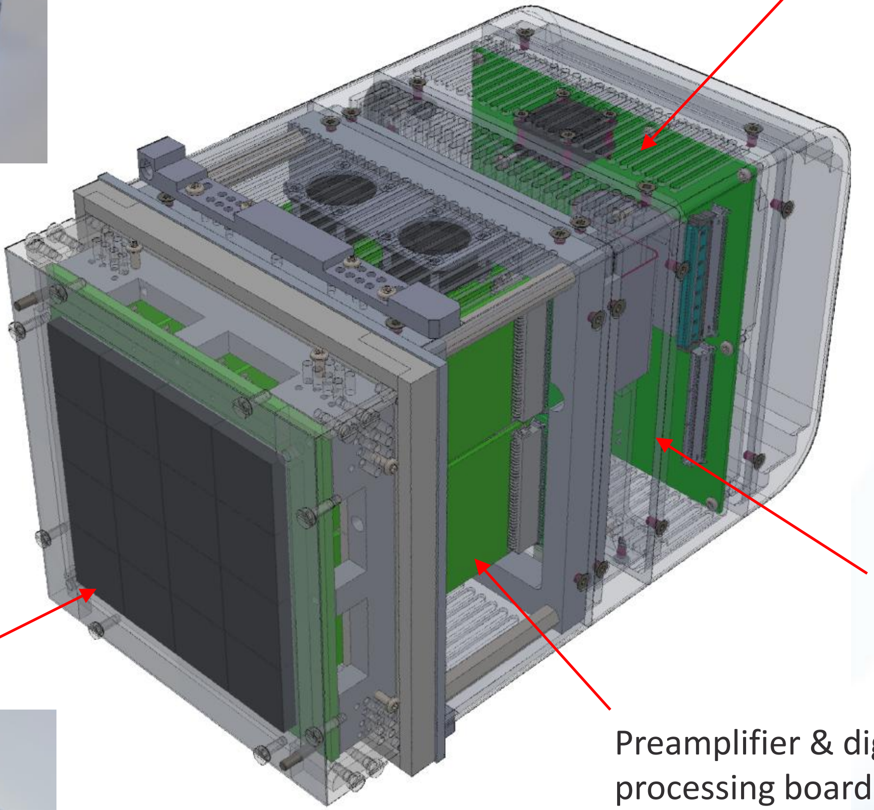

System manager/Interface board

4x4 CZT crystal plane

Preamplifier & digital
processing boards

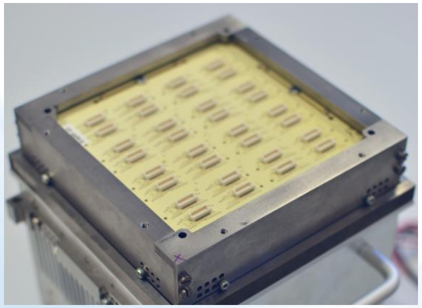

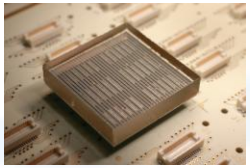

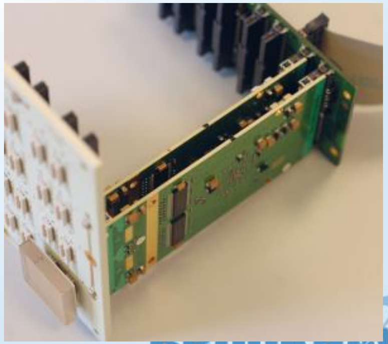

Detectors with electronics

CZT Coplanar Grid (CPG) detectors

- Source material: Redlen 19 x 19 x 5 mm^3 with 8 x 8 pixel
- Removal of pixel and backside contacts
- Deposition of CPG contacts and new backside contact
- Stack of two detectors used to increase volume ~4 cm^3

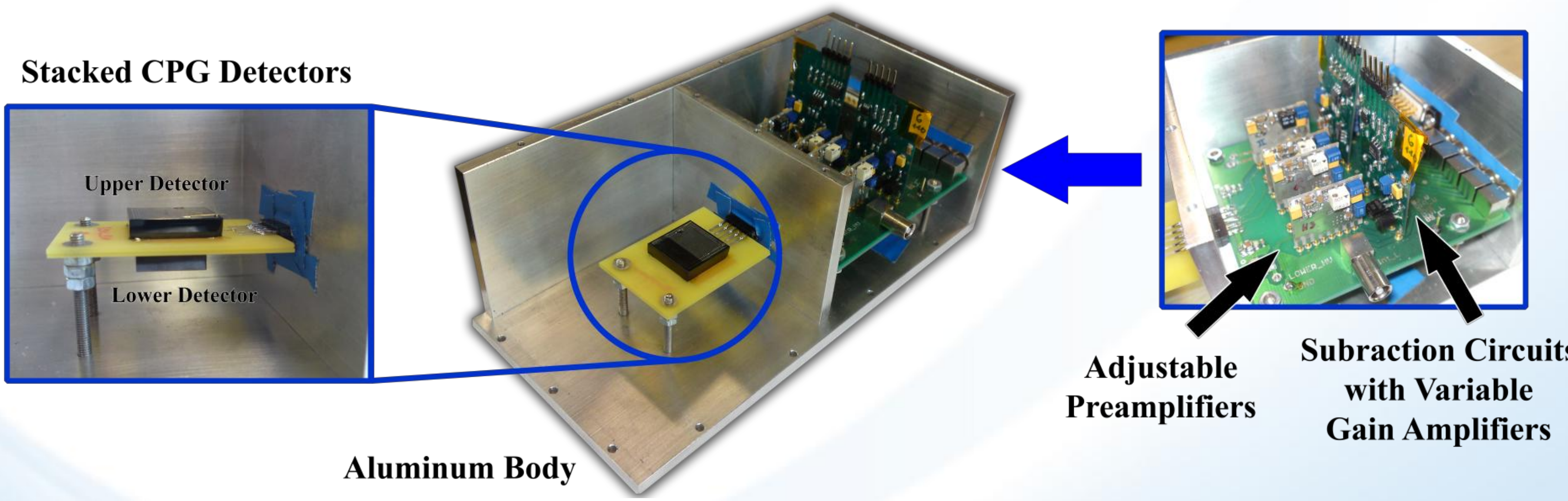

C. Disch: “Coincidence Measurements and long-term Stability Analysis with Stacked (Cd,Zn)Te Coplanar Grid Detectors”, RTSD.S Postersession I/II

Underground

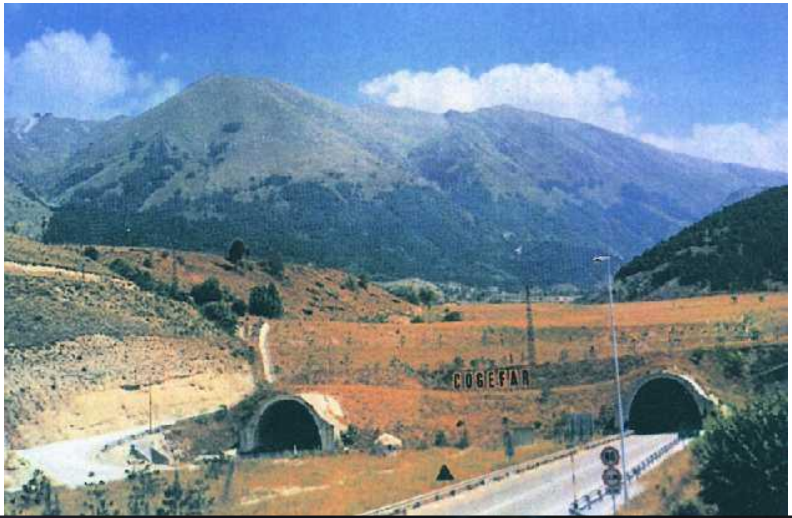

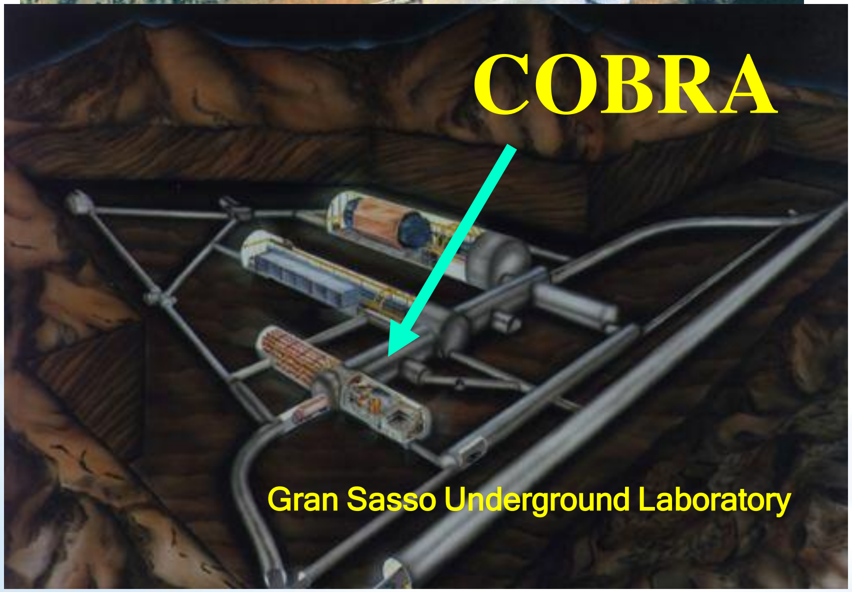

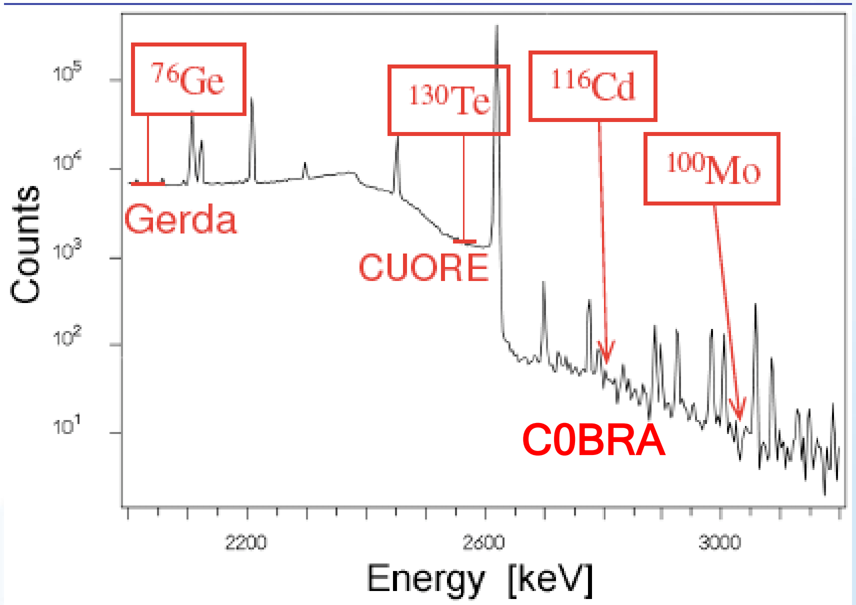

Pixel detectors

In collaboration with group of Z. He (Univ. Michigan)

The power of pixels!

Running at Gran Sasso Sep. 2009 – January 2010

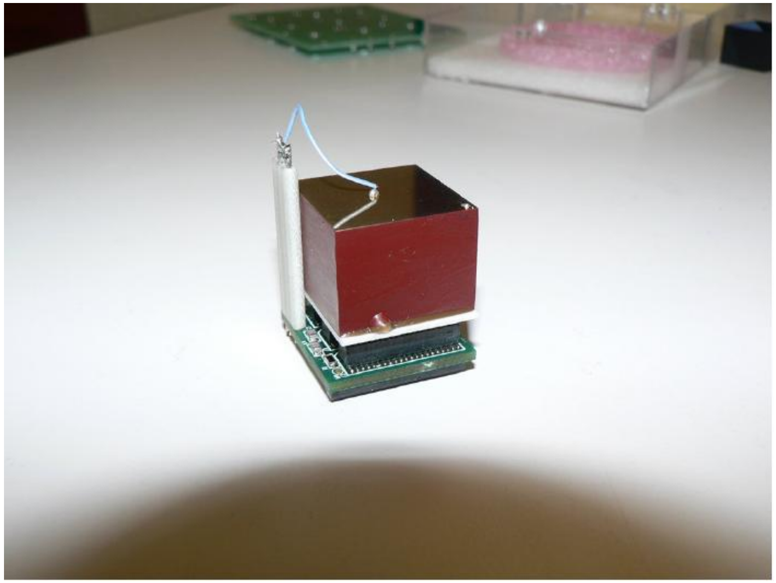

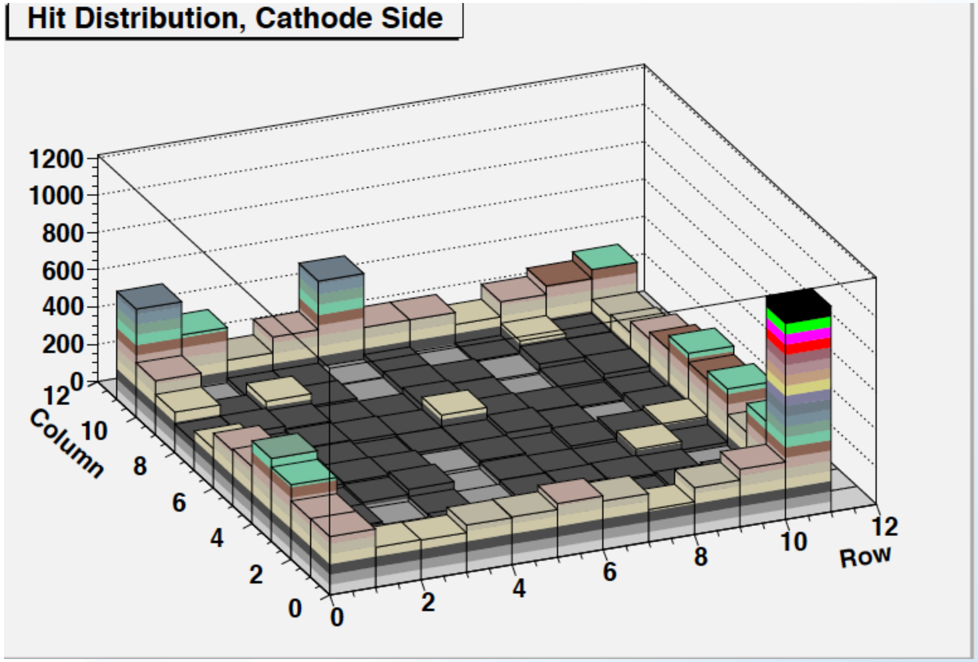

20x20x15 cm^3 CZT detector (as used in Polaris system)
11x11 pixels

NB: Also running a pixel system developed at Washington University at St. Louis at Gran Sasso

COBRA Set-up

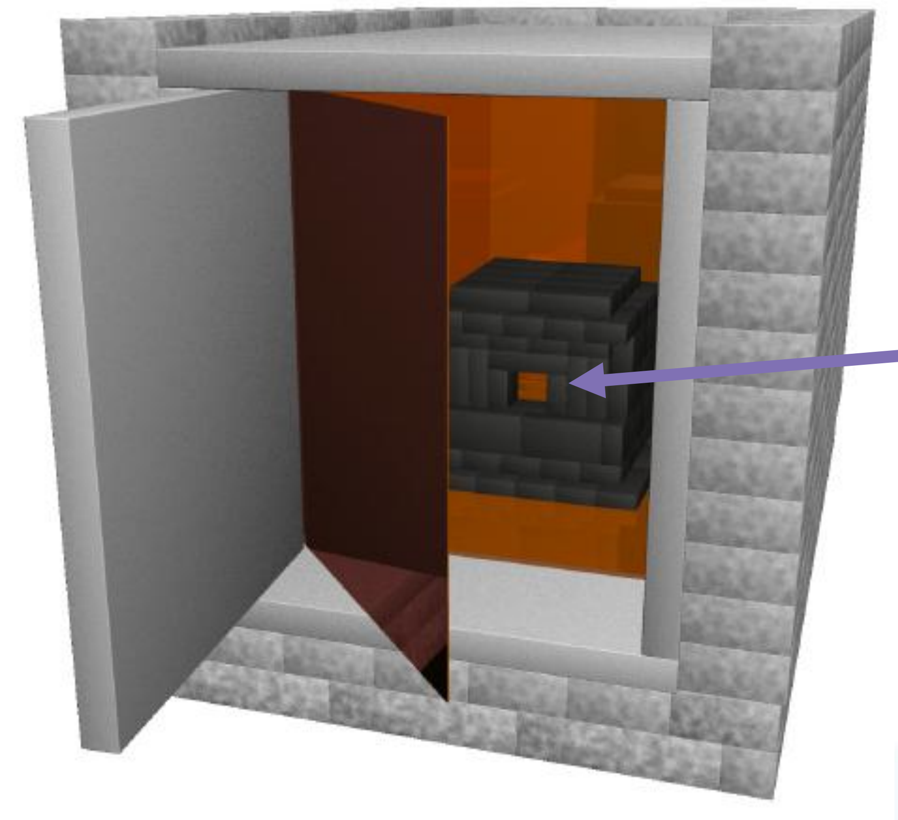

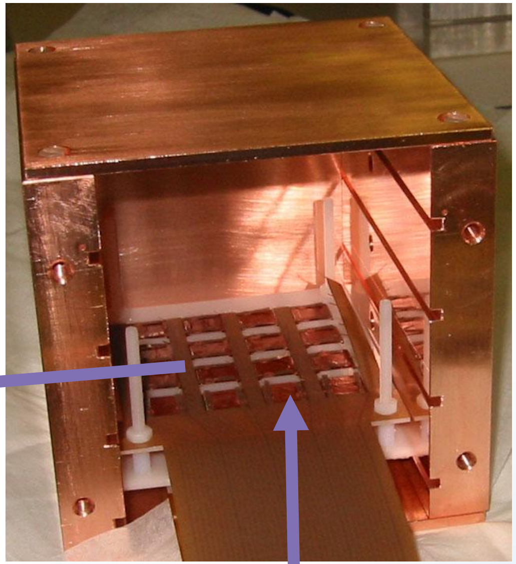

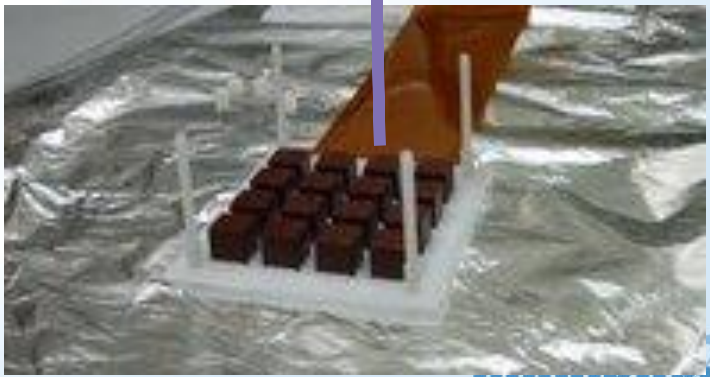

Learn about background using 1cm^3 CPG CZT detectors

Motivation

Dose rate monitoring network in Germany

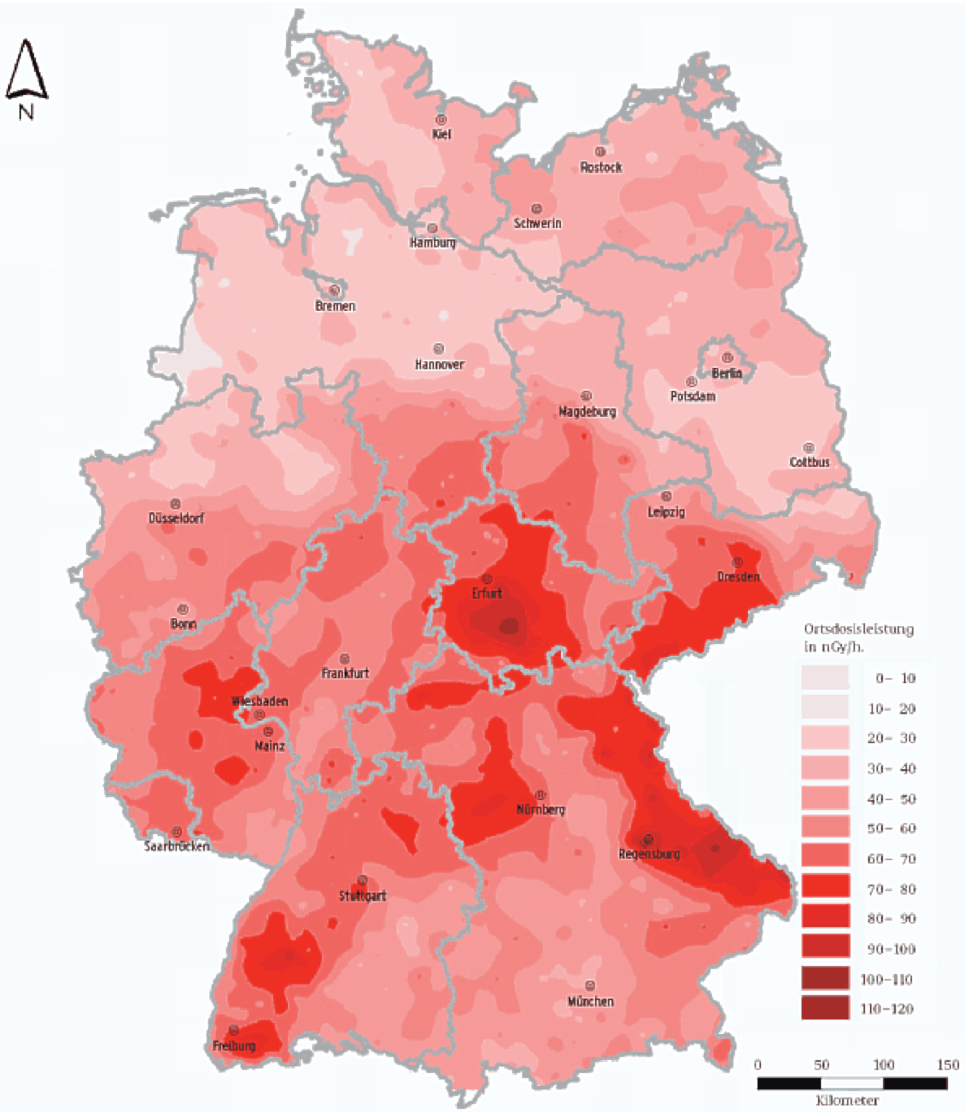

- ~1800 probes
- Geiger-Müller counters
- Connected to server via phone line

- No energy information → no particle identification
- ~200 spectroscopic systems planned

Spectroscopic concept

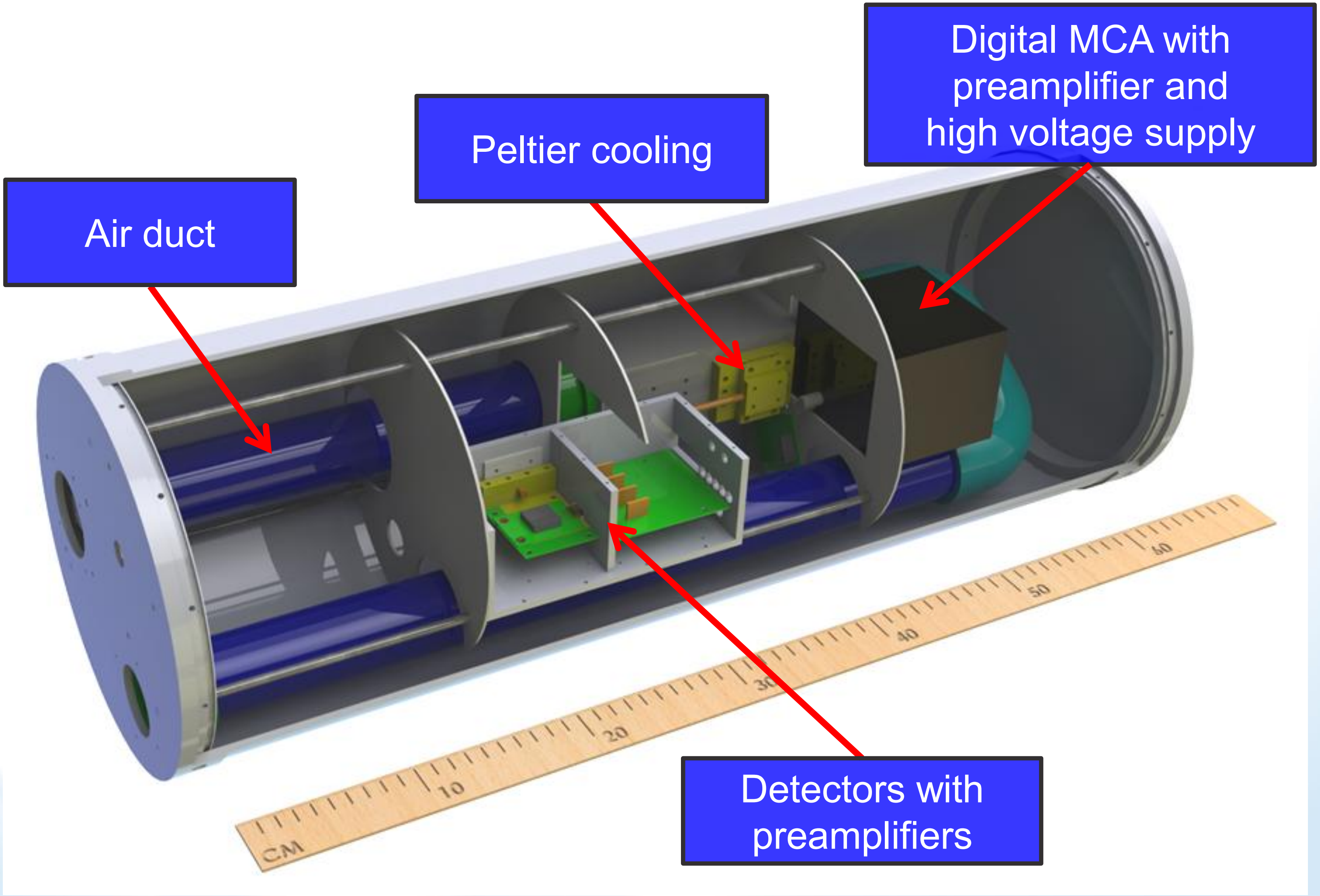

- Silicon and CZT in one copper box
  - 6.5 cm distance between
- Readouts coupled by 4 signals
  - Counter Clear
  - Counter Oscillator
    - 3.125 MHz
  - Busy In
  - Busy Out
- Selected events that:
  - Matched counters
  - Coincidence between both sides of Silicon
    - Energy match of 10 keV

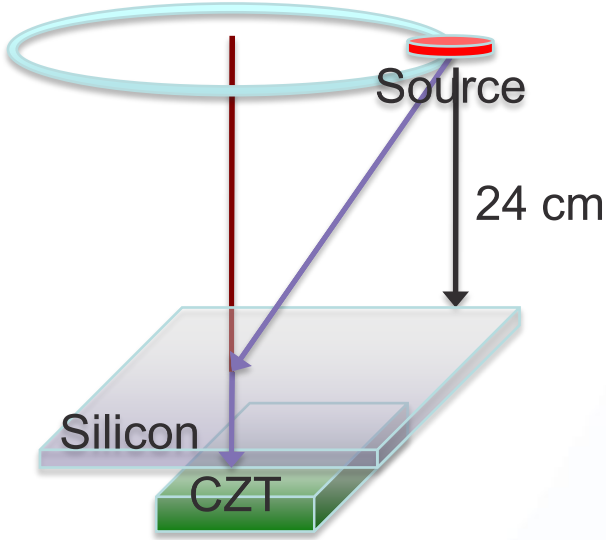

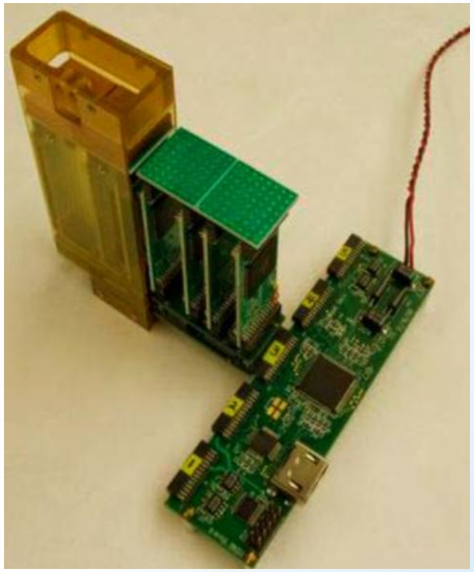

- Cs-137 source 24 cm away from Si
  - ~77 Bq
- Event Ordering
  - Assumed smallest interaction energy is first
    - True for ~75% of events at 662 keV
      - 0-76° scatter angles
    - Silicon scatter events
      - Lower Doppler broadening
  - Reconstruct cone of probable locations based on energy and locations of interactions
    - Angular resolution of 8.5° FWHM

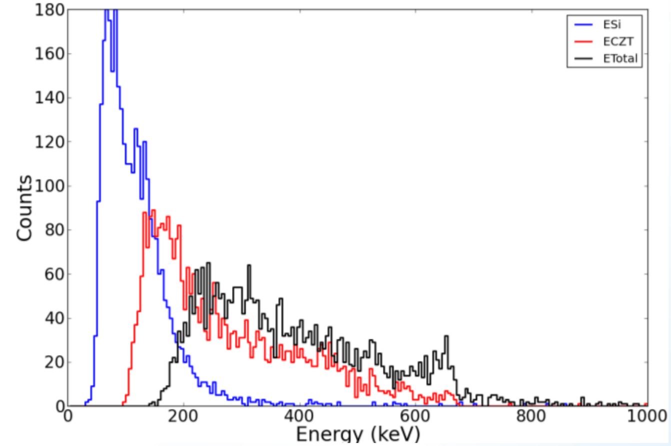

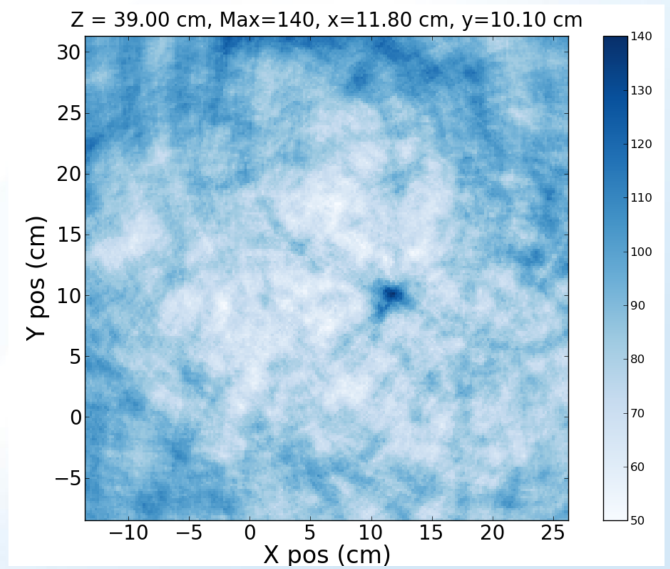

Caliste development

3 generations to reach optimal performance

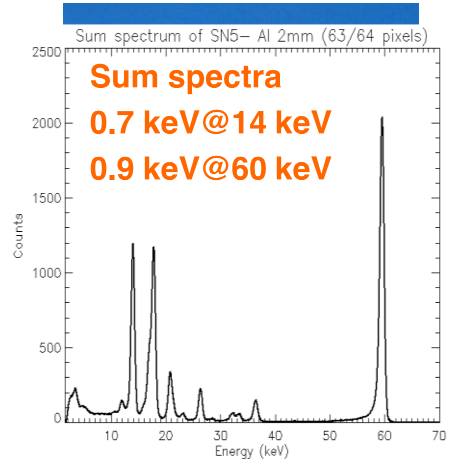

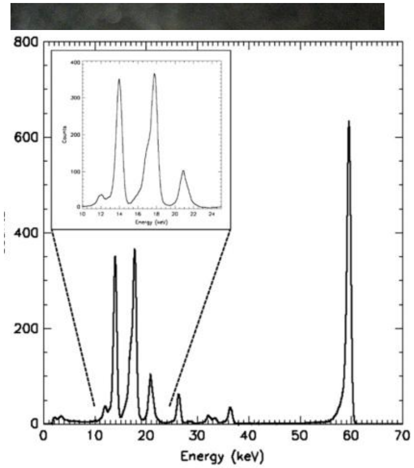

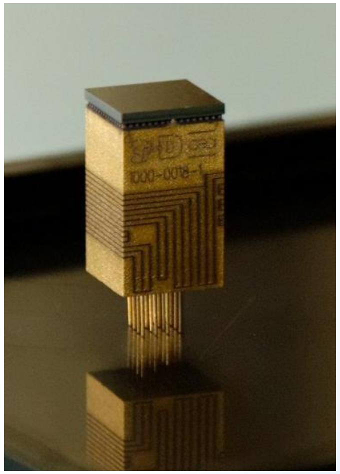

Features	Caliste 64	Caliste 256	Caliste HD
Pixel detector	8 × 8	16 × 16	16 × 16
Pixel pitch	1 mm	580 µm	625 µm
Guard ring	900 µm	200 µm	20 µm
Front-end	IDeF-X 1.1	IDeF-X v2	IDeF-X HD
Power consumption	200 mW	800 mW	200 mW
Pin grid array	7 × 7	7 × 7	4 × 4
Energy range	2-250 keV	2-250 keV	2 keV-1 MeV

Medipix-2 Detector Chip

- Photon Counting detectors
- 65,536 pixels (256 × 256)
- 55 × 55 μm^2 pixels
- 1.4 × 1.4 cm^2 area

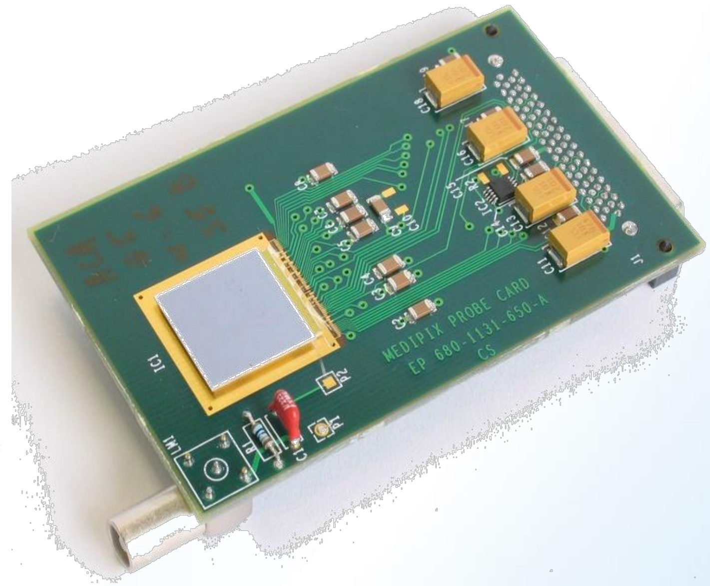

Fig (a) shows Medipix-2 detector chip

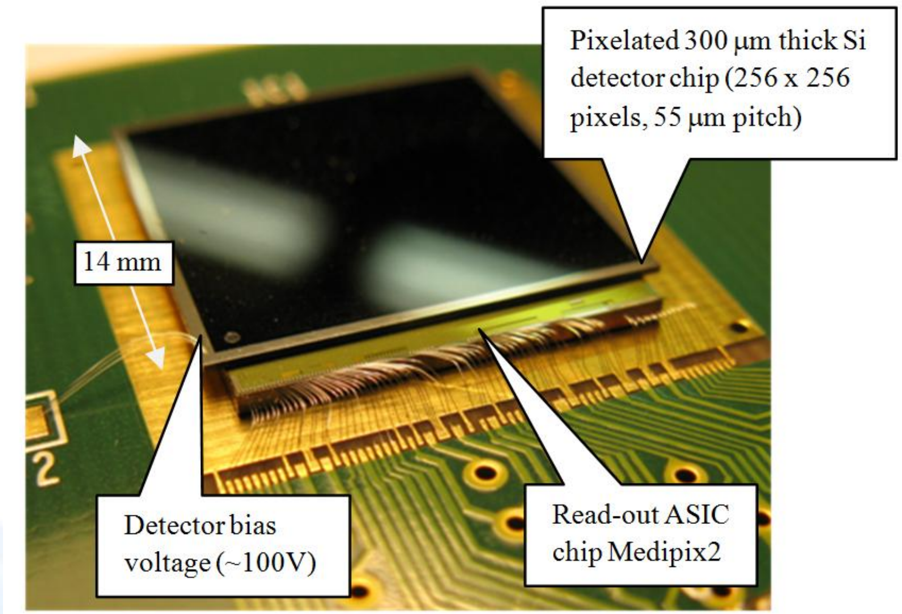

Fig (b) magnified view of (a)

Flood Frames

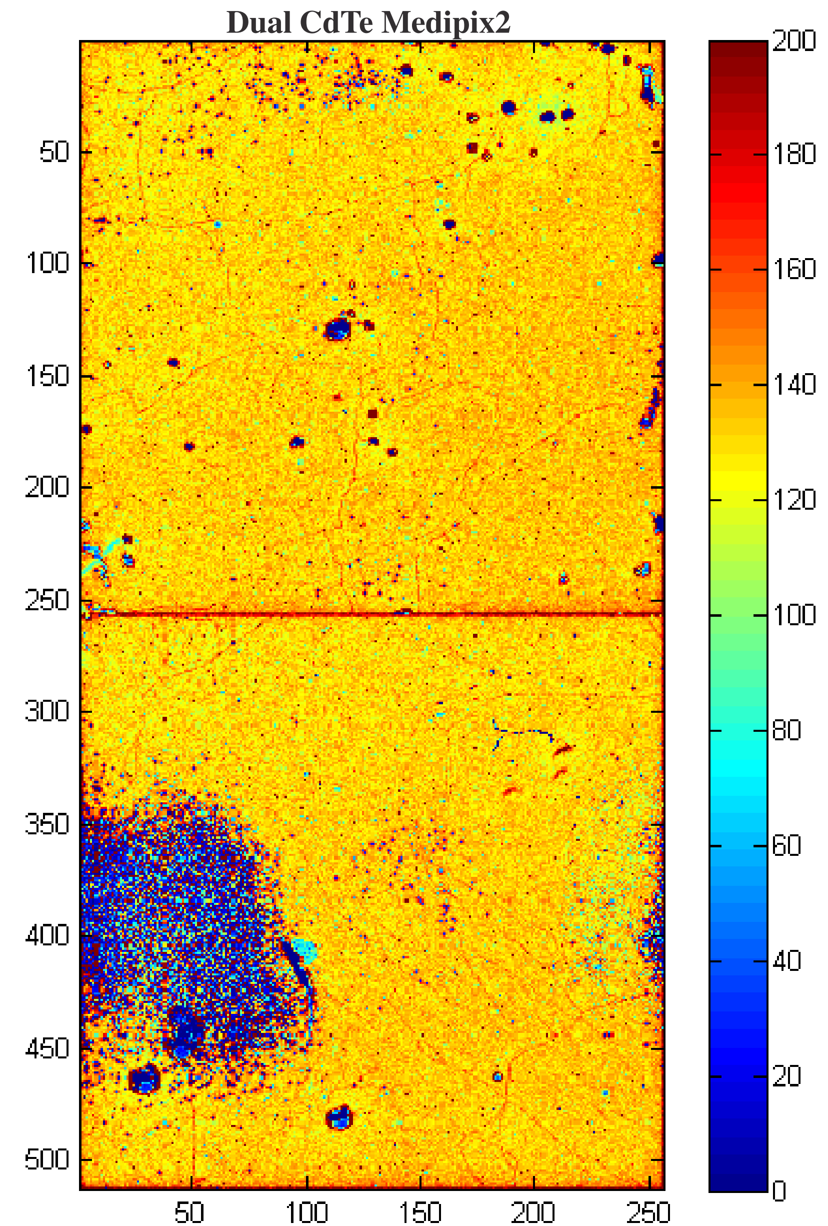

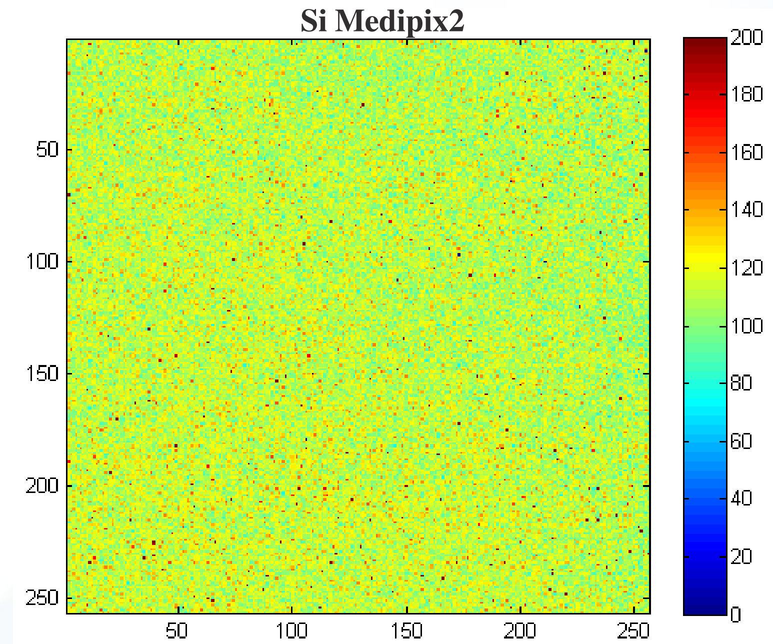

Image Correction Demonstration of Si

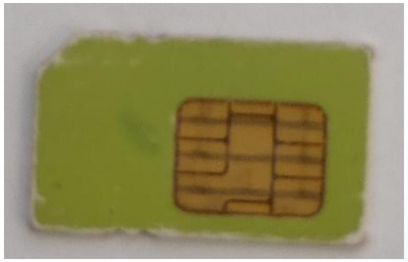

- **Detector parameters:**
  - 100 V bias
  - Low energy threshold ≈ 13 keV
  - 200 frames
  - Tube Current = 200μA
  - Shutter time = 40ms
  - SDD = 190mm

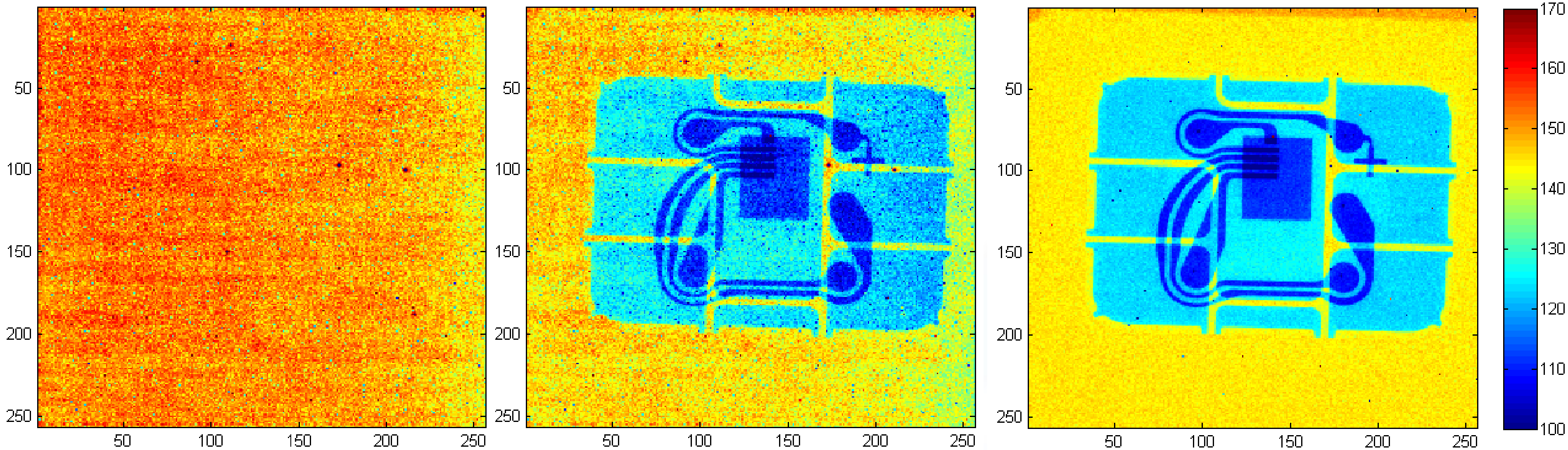

Mean of 200 open beam frame

Mean of 200 frame with mobile sim

Corrected Frame

Image Correction Demonstration of CdTe

- **Detector parameters:**
  - -438 V bias
  - Low energy threshold ≈ 13 keV
  - 200 frames
  - Tube Current = 23μA
  - Shutter time = 30ms
  - SDD = 190mm

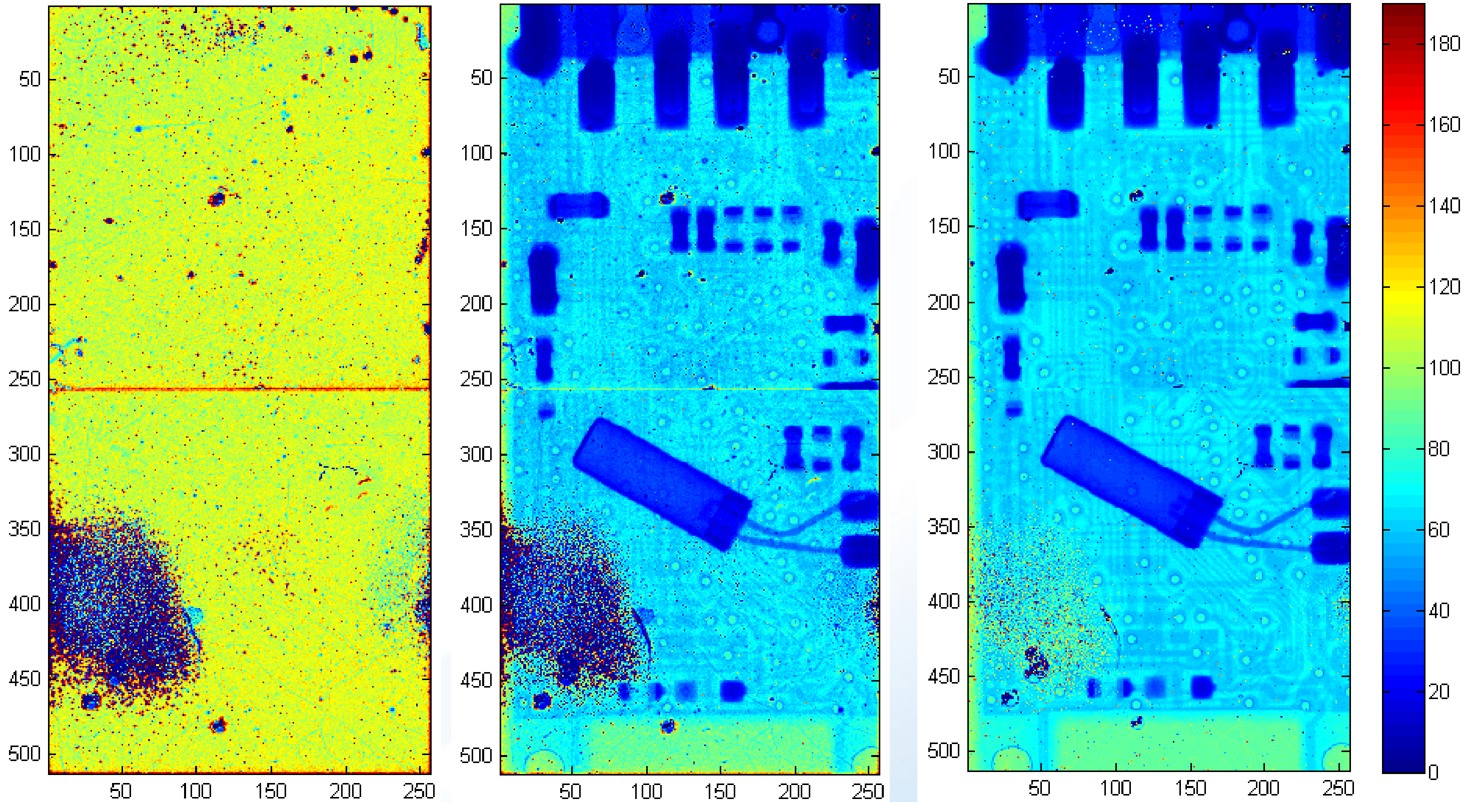

Mean of 200 open beam frame

Mean of 200 frame with USB

Corrected Frame

CT Images With Medipix2-CdTe

Mouse Sample

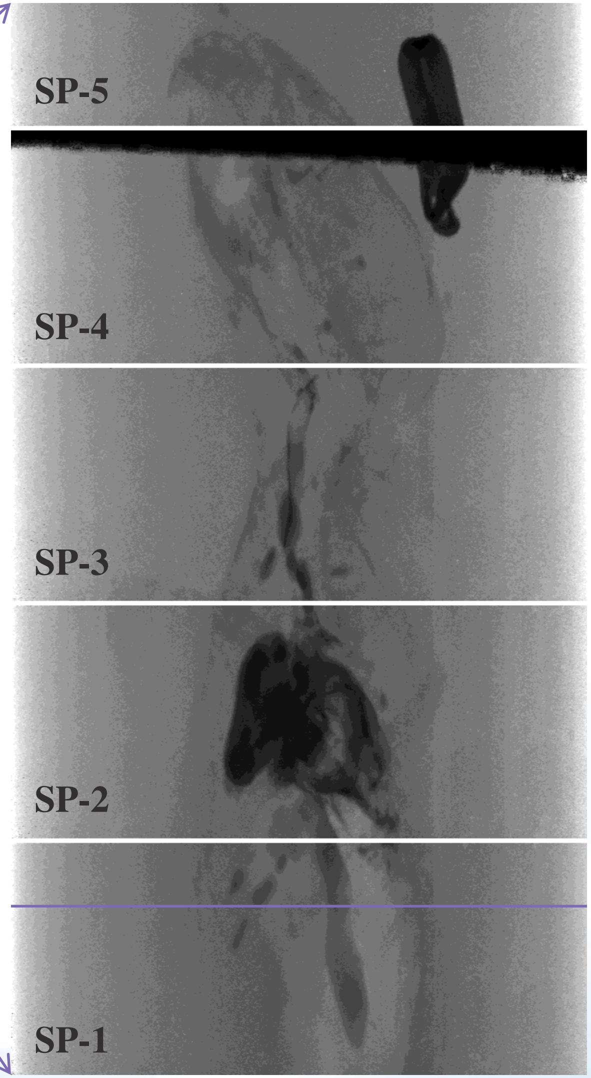

2-D Projection Images

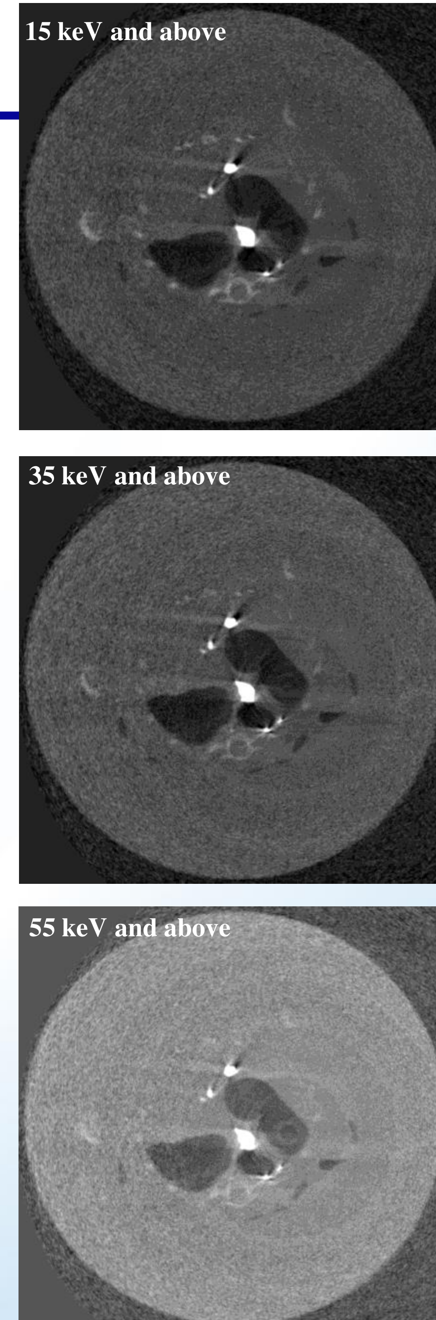

3-D CT images (selected region from projection image)

Conclusions

- Quality and high cost of crystals is the main factor limiting wide spread of CZT detectors
- Due to developments in readout electronics and charge loss correction techniques CZT detectors continue finding places in many areas of applications

Acknowledgements

Department of Nonproliferation and National Security: Giuseppe Camarda, Yonggang Cui, Anwar Hossain, Ge Yang, Istvan Dioszegi, Leon Forman, Vinita Ghosh, Walter Kane, Peter Vanier, Carl Czajkowski, Stephen Musolino and Joe Indusi

BNL’s Instrumentation Division: Graham Smith, Bo Yu, Paul O'Connor, Gabriella Carini, Gianluigi De Geronimo, Peter Siddons, Paul Vaska, and George Mahler, Dr. Ralph James